

**Modeling of Brick Masonry Infill for Seismic
Performance Evaluation of RC Frame Buildings**

JUNE 2013

DOCTOR OF ENGINEERING

MAIDIAWATI

TOYOHASHI UNIVERSITY OF TECHNOLOGY

Abstract

Brick masonry walls are commonly used as infill in Indonesian RC buildings. However, the presence of brick masonry infill in such buildings is usually neglected in seismic design calculations, assuming it to be a nonstructural element. According to experimental and analytical past studies by several researchers, the brick masonry infill significantly contributed to the seismic performance of this kind of building.

The current study focuses on evaluation of brick masonry infill contribution to the seismic performance of RC frames. In this study, site observation on two 3-story earthquake-damaged RC buildings with brick masonry infill was conducted after the 2007 Sumatra, Indonesia earthquakes. The two damaged buildings had similar structural characteristics, however, one of them totally collapsed and the other was moderately damaged. The seismic capacities of both buildings were evaluated for the first story, where the most severe damage was observed, based on the current Japanese standard without considering the brick infill effects. As the result, a similar seismic capacity was obtained for both buildings. It seemed that the brick infill, which was much larger in the surviving building, contributed to resist seismic loads and protected the building from collapsing.

To investigate the contribution of nonstructural brick infill to the actual performance of damaged building, a series of experimental tests on RC frames with/without brick infill representing the moderately damaged building was conducted. Four 1/2.5 scale one-bay RC frames with rigid beams were prepared: one bare frame and three infilled frames with different brick infill. One of brick wall was extracted from the moderately damaged building in Indonesia, transported to Japan, and then installed into one of the RC frames. On the other hand, two

other brick walls consisted of 1/2.5 scale bricks having the dimensions of 88 mm in length, 44 mm in width and 20 mm in height. One of them was applied finishing mortar with a thickness of 8 mm to both surfaces of the wall which resulted in infill thickness of 60 mm. These specimens were tested under quasi-static cyclic loading and constant vertical loading. The behavior and performance of test structures were observed at every peak and residual drift throughout loading. The brick wall contributions were quantitatively evaluated comparing the seismic performance and failure mechanism between bare frame and infilled frames.

An analytical model of masonry infilled frames was developed to evaluate the contribution of brick masonry infill to the seismic performance of RC frames. In this model, the masonry infill was replaced by a diagonal compression strut having the same thickness and material properties as those of the panel. The equivalent diagonal strut represents a distributed compression transferred diagonally between infill/frame interfaces. The Infill/frame contact length was determined by solving two equations, i.e., static equilibriums related to compression balance at infill/frame interface and lateral displacement compatibility. Consequently, the strut width was presented as a function of infill/column contact length, however, which was defined as the smallest contact lengths between both ends of strut. The lateral strength and stiffness of infill at yield were given based on the evaluated strut width.

Verification of the proposed analytical method was conducted through simulating the experimental results of brick masonry infilled frames. As the result, good agreements were observed between the experimental and analytical results on lateral stiffness, lateral strength, and ductility. It means that the performance of boundary frame as well as infill can be reproduced based on the proposed method. Moreover, the column performance was evaluated by considering the infill effects and displacement compatibility. Consequently, deformation capacities of columns in infilled frames were also evaluated appropriately.

The proposed analytical method was applied to non-structural brick infill in collapsed and

surviving buildings to recalculate the seismic performance of both buildings by considering the infill effects. Calculations were conducted in the East-West direction, to which the collapsed building actually toppled, on the basis of the Japanese standard. Although the brick infill was considered as an analytical parameter, the wing walls or walls with openings were neglected in calculations. The spandrel walls were considered to evaluate the clear height of columns. The seismic performance of both buildings was compared between the analyses with and without infill effects. A distinct difference was observed between the maximum strengths of buildings: it was higher in the case considering the infill. The strength of collapsed building drastically dropped when several short columns failed in shear. On the other hand, the strength of the surviving building was maintained up to much higher ultimate deformation of columns. These are possible reasons why one of the buildings could survive during the severe earthquake. It indicates that the nonstructural infill significantly contributed to prevent the surviving building from collapsing.

Acknowledgements

First, I would like to say “*Alhamdulillah rabbil 'aalamiin*”, thank Allah SWT, for ease during my doctoral journey.

I would like to express the deepest appreciation to my supervisor Prof. Yasushi Sanada for continues support of my PhD study and research, for his motivation, and immense knowledge. His guidance helped me in all the time and of research and lead me to finish my thesis step by step. His words can always inspire me and bring me to a higher level of thinking.

My sincere thanks also go Prof. Tomoya Matsui, who was my second and official supervisor, for help and guidance of defense preparation. I also want to thank Prof. Taiki Saito and Prof. Kinya Miura, who offered me the inspiring correction in the oral defense and for valuable suggestion in my thesis.

I am grateful to Indonesian Ministry of Higher Education for financial support during my study.

I thank my fellow lab. mates in concrete structure group in Toyohashi University of Technology for kind assistance to my experimental work and their friendship during my study. In particular, I am grateful to Mr. Kanada, who was an expert technician of concrete laboratory, and Mr Ishikawa, who was a skilled laborer, for their help and guidance in preparation and setting the specimens into the testing frame.

I would like to thank my beloved parents, elder and younger sisters and brothers, my aunt, Kartini, and her husband, Edwar Z. They were always pray for me with their best wishes.

Finally, I would like to thank my husband, Jafril Tanjung, and my lovely daughter, Zahra Nadya, for their unconditional support and encouragement to finish my PhD. Their love provided my inspiration and driving force. I would like to dedicate this thesis for them. I hope this work makes them proud.

Contents

Abstract.....	ii
Acknowledgments.....	v
List of tables.....	xi
List of figures.....	xii
List of Photos.....	xiv
Chapter 1-Introduction.....	1
1.1 Background.....	1
1.2 Research Objective.....	3
1.3 Dissertation Outline.....	3
Chapter 2-Literature Review.....	5
2.1 Introduction.....	5
2.2 Masonry Properties.....	6
2.3 Behavior of Masonry Infilled Frames.....	8
2.4 Seismic Performance of RC Frame Buildings with Masonry Infill.....	12
2.5 Review of Previous Analytical Models for Masonry Infill.....	14
2.6 Summary.....	20
Chapter 3-Field Investigation of Indonesian RC Buildings Damaged during the September 2007 Sumatra Earthquakes.....	22
3.1 Introduction.....	22

3.2 Description of the 2007 Earthquakes.....	23
3.3 Typical Building Damage.....	25
3.4 Field Investigation of Damaged RC Buildings	30
3.4.1 Collapsed Building.....	31
3.4.2 Surviving Building.....	31
3.5 Damage Grade Evaluation of Damaged Buildings.....	37
3.6 Seismic Performance Evaluation of Damaged Buildings.....	38
3.6.1 Basic Seismic Index E_0	38
3.6.2 Strength Index C	39
3.6.3 Ductility Index F	42
3.6.4 Seismic Performance of Damaged Buildings.....	45
3.7 Torsion Effect Evaluation of Damaged Buildings.....	46
3.8 Summary.....	50

Chapter 4-Experimental Evaluation on Contribution of Brick Masonry Infill to

Seismic Performance of RC Frames.....	51
4.1 Introduction.....	51
4.2 Test Models of RC Frames with/without Brick Infill.....	52
4.2.1 BF Specimen.....	52
4.2.2 IF_FB Specimen.....	52
4.2.3 IF_SBw/oFM and IF_SB Specimens.....	54
4.3 Material Properties.....	59
4.4 Experimental Methods.....	59
4.4.1 Loading Method.....	59
4.4.2 Measurement.....	61

4.5 Experimental Results.....	61
4.5.1 Failure Process and Mechanism.....	61
4.5.2 Lateral Force-Drift Ratio Relationship.....	66
4.6 Summary.....	67
Chapter 5-Analytical Modeling of RC Infilled Frames.....	68
5.1 Introduction.....	68
5.2 Proposal of Simple Model for Evaluating Infill-Frame Interaction.....	69
5.3 Experiments for Verification.....	75
5.4 Verification of Analytical Model.....	76
5.4.1 Seismic Contribution of Brick Masonry Infill.....	76
5.4.2 Effects on Columns.....	80
5.4.3 Evaluation of Column Ductility.....	80
5.4.4 Performance Curves of Infilled Frames.....	82
5.5 Summary.....	84
Chapter 6-Application of Proposed Model to Seismic Performance Evaluation of	
 RC Buildings.....	85
6.1 Introduction.....	85
6.2 Application of Proposed Model.....	86
6.3 Seismic Performance Evaluation of Earthquake-Damage RC Buildings.....	88
6.4 Summary.....	90
Chapter 7-Summary, Conclusions and Recommendations.....	91
7.1 Summary.....	91
7.2 Conclusions.....	93

7.3 Recommendations.....	94
References.....	96
Appendix A-An Example to Demonstrate the Calculation of Contact Length and Strut Width of Infill by the Proposed Model.....	100
Appendix B-Moment, Shear and Axial Force Distributions of Column.....	108
Appendix C-An Example to Demonstrate the Calculation of Column Performance.....	112
Publications.....	114.

List of Tables

Table 3.1: Member List of the Surviving Building.....	35
Table 3.2: Damage Class Definition of RC Columns.....	36
Table 3.3: Seismic Capacity Reduction Factor η	36
Table 3.4: Structure Parameters and Damage Grades.....	38
Table 3.5: Effective Strength factor.....	41
Table 4.1: Parameters for Specimens.....	52
Table 4.2: Material Properties of Specimens.....	58
Table 4.3a: Failure Processes of BF and IF_FB.....	63
Table 4.3b: Failure Processes of IF_SBw/oFM and IF_SB.....	64
Table A.1: Balancing Process of Beam Shear Affect to Columns' Deformation.....	102
Table A.2: Newton-Raphson Method for Finding Intersection Height.....	105
Table A.3: Iteration Process for Finding the Contact Length.....	106
Table B.1: Moment, Shear and Axial Forces of Compressive Column of IF_FB specimen.....	108

List of Figures

Figure 2.1 :	Testing Method for Shear Strength in Masonry Panel.....	7
Figure 2.2 :	Typical Deformation of Infilled Frame Under Lateral Loading.....	11
Figure 2.3 :	Knee-Braced Frame Model for Sliding Shear Failure of Masonry Infill.....	15
Figure 2.4 :	Diagonal Tensile and Compression Failure of Masonry Infill.....	15
Figure 2.5 :	Diagonal Compressive Strut on Masonry Panel.....	16
Figure 2.6 :	Contact of Wall and Frame of Infilled Framed at Failure.....	17
Figure 3.1 :	Epicenters of 8.4 M_L and 7.9 M_L Earthquakes.....	24
Figure 3.2 :	Investigated Areas.....	26
Figure 3.3 :	First floor Plan of Collapsed Building.....	32
Figure 3.4 :	First Floor Plan of Surviving Building and Damage Class of Each Column...33	
Figure 3.5 :	Structural Members of Surviving Building.....	34
Figure 3.6 :	Seismic Performances of Damaged Buildings without Infill Effects.....	46
Figure 3.7 :	Centers of Mass and Rigidity of Damaged Buildings.....	49
Figure 4.1 :	Detailed Drawing of BF Specimen.....	55
Figure 4.2 :	Detailed Drawing of IF_FB Specimen.....	56
Figure 4.3 :	Detailed Drawing of IF_SB Specimen.....	57
Figure 4.4 :	Schematic View of Test Set-Up.....	60
Figure 4.5 :	Lateral Loading History.....	61
Figure 4.6 :	Measurement.....	62
Figure 4.7 :	Final Crack Patterns.....	65
Figure 4.8 :	Lateral Force-Drift ratio Relationships of Infilled Frames.....	66

Figure 5.1 :	Modeling of Masonry-Infilled Frame.....	70
Figure 5.2 :	Considering of Axial Force at Column Bottom.....	73
Figure 5.3 :	Lateral Displacement Compatibility between Column and Infill.....	74
Figure 5.4 :	Flowchart for Identifying Infill/Column Contact Length.....	75
Figure 5.5 :	Lateral Force-Drift ratio Relationships of Infills.....	77
Figure 5.6 :	Comparison of Lateral Strength of Infill between Analytical and Experimental Results.....	78
Figure 5.7 :	Stress Diagrams of Compressive Column.....	79
Figure 5.8 :	Performance Curves of Compressive Column.....	81
Figure 5.9 :	Concrete Strength Degradation with Displacement Ductility.....	82
Figure 5.10:	Comparison of Experimental and Analytical Performance Curves of Infilled Frames.....	83
Figure 6.1 :	Infilled Frames and Column Detail on the First Floor Plan of RC Frame Buildings.....	87
Figure 6.2 :	Strut Model of Infill in Multi-Span Infilled Frames.....	88
Figure 6.3 :	Assumed Distributed Forces due to Strut at Column Ends.....	88
Figure 6.4 :	Comparison of Seismic Performance of Damaged Buildings.....	89
Figure A.1:	Modeling of Infilled Frame.....	101

List of Photos

Photo 3.1:	Typical Damage to RC-frame + URM Structures.....	27
Photo 3.2:	Comparison of Roofs Used in Sumatra and Java Islands.....	28
Photo 3.3:	Typical Damage to URM Structures.....	29
Photo 3.4:	Timber Houses with Rumbia Roofs.....	29
Photo 3.5:	Collapsed and Surviving Buildings just after the Earthquakes.....	30
Photo 3.6:	Collapsed Building.....	32
Photo 3.7:	Surviving Building.....	33
Photo 3.8:	Examples of Classified Columns.....	37
Photo 4.1:	Preparation of Brick Wall Specimen.....	53
Photo 4.2:	Installation of Brick Wall.....	53
Photo 4.3:	Initial Damage to Infilled Wall.....	54
Photo A.1:	IF_FB Specimen.....	101

Chapter 1

Introduction

1.1 Background

Brick masonry has been widely used as an infill in the reinforced concrete (RC) frame buildings in the high-risk seismic area such as Indonesia. Easy and low-cost constructing is known as a main reason for uses of the brick masonry in the developing countries. Damage to RC frame buildings after earthquakes in such countries shows that the brick masonry might play significant roles in the seismic resistant of this kind of structure, because RC frame buildings with brick masonry infill have been survived under strong ground motions comparing to bare RC frame structures. Unfortunately, there have been not clearly known how the brick masonry improved the seismic performance of RC frame buildings.

In most of cases of seismic resistant design procedures, particularly in Indonesia, the brick masonry infill in RC frame buildings is considered as nonstructural walls. Therefore, this consideration may result inaccurate prediction of the lateral stiffness, strength, and ductility of

RC frame buildings. Reluctance of numerous engineers to take into account the contribution of brick masonry infill has been due to the inadequate knowledge concerns infilled RC frame behavior, complication involved in structural analysis, and uncertainty about the non-integral action between infill and RC frame.

Recently, several researchers have been experimentally and analytically studied about the performance and behavior of brick masonry infill on RC frame structures as well-documented in (Polyakov, 1956; Holmes, 1961; Smith and Carter, 1969; Brokken and Bertero, 1981; Bertero and Brokken, 1983; Paulay and Priestley, 1992; Decanini et al., 2004; Hashemi and Mosalam, 2007; Baran and Sevil, 2010). Such experimental results showed that the performance and behavior of brick masonry on RC frame structures varied with levels of lateral loads applied to structures. Brick masonry infill remains in contact with RC frame structures under very low lateral loads and hence there is composite action between RC frame and brick masonry infill. Therefore, the stiffness of structural system becomes larger than bare RC frame structure. With increasing lateral loads, the brick masonry infill starts to crack at the interface between RC frame and brick masonry infill. Furthermore, separation between RC frame and brick masonry infill occurs at the tension zone when lateral loads further increased. On the other hand, on the compression zone, the brick masonry forms a diagonal strut action.

One of analytical methods to estimate the seismic performance of brick masonry in RC frame structures is on the basis of the diagonal strut action by defining its effective width as proposed by several researchers. Some of them focused on the contact length between brick masonry and RC frame for describing interaction between brick masonry and RC frame. However, there were no completed methods to precisely estimate behavior of brick masonry infilled frames. Therefore, this study proposes an alternative method of strut model for determining the equivalent strut width of infill with a simplified equation. In this model, a masonry infill is replaced by a diagonal compression strut, which represents a distributed

compression transferred diagonally between infill/frame interfaces. The infill/frame contact length can be determined by solving two equations, i.e., static equilibriums related to the compression balance at infill/frame interface and lateral displacement compatibility. Consequently, the equivalent strut width is presented as a function of infill/frame contact length.

1.2 Research Objective

The objective of this study is to propose a new simple analytical method for evaluating the seismic performance of the brick masonry infill in RC frame structures with high accuracy and efficiency. The proposed method starts from determining an equivalent strut width of compression diagonal strut by using simplified equations. The goal of this study is to make clear how the brick masonry affects the seismic performance of RC frame structures with brick masonry infill. To reach this objective, several stages of researches were conducted as follows:

1. Field investigation on damaged buildings due to September 2007 Sumatra, Indonesia earthquakes carried out after the earthquake event.
2. Experimental tests on an RC bare frame and several brick infilled frames representing one of the Indonesian earthquake-damaged buildings.
3. Developing a new analytical model of masonry infilled frames for evaluating contribution of masonry infill to lateral strength, stiffness and ductility of structure.
4. Evaluating the seismic performance of two RC buildings by applying the proposed analytical method to nonstructural brick infill.

1.3 Dissertation Outline

The dissertation is presented in seven chapters that are organized for following development of an analytical model. Chapter One introduces the background and objective of this research.

Chapter Two reviews the available literatures regarding to the behavior and seismic performance of masonry infilled frames. This chapter also introduces analytical modeling of masonry infill proposed by a number of researchers.

Chapter Three reports the field investigation in affected areas due to September 2007 Sumatra, Indonesia earthquakes. The seismic performance of two damaged buildings without considering the infill effects is presented in this chapter. The eccentricities of mass and rigidity of both buildings were also evaluated to investigate torsion effects on these building.

Chapter Four gives the results of experimental evaluation on contribution of brick masonry infill to seismic performance of RC frames. The test specimens are an RC bare frame and several brick infilled frames with different thickness and configuration of infill representing one of the Indonesian earthquake-damaged buildings. Infill was extracted from the damaged building, transported to Japan and installed into one RC frame. Moreover, scaled infill was also constructed by scaled bricks made in Japan, whose compressive strength of brick was arranged to be similar to that of Indonesian brick.

Chapter Five presents a new analytical model replacing infill by a compression strut to evaluate the seismic performance of masonry infilled RC frames. The proposed method introduces a simple approach to determine the equivalent strut width of infill based on compression balance at infill/frame interface and lateral displacement compatibility. Chapter Five also presents verification of the proposed method by simulating experimental test results on several brick infilled frames.

Chapter Six applies the proposed model to evaluate the seismic performance of earthquake-damaged RC buildings considering the infill effects. Finally, Chapter Seven summarizes the research finding and presents conclusions on research results. The recommendation for future study regarding to behavior and performance of masonry infilled frame structures is also presented in Chapter Seven.

Chapter 2

Literature Review

2.1 Introduction

Masonry walls, which are commonly used as infill walls in RC buildings in the world, consist of a variety of materials having specific physical and mechanical properties. The compressive and tensile strengths are the most important properties of masonry affect the structural performance. Several researchers have studied the behavior and performance of RC frame structures with masonry infill. They have revealed that the presence of masonry walls in RC frames as an infill can change the behavior and performance of whole structures. Therefore, to yield clear understanding of the structural behavior of RC frame with masonry infill, an extensive literature review of several past studies which are needed to develop rational theoretical models is presented in this chapter. Several analytical methods for evaluating the lateral strength of masonry infill from a number of researchers are also given in this section to compare with a new model developed in the current study.

Although the target of study is RC frames with unreinforced brick masonry infill, some experimental and analytical models for reinforced masonry infill and infilled steel frames are also included for references of masonry infill behavior.

2.2 Masonry Properties

Masonry is composite material consisting of masonry units (brick or blocks) and mortar which is commonly used for walls of buildings. The masonry unit can be solid or hollow and made from fired clay, concrete, calcium silicate or natural stone. Burned clay brick and concrete block are the most widely used as masonry units around the world. Mortar can be lime or a mixture of cement, lime, sand and water in various proportions. Consequently, masonry properties vary from one structure to others depending on the properties of and the interaction between components, type of units and mortar used. Mosalam mentioned in his report (Mosalam K. et al., 2009) that masonry and specially unreinforced masonry (URM) commonly has mechanical properties such as strength and ductility inferior to those of reinforced concrete and steel.

The compressive and tensile strength are the most important properties of masonry affect the structural performance. The compressive strength of masonry, which can be determined through the uniaxial compression tests of masonry prisms, is much higher than its tensile strength and substantially less than the unit strength due to the influence of the mortar. The bond between the mortar and the unit affected the tensile strength of masonry in which it is typically less than the tensile strength of either of the main component.

Bond between mortar and brick units is because of chemical or friction. As reported by Mosalam K. et al. (2009) that tensile strength at the interface is primarily due to chemical bond which depends upon the absorption rate of brick unit. High absorption rate decrease the strength of the bond. Hence, brick units are usually wetted before they are laid. Direct tension and

bending usually cause the bond to break where separation of bricks and mortar layer occurs. As reported by Page AW (1996), masonry bond strength can vary from zero to more than 1MPa depending on the correct match of the mortar and the units' properties, particularly the water retention of the mortar and the suction of the masonry units.

The shear behavior of masonry has been investigated by many researchers to investigate the shear strength of masonry under the shear loading. According to Paulay and Priestley mentioned in reference (Paulay and Priestley, 1992), different testing methods have been used for the simple masonry prism or masonry panel, as shown in Figure 2.1. However, none method give a good representation of the actual behavior under seismic force, where the cyclic reversal of force direction coupled with the influence of crack propagation along the mortar beds by flexural action may cause a reduction in the true shear strength compared with the values measured in simple monotonic test where flexural cracking inhibited.

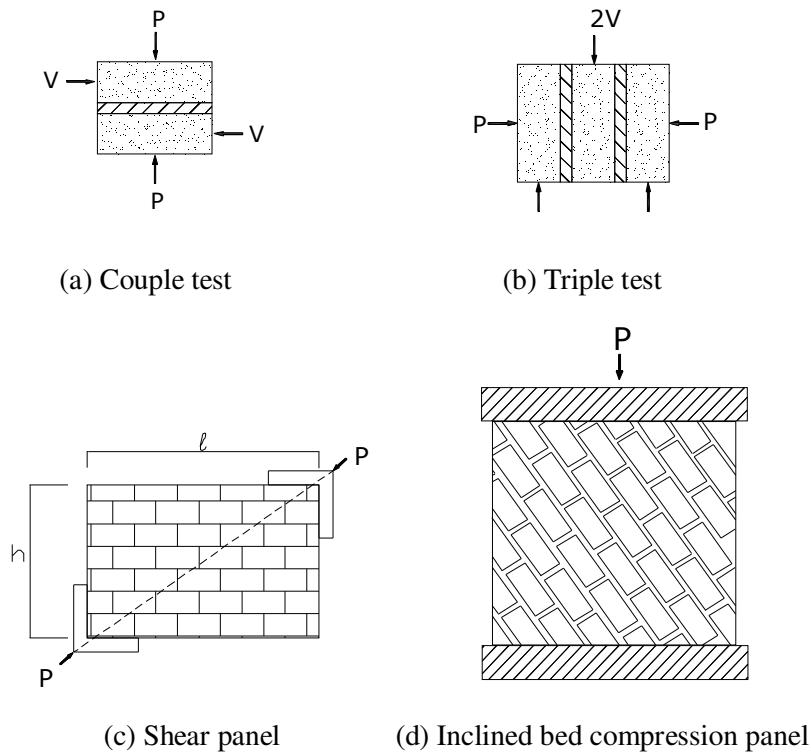


Figure 2.1. Testing method for shear strength in masonry panel.

Different test methods tend to give different shear strength. Shear stresses of infill can be expressed in Equation 2.1.

$$\tau = \frac{Q}{A} \quad (2.1)$$

Where, Q is shear force, A is net bonded area. The net bonded area is usually smaller than the cross-sectional area of wall.

2.3 Behavior of Masonry Infilled Frames

Behavior of masonry infilled frames subjected to in-plane lateral loads has been studied in the last four decades in attempts to develop a rational approach for design of such frames. The interactions of the infill with bounding frame and the impact of an infill on the lateral resistance and stiffness of a frame have been examined by number of researchers.

Fiorato et al. (1970) conducted monotonic tests as well as cyclic lateral loads on the 1/8-scale non-ductile reinforced concrete frames infilled with brick masonry. The tests showed that the horizontal sliding failure of masonry infill introduces a short-column effect, with plastic hinges and sometimes brittle shear failure developed at the mid-height of the column. They have found that masonry infill can increase the stiffness and strength but reduce the ductility of concrete frames.

Klingner and Bertero (1976), and Brokken and Bertero (1981) also performed tests on 1/3-scale, three-story-high, reinforced concrete frames infilled with fully grouted hollow concrete masonry under monotonic and cyclic lateral loading. The infill panels were reinforced with standard deformed bars in both vertical and horizontal directions. Additional shear steel that was beyond the minimum requirements of the ACI code was used to enhanced the shear

strength of the concrete columns. The tests results shown that infill panels can be effectively used to enhance the seismic performance of reinforced concrete frames in terms of strength and ductility. They have shown that the lateral stiffness and strength deteriorate with cyclic load reversals, the degree of which depends on the panel reinforcement and interface condition. The peak strength under cyclic loading is, in general, somewhat smaller than that obtained under monotonic loading, but it is always higher than that of a bare frame.

Kahn and Hanson (1979) have observed in their tests of RC frames with reinforced concrete panels as infill that separating the infill from the bounding columns and enhancing the shear transfer between the beam and the infill can prevent the brittle shear failure of the columns and, therefore, significantly enhance the ductility of a structure. They also found that, the failure of an infill panel transfers a big shear force to the columns, whose failure in shear will result in a fast degradation of the lateral load resistance of the system. They concluded that the shear failure of the columns could be prevented if the columns were confined with adequate shear reinforcement

Bertero and Brokken (1983) tested RC frames infilled with four types of masonry infill; two with hollow unit masonry, clay and concrete block, one with lightweight concrete panels, and one with solid clay brick infill reinforced with welded wire fabric at each face. The tests model consisted of eighteen 1/3-scale, three-story, one-bay, reinforced concrete. The results showed that the addition of infill increased significantly the lateral stiffness and lateral resistance of the frame. Further, they observed that almost all specimens exhibited concentrated failure at the bottom story. The fabrication method of infill including the quality control of material at the interface between the infill and bounding frames influenced to the response of an infilled frame. They also demonstrated that a properly designed infilled frame such as solid infill with welded wire fabric firmly tied on the bounding frames can exhibit superior performance as compared to bare frames. This interaction was succeeded through the wires of

the welded wire fabric that were spliced to dowels left anchored in the confined regions of the bounding frame members, so that the panel to be attached to the bounding frame

Mehrabi et al. (1994, 1996) tested two types of frame, non-ductile frame and ductile frame designed for Seismic Zone 4 according to the 1991 Uniform Building Code. They tested single-story, one-bay and single –story, two-bay reinforced concrete frames with unreinforced masonry infill, made with either hollow or solid concrete blocks. They demonstrated that the beneficial influence of the infill in terms of lateral strength, stiffness and energy dissipation capability and that the shear failure of the reinforced concrete columns can be prevented in a well designed frame. The most common failure mechanisms of unreinforced masonry infill in reinforced concrete frames were observed. Mehrabi et al. also introduced a limit analysis method for predicting the lateral strength and failure mechanism of an infilled reinforced concrete frame. In the later study, Shing and Mehrabi (2000) found that the infill walls have high lateral resistance and tend to partially separate from the boundary frames. And they form a compression strut mechanism as observed at a high lateral load level.

Baran and Sevil (2010) tested the infilled RC frames of one-bay, one and two-story, under the reversed cyclic lateral load. The infills were the hollow brick with and without plastering on both sides of infill. They found that infilled frames increased significantly in strength and stiffness for two and one-storey test frames. Application plaster on both sides of hollow brick infill increased lateral load carrying capacity of the frame. The two-storey and one-story equivalent test frame showed very similar behavior, especially lateral load capacities of equivalent pair were close.

Zovkic J. et al. (2012) performed the cyclic testing on one bare frame and nine of 1/2.5-scale of single bay reinforced concrete frames with various strength of masonry infill. The results showed that framed wall structure had much higher stiffness, dumping, and initial strength than the bare frame.

Most past studies demonstrated that the behavior of infilled frame at the initial stages of lateral loading is almost elastic and largely control by the characteristic of the masonry panel. The structure behaves as monolithic element due to the bond strength developed along the interface of structure. In this case, the columns act as tension or compression boundary members and the infill panel acts as connecting shear element. The masonry panel separates from the surrounding frame, except at the diagonally opposite compression corners as shown in Figure 2.2, as the lateral force increase where some parts of panel-frame interface crack due to the incompatible displacement resulting from different deformational characteristics. Further, the stresses at the tensile corners are relived while those near the compressive corner are significantly increased. The masonry panel subjected to compressive stresses along the loaded diagonal. In this stage, the principal stress perpendicular to the diagonal compression is compressive at the loaded corner and tensile at the center of the panel. Therefore, the loaded corners are subjected to biaxial compression, whereas the centre of the panel is under a tension-compression stress state.

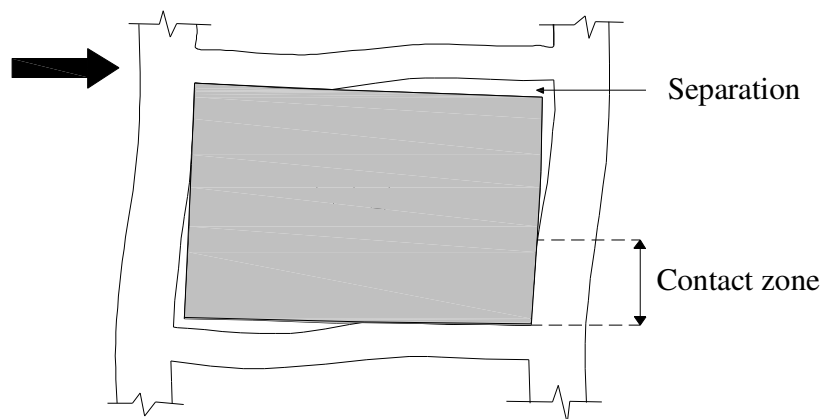


Figure 2.2. Typical deformation of infilled frame under lateral loading.

2.4 Seismic Performance of RC Frame Buildings with Masonry Infill

According to field investigations conducted by several researchers on seismic damaged building due to big earthquakes in many countries, the performance of RC buildings with masonry infill exhibited better performance as compared to the bare frame buildings. The observation results showed that masonry infill have the crucial role in preventing the collapsing of such buildings. As reported by Humar J. M. et al. (2001) on performance of buildings during the 2001 Bhuj earthquake that a large number of RC and masonry buildings suffered severe damage. Many reinforced concrete frames had infill masonry walls except in the first story, which was reserved for parking. The open first storey suffered severe damage or collapsed. However, it was found that the buildings with brick in cement mortar survived and showed better behavior although they suffered extensive cracks. The important observation to come out of the earthquake was that masonry infill, even when not tied to surrounding frame, could save building from collapse.

EEFIT (2008) reported that due to May 12, 2008 Wenchuan Earthquake about 70% of the structures had suffered some degree of damage with many suffering soft-storey failure at either the ground or first floor, mainly due to inconsideration of the added stiffness due to the presence of infill.

Observation on damage buildings due to L' Aquila, Italy earthquake occurred April 6, 2009 was carried by Kaplan H. et al. (2010). He discovered several RC and masonry buildings were collapsed and a number of out-of plane failures of non structural wall because of poor connection between frame and wall. However, the infill walls also played a positive role in preventing several non-ductile framed structures from collapsing because of the relatively short duration of ground shaking.

All above describe that the masonry infill appear to give great contributions to seismic performance of RC buildings. Therefore, based on a number of studies have conducted by

Fiorato et al. (1970), Klingner and Bertero (1976), Bertero and Brokken (1983), Mehrabi et al. (1996), Murty et al. (1996, 2000), Decainini et al. (2004), Hasemi and Mosalam (2007), Baran M. et al. (2010) and Zovkic et al. (2012), the effect of adding infill walls in frames are concludes as below

1. The Infill possesses large lateral stiffness and can significantly contribute to stiffness of infilled frame. Therefore, the infilled frames have much higher stiffness than those of the bare frame and the damaging behavior can be changed completely.
2. The masonry infill has considerable resisting to lateral load. Thus, the masonry infilled frames have the greater lateral strength compared to bare frames.
3. The masonry infill panel decreased the demand maximum displacement corresponding to the bare frame building. The ductility of infilled framed depends on infill properties, relative strength of frame and infill, ductile detailing of the frame when plastic hinging in the frame controls the failure, reinforcement in the infill when cracking in infill control the failure, distribution of infill in plan and elevation of the building.
4. Masonry infill gives a significant contribution to energy dissipation on frame structure. RC Frames with strong panels exhibited much better hysteretic energy dissipation than those with weak panels, regardless of the frame design.
5. The infill decreased the fundamental period of building.
6. The value of viscous damping ratio for whole building increase compare to bare frame
7. The presence of infill walls in frame structures completely alters the failure mechanism of infilled frame structure.

Paulay and Priestley (1992) conclude several different possible failure modes occur on infilled RC frame structure, namely

1. Tension failure of the tension column resulting from applied overturning moment. For infilled frames of high aspect ratio, the critical failure mode may be flexural, involving

tensile yield of the steel in the tension column, acting as a flange of the composite wall, and of any vertical steel in the tension zone of the infill panel. Under this condition the frame is acting as cantilever wall, and a reasonably ductile failure mode can be expected.

2. Sliding shear failure of the masonry along horizontal mortar courses generally at or close to midheight to the panel. If sliding shear failure of the masonry infill occur, the equivalent structural mechanism changes from the diagonally braced pin-jointed frame to the knee-braced frame, as shown in Figure 2.3 to form at approximately mid height and top or bottom of the columns or may result in column shear failure. Initially, the entire shear will be carried by the infill panel, but as the sliding shear failure develops, the increased displacement will induce moments and shear in the columns.
3. Diagonal tensile cracking of the panel. This does not generally constitute a failure condition, as higher lateral force can be supported by the following failure modes.
4. Compression failure of the diagonal strut. For masonry-infill panel, diagonal tensile splitting precedes diagonal crushing and the final infill failure force will be dictated by the compression strength, as shown in Figure 2.4 which may be used as the ultimate capacity. On elastic cycling the capacity of the diagonal strut will degrade, and the behavior will approximate the knee-braced frame. This failure mode is known as compression failure of diagonal strut.
5. Flexural or shear failure of the columns.

2.5 Review of Previous Analytical Model for Masonry Infill

The effect of masonry infill to seismic performance of infilled frame structure is commonly evaluated focusing on diagonal compression struts caused in the masonry infill as shown in Figure 2.5.

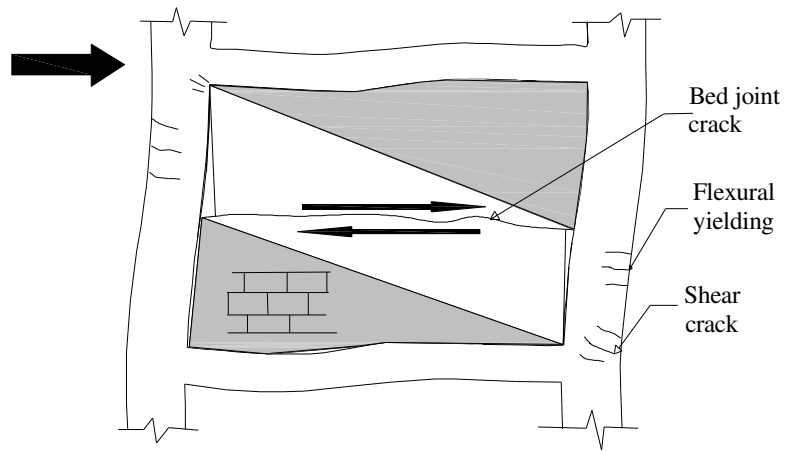


Figure 2.3. Knee-braced frame model for sliding shear failure of masonry infill.

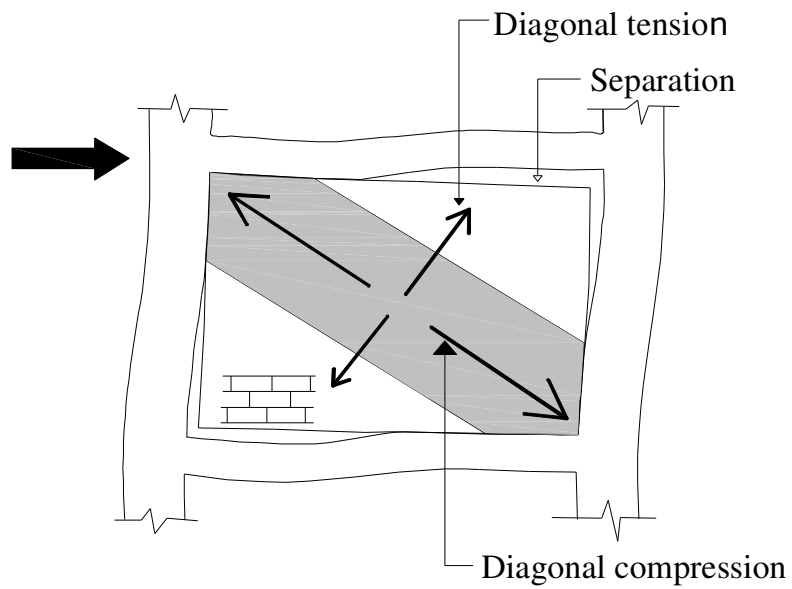


Figure 2.4. Diagonal tensile and compression failure of masonry infill.

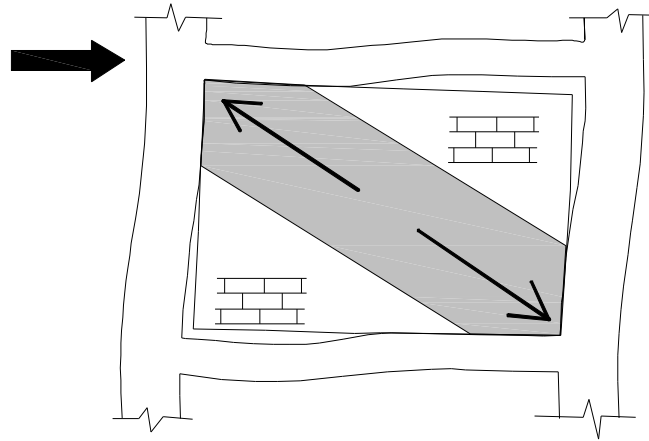


Figure 2.5. Diagonal compressive strut on masonry panel.

Several methods have been studied by researchers to define the effective width of diagonal strut of infill for determining the diagonal compression strength. This concept originally proposed by Polyakov in his research on “masonry in Framed Buildings” (1956). He performed a number of large-scale test including square as well as rectangular frames and found that the masonry infill and the members of the structural frame behave monolithically of infill-to-frame interface except for small regions at the two diagonally opposite corners. The diagonal cracks appeared in the center region of infill along the compression diagonal in a step-wise manner through mortar head and bed joints. Based on observation of the infill boundary separation, he suggested that the infilled frame system is equivalent to a braced frame with a compression diagonal strut replacing the infill wall.

Holmes (1961) continued the Polyakov idea to evaluate the infill effect in frame structure. Holmes tested infilled-steel frames with brickwork and concrete infilling under combination of vertical and horizontal loading to investigate the strength and stiffness of infilled frame. At failure, the wall and frame will only be contacted in the vicinity of the corner as shown in Figure 2.6 (Holmes, 1961). He suggested the wall panel was replaced by an equivalent

strut. Then, in his model, Holmes derived an equation to determine the ultimate lateral load capacity as given in Equation 2.2.

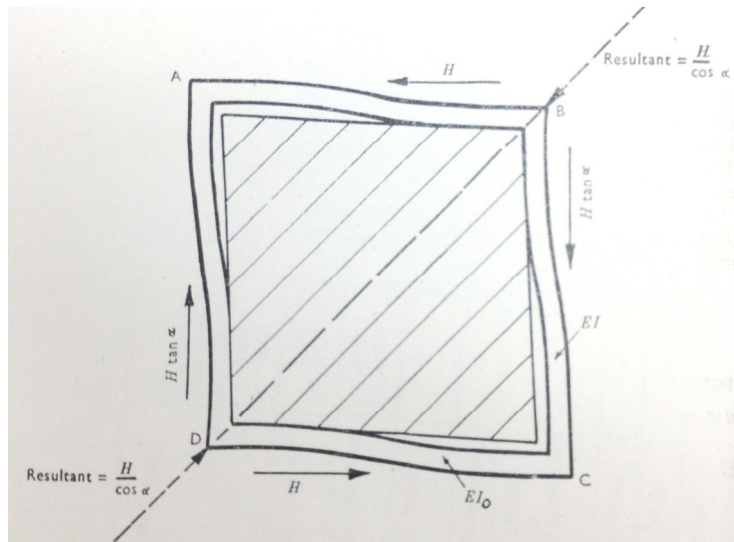


Figure 2.6. Contact of wall and frame of infilled framed at failure.

(Source: Holmes, 1961)

$$H = \frac{24EI e'_c d}{h^3 \left(1 + \frac{I}{I_0} \cot \theta\right) \cos \theta} + Af_c \cos \theta \quad (2.2)$$

where, H is horizontal load at failure, I is moment of inertia of the column of the frame, I_0 is the moment of the moment inertia of the beam of the frame, E is the modulus of elasticity of frame members, e'_c is the uniaxial compressive strain of the infill material at failure, h is the height of the infill, d is the diagonal length of the infill, θ is the angle of inclination of the diagonal strut to the horizontal, A is the section area of the equivalent diagonal strut and f_c is the ultimate compressive strength of the equivalent diagonal strut.

To consider the diagonal load distributed over the entire length of each side, Holmes

assumed the diagonal load as a triangular distribution of pressure and the effective area of equivalent strut was determined by conservative manner as $t.d/3$ for calculation, where t is thickness of infill. In this model, Holmes considered only the case of compressive failure of infill. He assumed that compressive failure would occur when the average diagonal strain reached a maximum value, which was measured from cylinder test or assumed. He ignored the variation of strain along loaded. However, the local strain could increase depend to the strength of the panel and the strain variation along the loaded diagonal was determined partly by the sides ratio of the panel and partly by the length of mutual contact of the frame and infill.

Stafford Smith (1967) and Smith and Carter (1969) conducted a series of tests on laterally loaded square mild steel frame models infilled with micro-concrete. He found that the load-deformation relation showed a high increase in strength of infilled frame compared to the bare frame. He observed that the wall could be replaced by an equivalent diagonal strut connecting the loaded corners. The effective width of diagonal strut of an infill is influenced the relative stiffness of the column-infill and the length/height proportions of the infill. The lengths of contact against the columns were showed to increase with each increase in the column section. Therefore, Stafford and Carter concluded that the large increase in the lateral stiffness response of the infill resulting from the increased length of the contact against the column. A non dimensional parameter, λh , is given in Equation 2.3 to determine the infill/frame contact length, α , which is given by Equation 2.4. From the tests it is shown that the stiffness of infill is independent of the beam section, however, the additional stiffness must be attributed to the effect of the increase in section of the column.

$$\lambda h = h \left(\frac{E_m t \sin 2\theta}{4E_c I h'} \right)^{1/4} \quad (2.3)$$

$$\frac{\alpha}{h} = \frac{\pi}{2\lambda h} \quad (2.4)$$

Where, h is height of column between centre-lines of beam, E_m is young's modulus of the infill material, E_c is young's modulus of column, t is thickness of the infill wall, h' is height of the infill, I is moment of inertia of the frame columns, θ is angle between diagonal of the infill and the horizontal.

In his model, Smith assumed triangular distributions of compressive and shear interaction act on the infill over the length of contact against the column and over half the span of the beam. The proportions of the total diagonal force transmitted from the beams or column were determined by calculating the resultant force of each triangular distribution to give balanced couples acting on the infill. The collapse may be assumed due to the plastic type of the infill failure. The corner region of the infill, which crushed and which might be considered to have been in plastic condition just before failure, extended along the column over the length of contact. The diagonal compressive strength of infill, R_c , is expressed by Equation 2.5. Lateral shear of infilled frame, H_c , to give compressive failure of the infill is given in Equation 2.6.

$$R_c = \alpha t \sec \theta f_c' \quad (2.5)$$

$$H_c = \alpha t f_c' \quad (2.6)$$

Mainstone (1971) presented results of series of test on model with infill of micro-concrete and model brickwork along with a less number of full-scale tests. Moinstone adopted the concept of replacing the infill with equivalent pin-jointed diagonal strut and only justified for behavior prior to first cracking of the infill. Based on experimental data and analytical result by

finite element analysis, Mainstone obtained the ratio of strut width to diagonal length of infill as given in Equation 2.7.

$$\frac{w}{d} = 0.175(\lambda h)^{-0.4} \quad (2.7)$$

where, w is width of equivalent strut, d is the diagonal length of of infill panel, and λh is non dimensional parameter given in Equation 2.3.

Liauw and Kwan (1984) studied experimentally and analytically the behavior of non-integral infilled frames and proposed Equation 2.8 for the width of the diagonal strut and Equation 2.9 for the width of diagonal strut for very stiff frames with flexible infill.

$$w = \frac{0.95 h \cos \theta}{\sqrt{\lambda h}} \quad (2.8)$$

$$w = \frac{0.86 h \cos \theta}{\sqrt{\lambda h}} \quad \text{or} \quad 0.45 h \cos \theta \quad (2.9)$$

Where, w is width of equivalent strut, h is story height, θ is slope of infill diagonal to the horizontal, λ is characteristic stiffness parameter.

Paulay and Priestley (1992) recommended that the width of diagonal strut be estimated as one-fourth of infill's diagonal length for a force equal to one-half of the ultimate load.

2.6 Summary

The brick wall is recognized as material with brittle behavior and low resistance to seismic action. On the other hand, the RC frame behaves more flexible than infill panel. Thus, combination of brick panel with RC frame can change the behavior and performance of infilled

RC frame structures.

A number of experimental tests have been carried by numerous researchers to investigate the effect of masonry infill on seismic performance of infilled frame structures. And several numerical methods have been developed to evaluate the strength and stiffness of masonry infill. The results show that the masonry infill has a significant effect on strength and stiffness. Therefore, the presence of masonry infill in frames have a significant impact on the seismic response of RC buildings, increasing structural strength and stiffness, increasing energy dissipation, but at the same time decreasing the lateral deformation and changing the failure mechanism of structures. It can be exhibited from past earthquakes where the RC buildings with masonry infill exhibited better performance when compared to the bare frame buildings.

Chapter 3

Field Investigation of Indonesian RC Buildings Damaged during the September 2007 Sumatra Earthquakes

3.1 Introduction

Sumatra Island, Indonesia is located close to a major earthquake fault line, where destructive earthquakes have occurred during the recent years. The greatest at 9.1 on the Richter scale (M_L), which caused a huge tsunami, occurred at Aceh, northern Sumatra on December 26, 2004. Then, a magnitude 8.6 M_L earthquake struck Nias Island in North Sumatra province on March 28, 2005. In 2007, there were three earthquakes of magnitude 6.4 M_L and greater around Padang, the capital of West Sumatra province: a 6.4 M_L quake struck Bukit Tinggi about 49 km north of Padang on March 6, 2007; on September 12, 2007 a 8.4 M_L quake occurred offshore of Bengkulu in southern Sumatra about 410 km from Padang; and the following 7.9 M_L on September 13, 2007 quake occurred near Kepulauan Mentawai, an offshore area about 190 km southeast of Padang. On September 30, 2009 at 5.16 PM local time in Indonesia, an earthquake

7.6 M_L struck again the west coast of Sumatra.

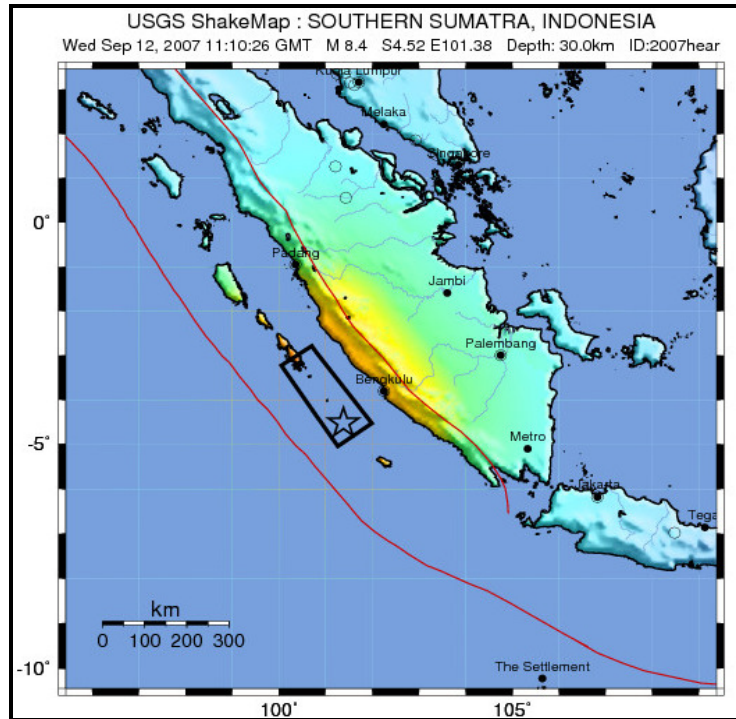
Padang city suffered moderate/serious damage due to the 2007 and 2009 earthquakes as reported by Maidiawati et al. (2008) and EERI (2009). In particular, the latest one caused thousands deaths and a large number of RC buildings totally collapsed. A lot of the concrete frame, infill wall and houses were damaged intensively due to this earthquake (EERI, 2009).

To investigate the typical damage on engineered and non-engineered buildings due to the earthquakes, the authors conducted a post-earthquake field investigation in Padang city and nearby areas after the 2007 event. Detailed investigation was conducted on two 3-story RC buildings with unreinforced brick masonry walls, standing side by side: one totally collapsed and other moderate damaged.

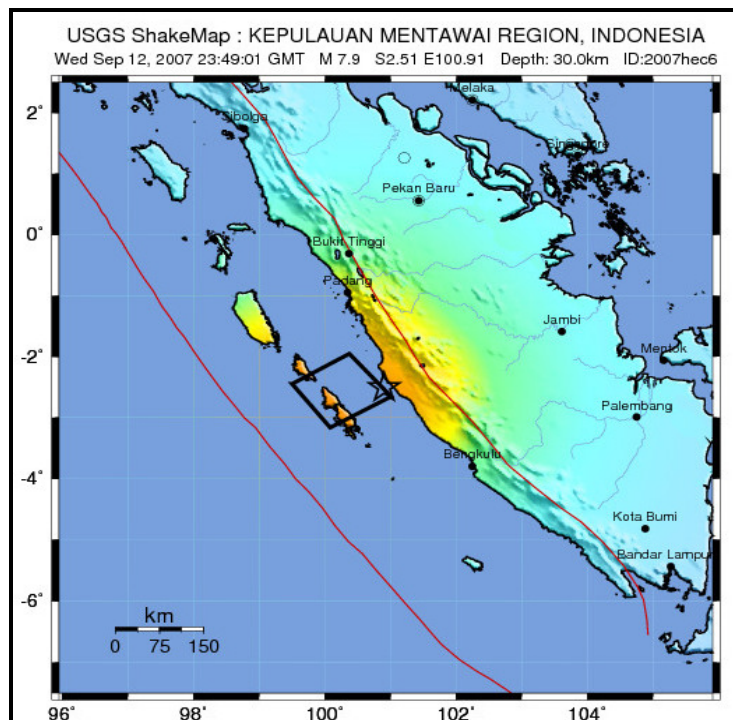
Moreover, the seismic capacity of both buildings was evaluated for the first story, where the most severe damage was observed, on the basis of current Japanese standard, without considering the brick infill effects.

3.2 Description of the 2007 Earthquakes

According to information provided by the U.S. Geological Survey (USGS, <http://earthquake.usgs.gov/>), the epicenters of September 12, 2007 earthquake 8.4 M_L , occurring at 06:10:26 PM was centered about 34 km underground, located at 4.520°S, 101.374°E, about 130 km southwest of Bengkulu on the southwest coast of Sumatra as shown in Figure 1(a). It was followed by several aftershocks of magnitude 5 and 6 along the same fault of west Sumatra. The second largest earthquake of 7.9 M_L occurred on September 13 at 06:49:04 AM local time in Indonesia, at 2.506°S, 100.906°E, Kepulauan Mentawai Indonesia at a depth of 30 km, as shown in Figure 1(b).



(a) 8.4 M_L earthquake



(b) 7.9 M_L earthquake

Figure 3.1. Epicenters of 8.4 M_L and 7.9 M_L earthquakes (Source: USGS).

Based on data reported by the National Disaster Management Coordinating Board of Indonesia (BAKORNAS, <http://bakornaspb.go.id/website>), the earthquakes killed 25 persons, seriously injured 41, and lightly injured 51. The earthquakes collapsed two engineering buildings in Padang, and many other buildings were damaged in Bengkulu and West Sumatra. In Bengkulu, 7,050 residences collapsed, 10,522 were heavily damaged, and 35,041 were slightly damaged. In West Sumatra, 10,915, 10,505, and 14,392 residences suffered heavy, medium, and light damage, respectively. In particular, Pesisir Selatan, a coastal area, and Kepulauan Mentawai suffered the most severe damage.

3.3 Typical Building Damage

The first stage of the investigation was a preliminary damage survey in Padang city and nearby areas along the coast, as shown in Figure 3.2, which was carried out to observe typical buildings and their damage. Most of the buildings can be classified into four types.

1. RC-frame + URM: RC moment-resisting frame structure with URM brick walls.
2. RC-tie + URM: URM brick structure confined with RC ties.
3. URM: URM brick structure.
4. TIM: Timber structure.

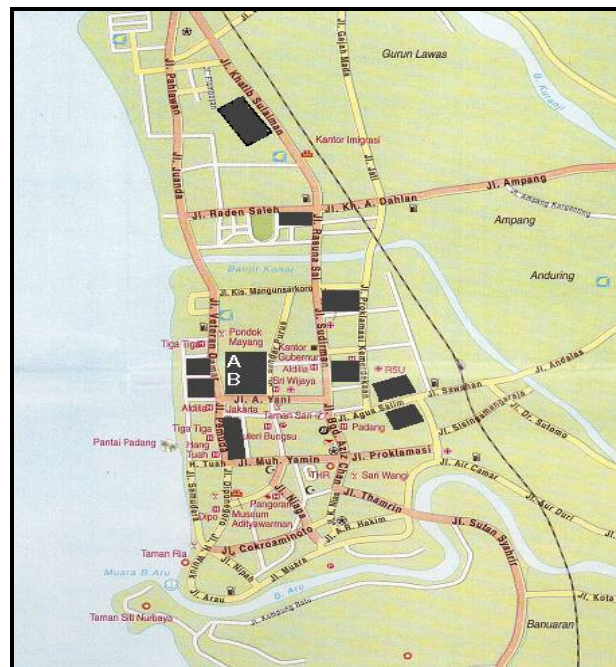
The former three types were popular in the city. On the other hand, the latter three were common in provincial areas.


The RC-frame + URM type is commonly constructed for buildings of more than two stories. Concrete slabs or tile roofs are conventionally used for roofing. Several examples of typical damage were observed for this type: total collapse of buildings as shown in Photo 3.1(a), shear failure of columns as shown in Photo 3.1(b), flexural failure of columns due to buckling of longitudinal reinforcements as shown in Photo 3.1(c), collapse and/or damage of infill walls as shown in Photo 3.1(d), and falling roof tiles and ceilings as shown in photos 3.1(e) and 3.1(f).

One of the collapsed buildings, shown in Photo 3.1(a), was investigated in detail as described in the following section.



(a) Black line show the survey route map



 : Investigated areas. A, B: Buildings for detailed investigation

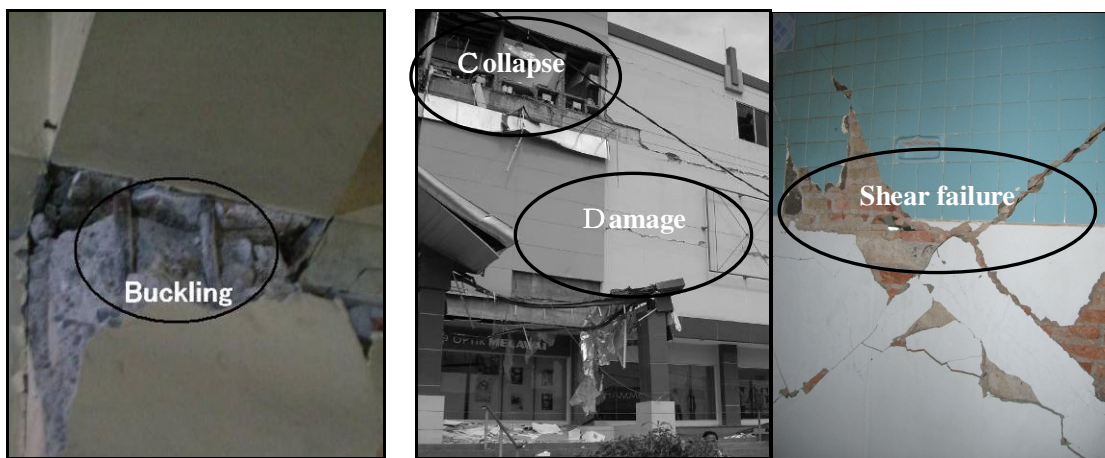
(b) Padang city map

Figure 3.2. Investigated areas.



(a) Total collapse of three story buildings

(b) Shear failure of column



(c) Flexural failure due to buckling of reinforcements

(d) Collapse and damage of infill walls



(e) Roof tiles fell



(f) Ceilings fell

Photo 3.1. Typical damage to RC-frame + URM structures.

The RC-tie + URM type is commonly applied for single-story residences or stores. In this type of building, slender RC columns and beams are provided along the perimeters of masonry walls. Major observed damage was shear cracking of walls. Moreover, this type generally has a corrugated iron roof as shown in Photo 3.2(a), which is much lighter than a tile or concrete slab roof. Compared to Javanese residences with clay tile roofing, damaged by the Central Java earthquake, 2006 (AIJ report, 2007) as shown in Photo 3.2(b), light roofing seems to contribute to significantly reducing roof damage.



(a) Residence with corrugated iron roofing



(b) Residence with tile roofing damaged due to the central Java earthquake

Photo 3.2. Comparison of roofs used in Sumatra and Java Islands.

The URM type consists of brick walls without confinement and a wooden roof truss, which is supported by the walls as shown in Photo 3.3(a). This type lacks adequate strength and ductility to resist earthquakes because it often suffers from out-of-plane failure of walls and a resultant total collapse due to roof fall. It is used particularly for residences. Major damage to walls observed during the investigation included complete collapse, shear cracking, separation at corners, and cracking around openings, as shown in Photo 3.3.



(a) Wooden roof truss supported by brick walls



(b) Collapsed brick wall and cracks around the opening



(c) Shear crack on wall



(d) Separation at the corner of walls

Photo 3.3. Typical damage to URM structures.



Photo 3.4. Timber houses with rumbia roofs.

The TIM structure is a traditional residence, as shown in Photo 3.4. This type of structure usually has a traditional roof called a *rumbia roof*, which is made from rumbia tree leaves. Almost no damage was observed as shown in the photo. It seems to behave well because of its lightweight materials compared to other building types.

3.4 Field Investigation of Damaged RC Buildings

The second stage of the investigation focused on one of the collapsed buildings in Padang, which was located at the eastern side of Jl. Veteran Damar as shown in Figure 3.2(b). A neighboring building survived the earthquakes as shown in photo 3.5, nevertheless the structure type was the same as that of the collapsed building. Therefore, a further detailed investigation was conducted to compare damage grades and seismic performance. Structural details of both buildings were collected through on-site inspections and interviews with occupants as well as the owner.



Photo 3.5. Collapsed and surviving buildings just after the earthquakes.

3.4.1 Collapsed Building

The collapsed building was a three-story RC-frame + URM building constructed in 1980, which was used for a car showroom. It was constructed as a two-story building and then the third story was added. Based on photos taken just after the collapse, and information obtained from interviews, this building toppled toward the west, as shown in Photo 3.5.

This building had a regular plan as illustrated in Figure 3.3 and Photo 3.6. As shown, the cross-sectional dimensions of columns were 350 x 400 mm for the first story and many spandrel walls were used as exterior walls. Nonstructural brick walls were used for partition walls.

3.4.2 Surviving Building

The surviving building is a three-story RC-frame + URM building, as shown in Photo 3.7, which in common with the collapsed building also has a regular plan as illustrated in Figure 3.4. Details of the building, related to cross-sectional dimensions of structural components, arrangements of reinforcing bars, and damages to columns and walls, were collected to evaluate its damage grade and seismic performance.

The inspection results for the first story are indicated in Figure 3.4, and several examples of the classified columns are shown in Photo 3.8. The structural members and details of surviving building are shown in Figure 3.5 and listed in Table 3.1, respectively.

Damage to the columns was categorized into five classes according to Table 3.2, based on Nakano et al. (2004). Moreover, the damage grade of both building was evaluated based on damage class of columns and the residual capacity index, R , calculated by Equation 3.1 (Nakano, 2004).

$$R = \frac{\sum_{j=0}^5 \eta_j A_j}{A_{org}} \quad (3.1)$$

where, A_j is total number of columns having damage class 0 through V, A_{org} is total number of investigated columns, and η_j is seismic capacity reduction factor from Table 3.3.



Photo 3.6. Collapsed building.

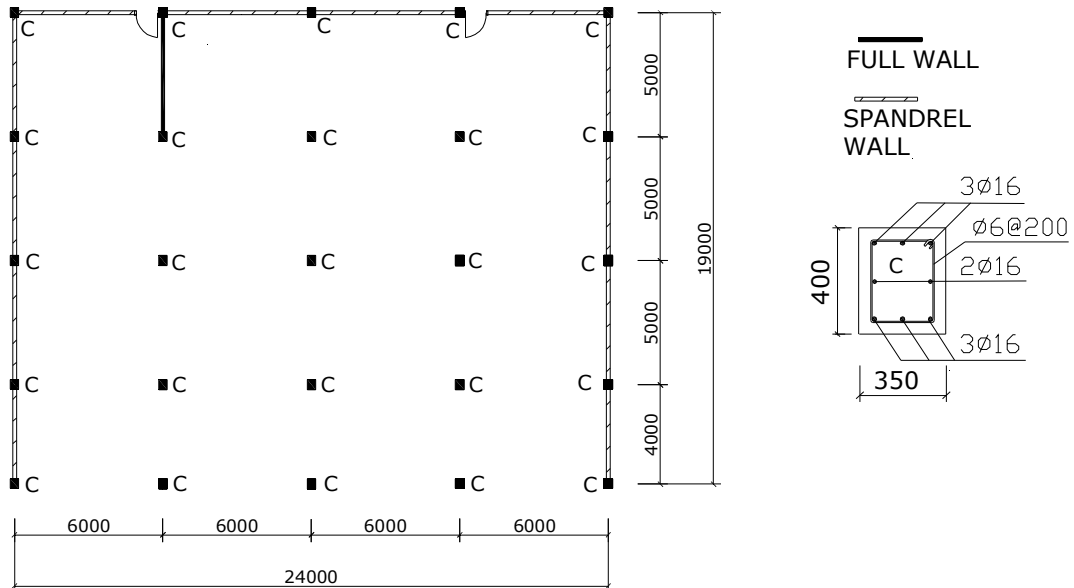


Figure 3.3. First floor plan of collapsed building.



Photo 3.7. Surviving building.

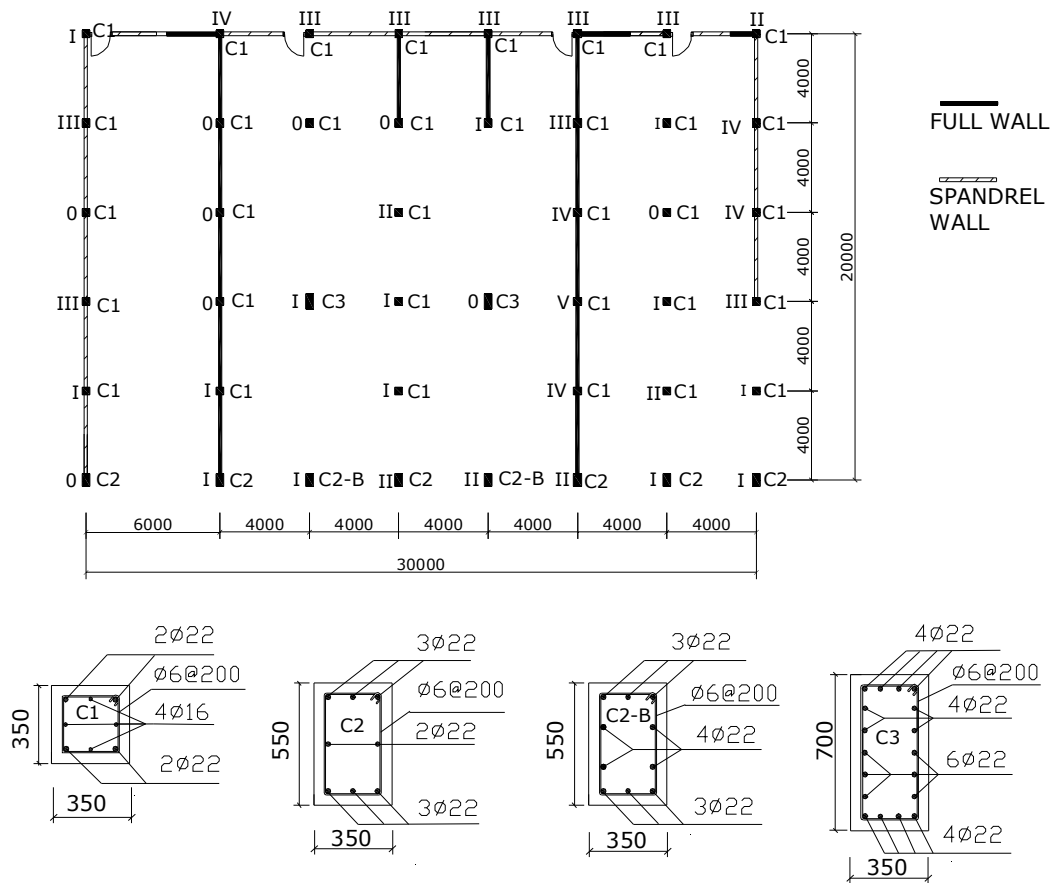


Figure 3.4. First floor plan of surviving building and damage class of each column.

C1	C1	C1	C1	C1	C1	C1	C1
C1	C1	C1	C1	C1	C1	C1	C1
C1	C1		C1		C1	C1	C1
C1	C1	C4	C1	C4	C1	C1	C1
C1	C1		C1		C1	C1	C1
C2	C2	C3	C2	C3	C2	C2	C2

(a) Columns

	G1	G1	G1	G1	G1	G1	G1
G1	G1	G1	G1	G1	G1	G1	G1
G1	G1	G2	G2	G2	G2	G1	G1
G1	G1	G1	G1	G1	G1	G1	G1
G1	G1	G2	G2	G2	G2	G1	G1
G1	G1	G1	G1	G1	G1	G1	G1

(b) Beams

Figure 3.5. Structural members of Surviving building

The damage grade of a building is defined according to the following classification based on R value.

Slight damage: $95 \% \leq R$

Light damage: $80 \% \leq R < 95 \%$

Moderate damage: $60 \% \leq R < 80 \%$

Heavy damage: $R < 60 \%$

Collapse: $R \approx 0$

As a result, the damage grade of the surviving building was classified as “moderate” for the first story.

Table 3.1. Member list of the surviving building.

Story	Column	C1	C2	C3	C4
1	BxD	350×350	350×550		350×700
	Main rebar	4- ϕ 22 4- ϕ 16	8- ϕ 22 10- ϕ 22	10- ϕ 22	18- ϕ 22
	Hoop	2- ϕ 6@200			
2	BxD	350×350	350×550		350×700
	Main rebar	4- ϕ 22 4- ϕ 16	4- ϕ 22 6- ϕ 16	4- ϕ 22	4- ϕ 22 14- ϕ 16
	Hoop	2- ϕ 6@200			
3	BxD	350×350	350×550		350×700
	Main rebar	8- ϕ 16			18- ϕ 16
	Hoop	2- ϕ 6@200			
Floor	Beam	G1	G2	G3	
2	BxD	350×550	250×420	350×720	
	Main rebar	4- ϕ 16 4- ϕ 12	10- ϕ 16 2- ϕ 12	10- ϕ 12	
	Stirrup	2- ϕ 6@100 (Middle: 2- ϕ 6@150)			
3	BxD	300×450	250×420	300×600	
	Main rebar	4- ϕ 16 4- ϕ 12	10- ϕ 16 2- ϕ 12	6- ϕ 22	
	Stirrup	2- ϕ 6@100 (Middle: 2- ϕ 6@150)			
R	BxD	300×450	250×420	300×550	
	Main rebar	4- ϕ 16 4- ϕ 12			4- ϕ 22 4- ϕ 12
	Stirrup	2- ϕ 6@100 (Middle: 2- ϕ 6@150)			

Table 3.2. Damage class definition of RC columns.

Damage Class	Description of Damage
I	- Visible narrow cracks on concrete surface (crack width of less than 0.2 mm)
II	- Visible clear cracks on concrete surface (crack width of about 0.2–1.0 mm)
III	- Local crushing of concrete cover - Remarkably wide cracks (crack width of about 1.0–2.0 mm)
IV	- Remarkable crushing of concrete with exposed reinforcing bars - Spalling off concrete cover (crack width of more than 2.0 mm)
V	- Buckling of reinforcing bars - Cracks in core concrete - Visible vertical and/or lateral deformation in columns and/or walls - Visible settlement and/or leaning of building

Table 3.3. Seismic capacity reduction factor η .

Damage class	Brittle column ($h_0/D \leq 3$)	Ductile column ($h_0/D > 3$)
I	0.95	0.95
II	0.60	0.75
III	0.30	0.50
IV	0	0.10
V	0	0

where, h_0 : column clear height, D : column depth.



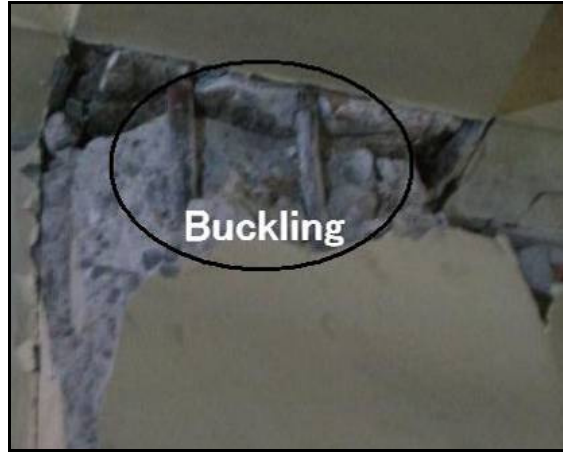
(a) Class III: crack widths of about
1.0-2.0 mm



(b) Class IV: crack widths of more than
2 mm



(c) Class IV: exposed reinforcing bars
without buckling



(d) Class V: buckling of longitudinal
reinforcements

Photo 3.8. Examples of Classified Columns.

3.5 Damage Grade Evaluation of Damaged Buildings

Table 3.4 shows several structural parameters for collapsed and surviving buildings with their damage grades. The column and wall ratios (=gross cross-sectional area of columns or walls/floor area) of both buildings are larger in the case of the surviving building, which is

consistent with its lighter damage grade. In these buildings, however, many spandrel walls were used as exterior walls. Because they must have affected structural behavior during the earthquakes, another investigation was conducted as described in other section.

Table 3.4. Structure parameters and damage grades.

Building	Column ratio (%)	Wall ratio (%)*		Damage grade
		NS	EW	
Collapsed	0.76	0.0	0.16	Collapsed
Surviving	1.06	0.0	1.19	Moderate

* Spandrel walls are not considered.

3.6 Seismic Performance Evaluation of Damaged Buildings

Seismic performance of collapsed and surviving buildings was evaluated on the basis of the current Japanese standard (JBDPA, 2005). There are three levels of seismic evaluation methods in the standard, namely the first, the second, and the third level screening procedures. In the first level screening procedures, the material strength and contribution of cross section area of vertical members are considered. In the second level method, ductility or deformation capacity and strength of vertical members are considered. The seismic capacity of the collapsed and surviving buildings was evaluated according to the second level screening procedure.

3.6.1 Basic Seismic Index E_0

The seismic performance of collapsed and surviving buildings is presented by the basic seismic index of structure, E_0 , of each story which is evaluated based on relation between the cumulative strength index, C , and the ductility index, F , as given in Equations 3.2 and 3.3.

The larger one of the basic seismic index of structure, E_0 , from Equations 3.2 and 3.3 is defined as seismic capacity of building. The Equation 3.2 is the ductility-dominant basic seismic index of structure and the Equation 3.3 is strength-dominant basic seismic index of the structure. Assuming the collapsed and surviving building as a strength dominant structure, the basic seismic index of both buildings were given by Equation 3.3.

$$E_0 = \frac{n+1}{n+i} \sqrt{E_1^2 + E_2^2 + E_3^2} \quad (3.2)$$

$$E_0 = \frac{n+1}{n+i} \left(C_1 + \sum_j \alpha_j C_j \right) F_1 \quad (3.3)$$

Where, $E_1 = C_1 F_1$, $E_2 = C_2 F_2$, $E_3 = C_3 F_3$, C_1 is the strength index C of the first group (with small F index), C_2 is the strength index C of the second group (with medium F index), C_3 is the strength index C of the third group (with large F index), F_1 is the ductility index F of the first group, F_2 is the ductility index F of the second group, F_3 is the ductility index F of the third group.

3.6.2 Strength Index C

The cumulative strength index, C , at a certain ductility index, F , was calculated by Equation 3.4.

$$C = C_i + \sum \alpha_j C_j \quad (3.4)$$

$$C_i = \frac{Q_u}{\sum W} \quad (3.5)$$

where, C_i is strength index of the i -th group of vertical members having the same ductility index, given by Equation 3.5, α_j is effective strength factor of the j -th group at the ultimate deformation R_j corresponding to the first group (ductility index of F_j) of i - and j -th groups, given in Table 3.5., C_j is strength index of the j -th group having the same ductility index larger than that of i -th group, Q_{ui} is ultimate lateral load-carrying capacity of the i -th group of columns which is evaluated as the smaller value between the shear force at flexural yielding, Q_{mu} , and the ultimate shear strength, Q_{su} , $\sum W$ is total weight of building supported by the story concerned.

The Q_{mu} and Q_{su} are calculated by Equations 3.6 and 3.8 respectively (JBDPA, 2005)

$$Q_{mu} = \frac{2M_u}{h_0} \quad (3.6)$$

$$M_u = 0.8 \cdot a_t \cdot \sigma_y \cdot D + 0.5 \cdot N \cdot D \left(1 - \frac{N}{b \cdot D \cdot F_c} \right) \quad (3.7)$$

$$Q_{su} = \left[\frac{0.053 \cdot p_t^{0.23} \cdot (18 + F_c)}{M/(Q \cdot d) + 0.12} + 0.85 \sqrt{p_w \cdot \sigma_{wy}} + 0.1 \cdot \sigma_o \right] \cdot b \cdot j \quad (3.8)$$

Where, M_u is flexural strength of column calculated by Equation 3.7, h_0 is clear height of column, a_t is total cross-sectional area of tensile reinforcing bars, σ_y is yield stress of longitudinal reinforcement, D is column depth, N is axial force on column due to weight of upper floor, b is column width, F_c is compressive strength of concrete, p_t is tensile reinforcement ratio calculated by $p_t = \frac{a_t}{b \cdot D}$, M/Q is shear span length in which the default value is $h_0/2$, d is effective depth of

column., p_w is shear reinforcement ratio calculated by $p_w = \frac{a_w}{b \cdot s}$, σ_{wy} is yield stress of shear reinforcement, σ_o is axial stress in column by $\sigma_o = \frac{N}{b \cdot D}$, j is distance between tension and compression forces, default value is $0.8D$. a_w is cross-sectional area of shear reinforcing bars, s is spacing of hoops. If the value of $M/(Q \cdot d)$ is less than unity or greater than 3, the value of $M/(Q \cdot d)$ to be unity or 3, respectively, and the value of σ_o is not more than 8 N/mm^2 .

Table 3.5. Effective strength factor.

Cumulative point of the first group $F_1 \geq 1.0$ (drift angle $R_1 \geq R_{250} = 1/250$)				
	F_1	$F_1 = 1.0$	$1 < F_1 < 1.27$	$1.27 \leq F_1$
	R_1	R_{250}	$R_{250} < R_1 < R_{150}$	$R_{150} \leq R_1$
Second and higher group	Shear ($R_{su} = R_{250}$)	1.0	0.0	0.0
	Shear ($R_1 < R_{su}$)	α_s	α_s	α_s
	Flexural ($R_{my} < R_1$)	1.0	1.0	1.0
	Flexural ($R_1 < R_{my}$)	α_m	α_m	1.0
	Flexural ($R_{my} < R_{150}$)	0.72	α_m	1.0

where,

α_s : Effective strength factor of a shear column, calculated by $\alpha_s = Q_{(F1)}/Q_{su} = \alpha_m Q_{mu}/Q_{su} \leq 1.0$.

α_m : Effective strength factor of a flexural column, calculated by $\alpha_m = Q_{(F1)}/Q_{mu} = 0.3 + 0.7R_1/R_{my}$

R_{my} : Drift angle at flexural yielding

R_{su} : Drift angle at shear strength

$Q_{(F1)}$: Shear force at deformation capacity R1 of a column in the second ad higher groups.

Q_{su} : Shear strength of a column in the second and higher groups

Q_{mu} : Shear force at flexural yielding of a column in the second and higher group.

3.6.3 Ductility Index F

The ductility index, F represents deformability of certain vertical members calculated according to structural specifications; member type, failure mode, strength, dimension, etc. (JBDPA, 2005). This index for columns, excepting extremely short ones, ranges between 1.0 and 3.2, which corresponds to a lateral drift ratio of 1/250 and 1/30, respectively. The ductility index of the shear column is calculated by Equation 3.9 based on the story angle at the ultimate deformation capacity in shear failure of the column, R_{su} , which is presented by Equation 3.10.

$$F = 1.0 + 0.27 \frac{R_{su} - R_{250}}{R_y - R_{250}} \quad (3.9)$$

$$R_{su} = \frac{Q_{su} / Q_{mu} - 0.3}{0.7} \cdot R_{my} \geq R_{250} \quad \text{for } \alpha_c \cdot Q_{mu} < Q_{su} \quad (3.10)$$

$$R_{su} = R_{250} \quad \text{for } \alpha_c \cdot Q_{mu} \geq Q_{su}$$

$$R_{my} = \left(h_o / H_o \right) \cdot R_{my} \geq 1/250 \quad (3.11)$$

where, R_{my} is the inter-story drift angle at the flexural yielding of column evaluated by Equation 3.11. α_c is effective strength factor of the column which is calculated by $\alpha_c = 0.3 + 0.7 \left(R_{250} / R_{my} \right)$, and R_{250} is standard inter-story drift angle that is 1/250.

The ductility index of flexural column is given in Equation 3.12 based on the inter-story drift angle at the ultimate deformation capacity in the flexural failure of the column, R_{mu} .

In the case of $R_{mu} < R_y$.

$$F = 1.0 + 0.27 \frac{R_{mu} - R_{250}}{R_y - R_{250}} \quad (3.12a)$$

In the case of $R_{mu} \geq R_y$.

$$F = \frac{\sqrt{2R_{mu} / R_y - 1}}{0.75 (1 + 0.05 R_{mu} / R_y)} \leq 3.2 \quad (3.12b)$$

where, R_y is yield deformation in terms of inter-story drift angle, which in principle shall be taken as 1/150

The ultimate deformation in the flexural failure of the column, R_{mu} was evaluated based on the inter-story drift angle at ultimate flexural strength and yield deformation occurred on column. The inter-story drift angle at ultimate flexural strength of column, R_{mu} is given in Equation 3.13.

$$R_{mu} = (h_o / H_o) \cdot {}_c R_{mu} \geq R_{250} \quad (3.13)$$

$${}_c R_{mu} = {}_c R_{my} + {}_c R_p \leq {}_c R_{30} \quad (3.14)$$

$${}_c R_{mp} = 10(Q_{su} / Q_{mu} - q) \cdot {}_c R_{my} \geq 0 \quad (3.15)$$

where, H_o is standard clear height of column from bottom of the upper floor beam to top of the lower floor slab, ${}_c R_{mu}$ is drift angle at ultimate the ultimate flexural strength of column is given in Equation 3.14, ${}_c R_{my}$ is yield drift angle of column measured in the clear height of the column that is 1/150 for $h_o/D \geq 3.0$ and 1/250 for $h_o/D \leq 2.0$, and it set by interpolation for $2 < h_o/D < 3.0$,

${}_cR_p$ is plastic drift angle of the column is calculated by Equation 3.15, and ${}_cR_{30}$ is standard drift angle of the column of 1/30. $q = 1.0$ for s (=spacing of hoop) ≤ 100 mm, and $q = 1.1$ for $s > 100$ mm.

The value of ${}_cR_{mu}$ must be less or equal to the upper limit of the drift angle of the flexural column, ${}_cR_{max}$. The value of ${}_cR_{max} = \min\{{}_cR_{max (n)}, {}_cR_{max (s)}, {}_cR_{max (t)}, {}_cR_{max (b)}, {}_cR_{max (h)}\}$ which is defined as below.

1. ${}_cR_{max (n)}$: the upper limit of the drift angle of the flexural column determined by the axial force.

$${}_cR_{max (n)} = 1/250 \text{ for } \eta > \eta_H.$$

$${}_cR_{max (n)} = 1/30 \left(\frac{1/250}{1/30} \right)^{n'} \leq 1/30 \text{ for other case.}$$

$$\text{where, } n' = (\eta - \eta_L)(\eta_H - \eta_L),$$

$$\eta = N_s / (b.D.F_c) .$$

$$\eta_L = 0.25 \text{ and } \eta_H = 0.5 \text{ for } s \leq 100 \text{ mm.}$$

$$\eta_L = 0.2 \text{ and } \eta_H = 0.4 \text{ for } s > 100 \text{ mm.}$$

2. ${}_cR_{max (s)}$: the upper limit of the drift angle of the flexural column determined by the shear force.

$${}_cR_{max (s)} = 1/250 \text{ for } {}_c\tau_u / F_c > 0.2.$$

$${}_cR_{max (s)} = 1/30 \text{ for others case.}$$

3. ${}_cR_{max (t)}$: the upper limit of the drift angle of the flexural column determined by the tensile reinforcement ratio.

$${}_cR_{max (t)} = 1/250 \text{ for } p_t > 1.0\%.$$

$${}_cR_{max (t)} = 1/30 \text{ for other case.}$$

4. ${}_cR_{max (b)}$: the upper limit of the drift angle of the flexural column determined by the spacing of hoops.

$${}^cR_{max (b)} = 1/50 \quad \text{for } s/d_b > 8.$$

$${}^cR_{max (b)} = 1/30 \quad \text{for other cases.}$$

5. ${}^cR_{max (h)}$: the upper limit of the drift angle of the flexural column determined by the clear height.

$${}^cR_{max (h)} = 1/250 \quad \text{for } h_c/D \leq 2.$$

$${}^cR_{max (h)} = 1/30 \quad \text{for other case.}$$

where, N_s is additional axial force of column due to earthquakes, ${}^c\tau_u$ is shear stress at the column strength that is the $\min \{ Q_{mu} / (b \cdot j), Q_{su} / (b \cdot j) \}$, s is spacing of hoops, d_b is diameter of the flexural reinforcing bar of the column.

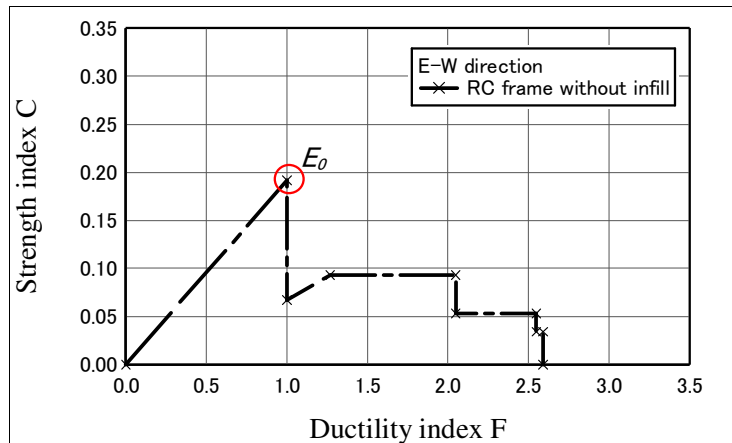
3.6.4 Seismic Performance of Damaged Buildings

Seismic performance of collapsed and surviving buildings was evaluated for the first story, where the most severe damage was observed to both buildings. However, the infill walls were neglected as an analytical parameter, the spandrel walls were considered to evaluate the clear heights of columns.

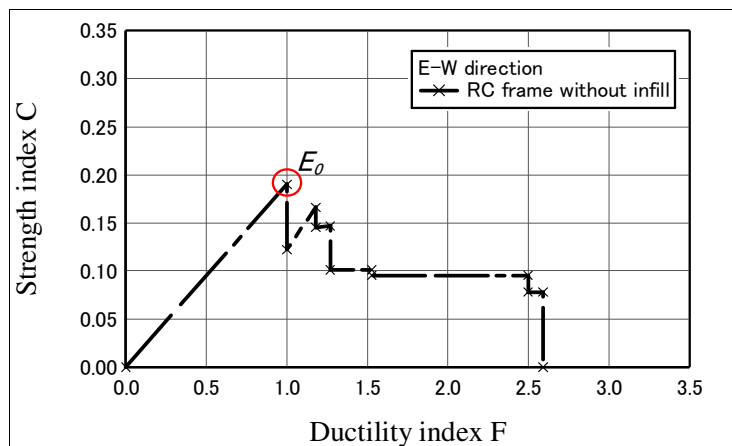
Material properties of building were obtained from material test of concrete and steel bars, which the material pieces of concrete were collected from the existing building by using concrete core drilling machine. Due to the properties of hoop reinforcing bars was not available, the yield strength of hoop was assumed equal to those of the bars commonly used in Indonesia. In the case of collapsed building, its properties was assumed equal to the survived building that were 27.6 N/mm^2 , 306.9 N/mm^2 and 240.0 N/mm^2 for compressive strength of concrete, yielding strength of longitudinal and shear reinforcements, respectively.

Calculated seismic performance of both buildings based on the larger basic seismic, E_0 , obtained by Equation 3.3 is compared in the E-W direction to which one of the collapsed building toppled, as shown in Figure 3.6. However, the similar strength was obtained for

seismic performance of both buildings, nevertheless one of them totally collapsed and other survived during the earthquake. It seemed that the brick infill which was much larger in surviving building significantly contributed to resist seismic load of such building.



(a) Collapsed building



(b) Surviving building

Figure 3.6 Seismic performances of damaged buildings without infill effects.

3.7 Torsion Effect Evaluation of Damaged Buildings

The torsion effect of collapsed and surviving building was evaluated by determining the

eccentricities in mass and stiffness distribution which can cause a torsion response coupled with translation response. Horizontal twisting occurs in buildings when the center of mass, CM does not coincide with the center of rigidity, CR . The large eccentricity, e , the distance between the centers of mass and rigidity, can cause the torsion moment that must be resisted by buildings under the seismic force.

The center of mass on floor was evaluated corresponding to the center of the gravity load of the structure elements. The center of mass of collapsed and surviving building was determined by indentifying the gravity and its coordinate of structural member with respect to the x and y axes of floor, which was assumed at the center of slab. The brief structural members of surviving buildings are shown in Figure 3.5 and their details are given in Table 3.1. However, the structural details of the collapsed building excluding the first story column could not be collected before the building was demolished. Therefore, column details in the second and third stories were assumed to be identical to those in the first story, and beam details were referred to a typical beam in the other building (G1 in Table 3.1).

The center of rigidity, CR , was evaluated based on lateral load, which was based on the base shear of seismic static equivalent, acting on each vertical member. The base shear of collapsed and surviving buildings was evaluated according Indonesian standard (SNI 03-1726-2003). The brick walls were considered for evaluating the rigidity of both buildings. However, the spandrel walls were considered for clear height of columns.

Consequently, the center of mass, CM , and the center of rigidity, CR , for both buildings are located as shown in Figure 3.7. The figures show that the stiffness eccentricities, e_{rx} and e_{ry} , are 1,191 mm and 1,670 mm for collapse building, and 1,901 mm and 3,247 mm for surviving building, respectively. These eccentricities should neither exceed 0.3 times the maximum plan dimension of the structure at that level. As the results, the eccentricities of collapsed building, $e_{rx}=1191<7200$, and surviving building, $e_{rx}=1901<9000$, are under limitation of requirements.

Japanese standard recommended providing the modulus of eccentricity, R_e , of each level have to satisfy the condition (Paulay, 1996 and AIJ, 1994).

$$R_{ex} = \frac{e_{rx}}{r_{kx}} \leq 0.15 \quad (3.16)$$

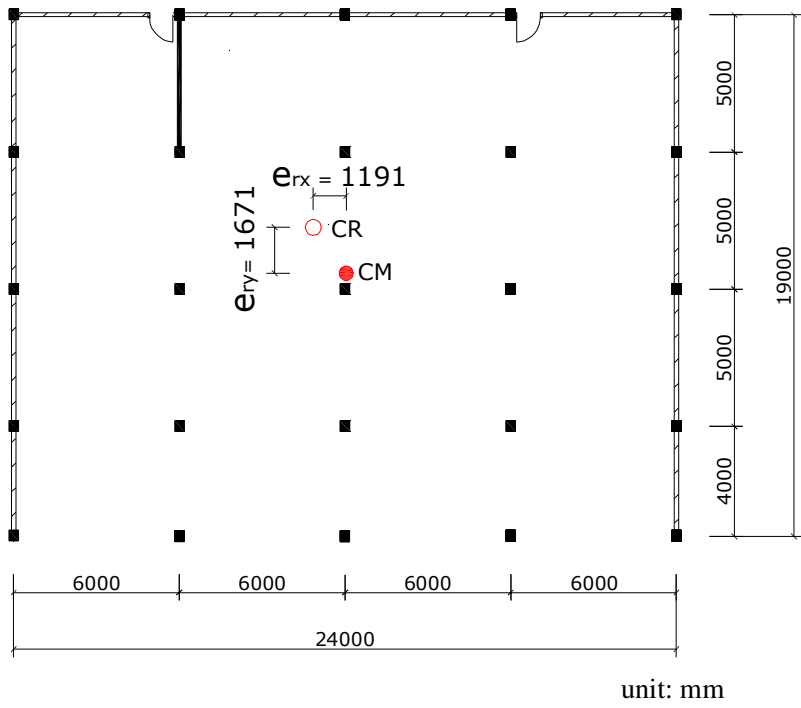
$$R_{ey} = \frac{e_{ry}}{r_{ky}} \leq 0.15$$

$$r_{kx} = \sqrt{\frac{K_t}{\sum k_{yi}}} \quad \text{and} \quad r_{ky} = \sqrt{\frac{K_t}{\sum k_{xi}}} \quad (3.17)$$

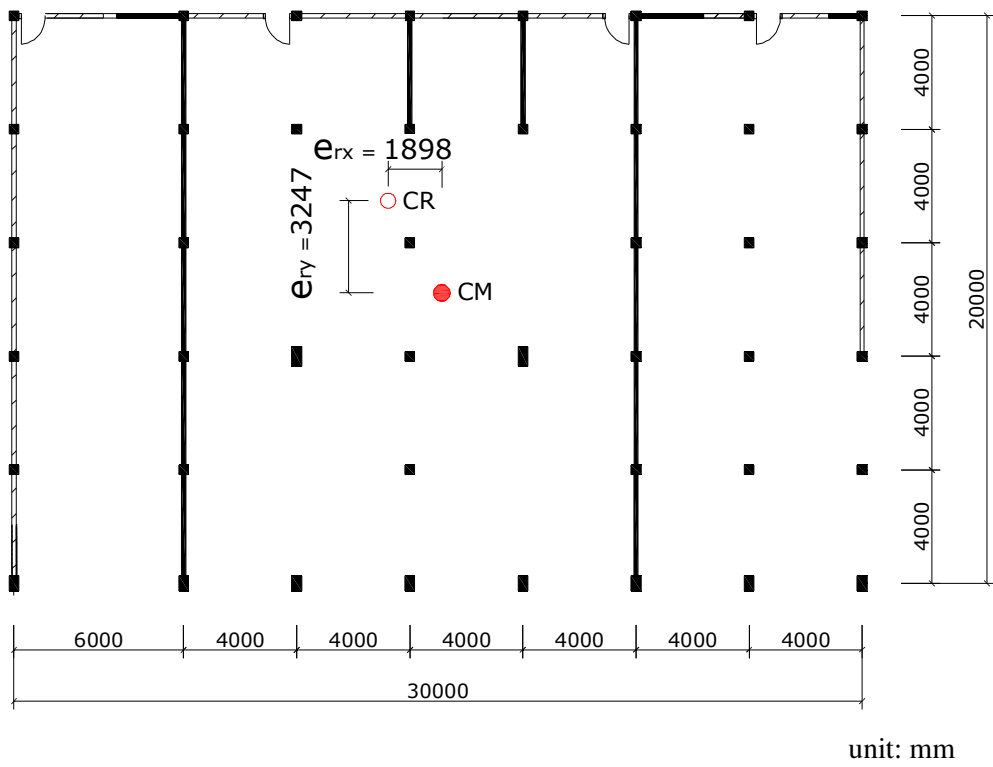
$$K_t = \sum x_i^2 k_{yi} + \sum y_i^2 k_{xi} \quad (3.18)$$

Where, r_{kx} and r_{ky} are elastic radius of stiffness to the x and y axes, respectively. k_{yi} and k_{xi} are translation stiffness of vertical elements with respect to the x and y axes, respectively. K_t is rotational stiffness, x_i and y_i are the distance of i^{th} element to y and x axes, respectively. According to eccentricities of both building, the R_{ex} and R_{ey} of collapsed building are 0.06 and 0.08, respectively. The R_{ex} and R_{ey} of surviving building are 0.10 and 0.11, respectively.

According to required limitation of $e_{rx} < 0.3 B$, $R_{ex} \leq 0.15$ and $R_{ey} \leq 0.15$, the design requirement related to torsion on building were satisfied. Although the eccentricities and modulus of rigidity of collapsed building were much lower than that of surviving building, it was toppled under the earthquake action. It indicates that the building was not collapsed due to the torsion effect.



a) Collapsed building



b) Surviving building

Figure 3.7 Centers of mass and rigidity of damaged buildings.

3.8 Summary

Post-earthquake investigation of building structures damaged due to the September 2007 Sumatra 8.4 and 7.9 M_L earthquakes were carried out in Padang and nearby areas. This section reports the investigation results, and damage grades of investigated buildings. Major findings are summarized as follows.

1. Two RC frame structures with URM infill walls totally collapsed and many of the same type of building suffered severe damage: shear and flexural failure of columns, collapse and/or damage of infill walls, and falling roof tiles and ceilings.
2. Confined and simple masonry structures also suffered damage. Among these types, however, light roofing seems to have contributed to reducing roof damage.
3. On the contrary, almost no damage was observed in traditional timber structures.
4. One of the collapsed RC frame buildings in Padang was selected for a further detailed investigation. Damage grades and seismic performance of the collapsed building and its neighboring building were briefly evaluated.
5. The seismic performance of collapsed and surviving buildings was evaluated for the first story only in East-West direction, where the most severe damage was observed, on the basis of the current Japanese standard by neglecting the infill effect. Consequently, the similar strength was observed for both damaged buildings.
6. According to the eccentricities e_x and e_y of collapsed and surviving buildings, the both buildings seemed not to be damaged by torsion effect.
7. According to comparison of seismic performance of both buildings, it was briefly concluded that the brick infill, which existed more in the surviving building, significantly contributes to the resistance to seismic loads and prevents the building from collapsing.

Chapter 4

Experimental Evaluation on Contribution of Brick Masonry Infill to Seismic Performance of RC Frames

4.1 Introduction

According to seismic performance of two earthquake-damaged RC buildings, one totally collapsed and other moderate damaged, which was evaluated without considering the brick infill effects based on the current Japanese standard (JBDPA, 2005), both of the buildings had similar seismic capacities. Therefore, it was briefly concluded that the nonstructural brick walls, which existed significantly more in the surviving building, contributed to resist the seismic loads and had a role to protect the surviving building from collapsing during the earthquakes. To evaluate the contribution of brick masonry infill, which is not considered in seismic design, to the actual performance of damaged buildings, a series of structural tests on one-bay RC bare frames and several infilled frames with different thickness and configuration of brick infill representing the moderate damage building was conducted.

The bare frame and infilled frame specimens were tested under quasi-static cyclic and constant vertical loadings. The comparison of failure mechanism and performance curves of bare frame and infilled frames are discussed.

4.2 Test Models of RC Frames with/without Brick Infill

4.2.1 BF Specimen

Four 1/2.5 scale RC one-bay frame specimens with rigid beams were prepared: one bare frame (BF) and three infilled frames with brick masonry (IF_FB, IF_SBw/oFM and IF_SB as described below. Table 4.1 summarizes the combination of test parameters. Figure 4.1 shows the configuration and bar arrangements of the BF specimen.

Table 4.1. Parameters for specimens

Specimens	Column	Experimental parameters	
		Brick wall	Plaster
BF	cross-section: 140x140 main bar: 4-Ø9 hoop: 2- Ø4@100	none	none
IF_FB		thickness: 100 mm	20 mm (each side)
IF_SBw/oFM		thickness: 44 mm	none
IF_SB		thickness: 44 mm.	8 mm (each side)

4.2.2 IF_FB Specimen

IF_FB specimen had a full-scale brick infill, which was extracted from the referential building, as shown in Photo 4.1(a). It was transported to Toyohashi University of Technology, Japan, as shown in Photo 4.1(b).



(a) Extracting wall.



(b) Transporting wall.

Photo 4.1. Preparation of brick wall specimen.



(a) Cutting off wall



(b) Installing wall.

Photo 4.2. Installation of brick wall.

The imported brick wall was installed in one of the RC frame specimens, as shown in Photo 4.2(b), after it was cut to dimensions of 1,420 mm in width x 960 mm in height, as shown in Photo 4.2(a). In this specimen, however, the wall thickness of 140 mm was not reduced because of technical difficulties related to scale reduction. Mortar was produced with a volume ratio of cement : sand : water = 1 : 4 : 1.3, and was applied between the main frame and inserted wall as a joint material. The thickness of the mortar joint was 20 mm, as shown in Figure 4.2. Initial slight damage was observed in the infilled wall, as shown in Photo 4.3. Material

properties including mortar are shown in Table 4.2



Photo 4.3. Initial damage to infilled wall.

(note: dashed lines on the wall surface represent initial damage).

4.2.3 IF_SBw/oFM and IF_SB Specimens

IF_SBw/oFM and IF_SB specimens had a scaled brick infill consisting of 1/2.5 scale bricks having dimensions of 88 mm in length, 44 mm in width and 20 mm in height. Although the compressive strength of the scaled bricks made in Japan was arranged to be similar to that of Indonesian bricks, the masonry prisms with mortar beds exhibited higher strengths for IF_SBw/oFM and IF_SB specimens from material tests, as shown in Table 4.2. Bricks were laid up in the interior clear height of frames with mortar beds at a volume ratio of cement: sand: water = 1: 4: 1.4. Finishing mortar with a thickness of 8 mm was applied only to the wall surfaces of IF_SB specimen, which resulted in an infill thickness of 44 mm and 60 mm for IF_SBw/oFM and IF_SB, respectively. Figure 4.3 is a detailed drawing of the IF_SB specimen.

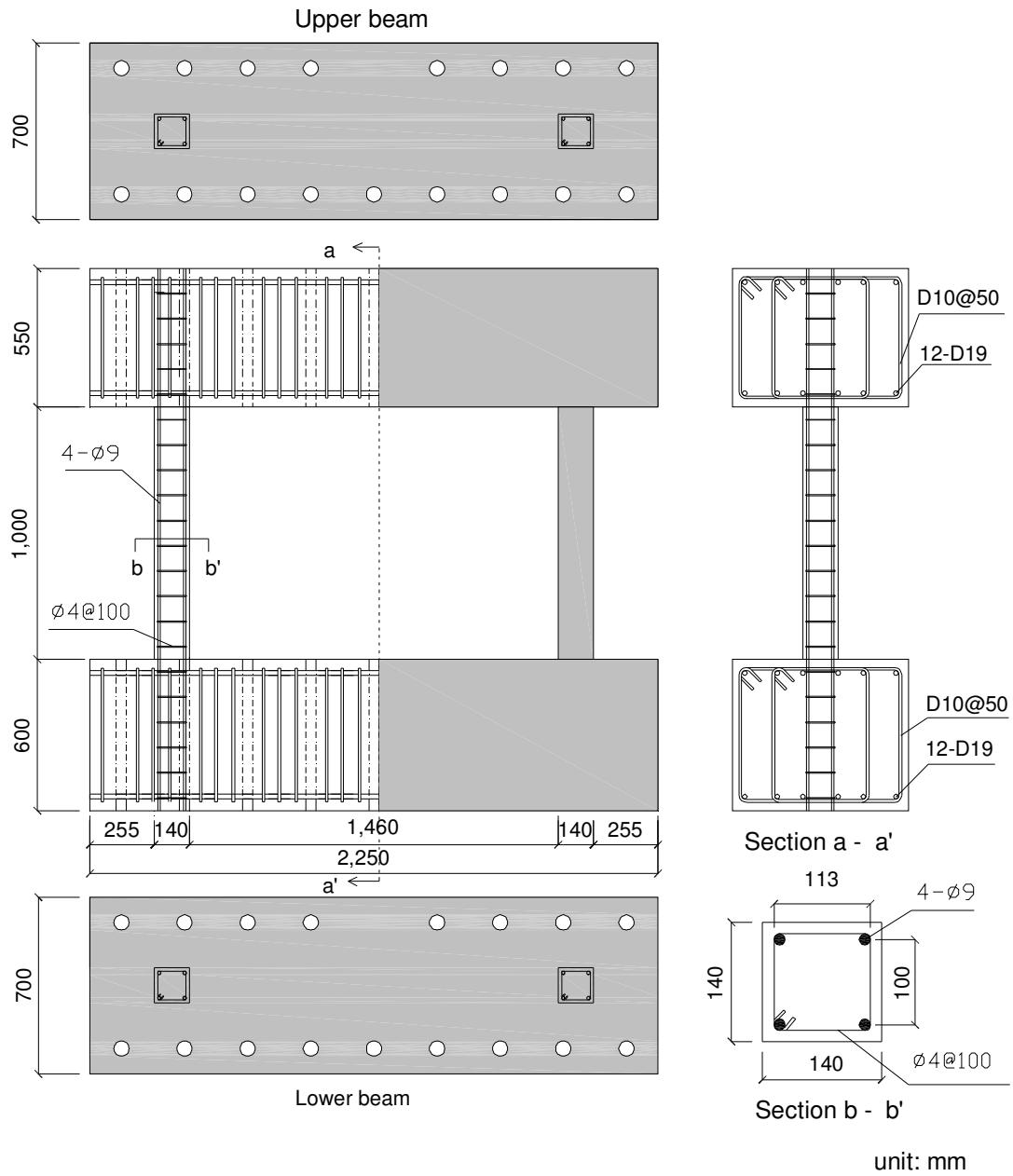


Figure 4.1. Detailed drawing of BF specimen.

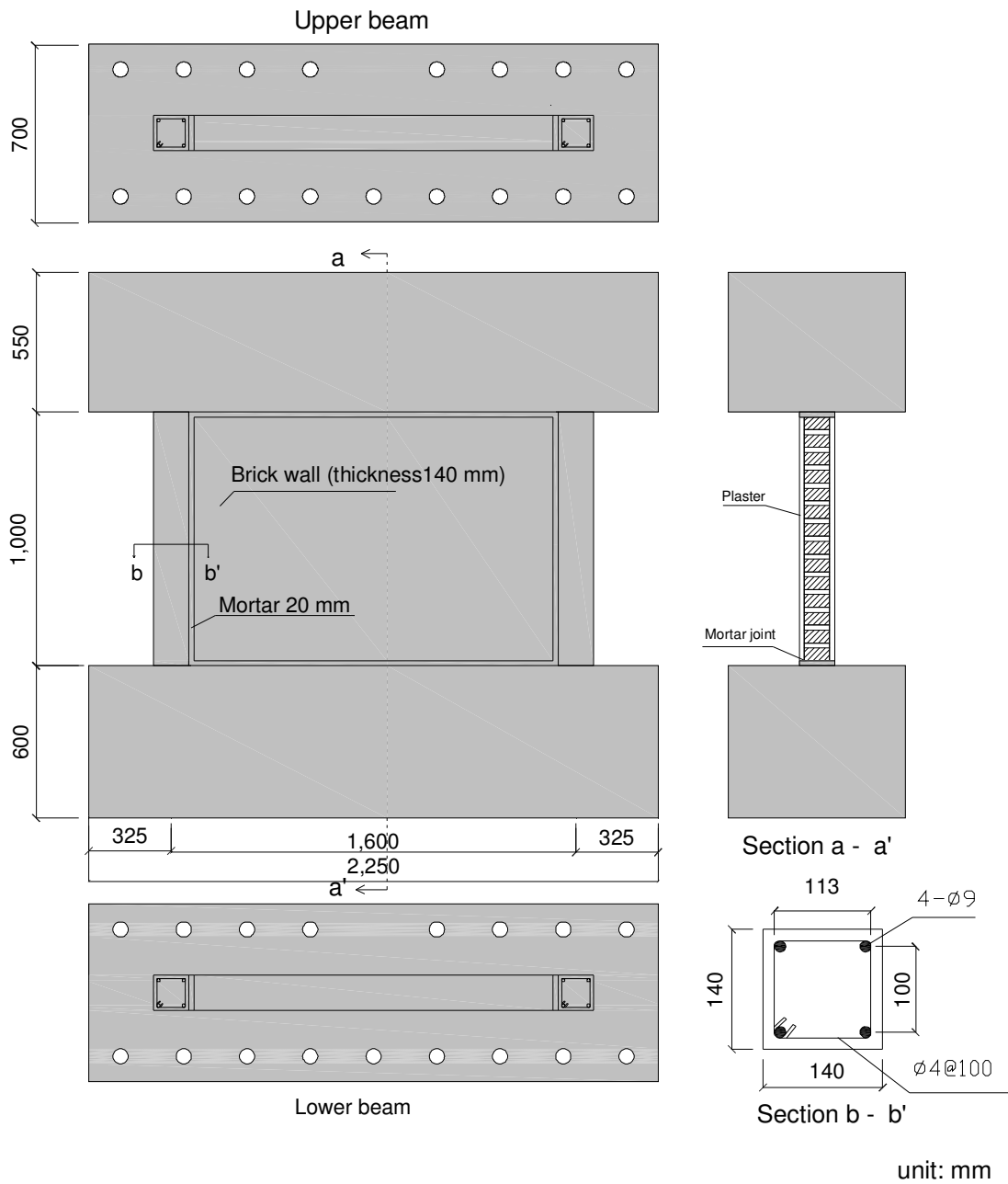


Figure. 4.2. Detailed drawing of IF_FB specimen.

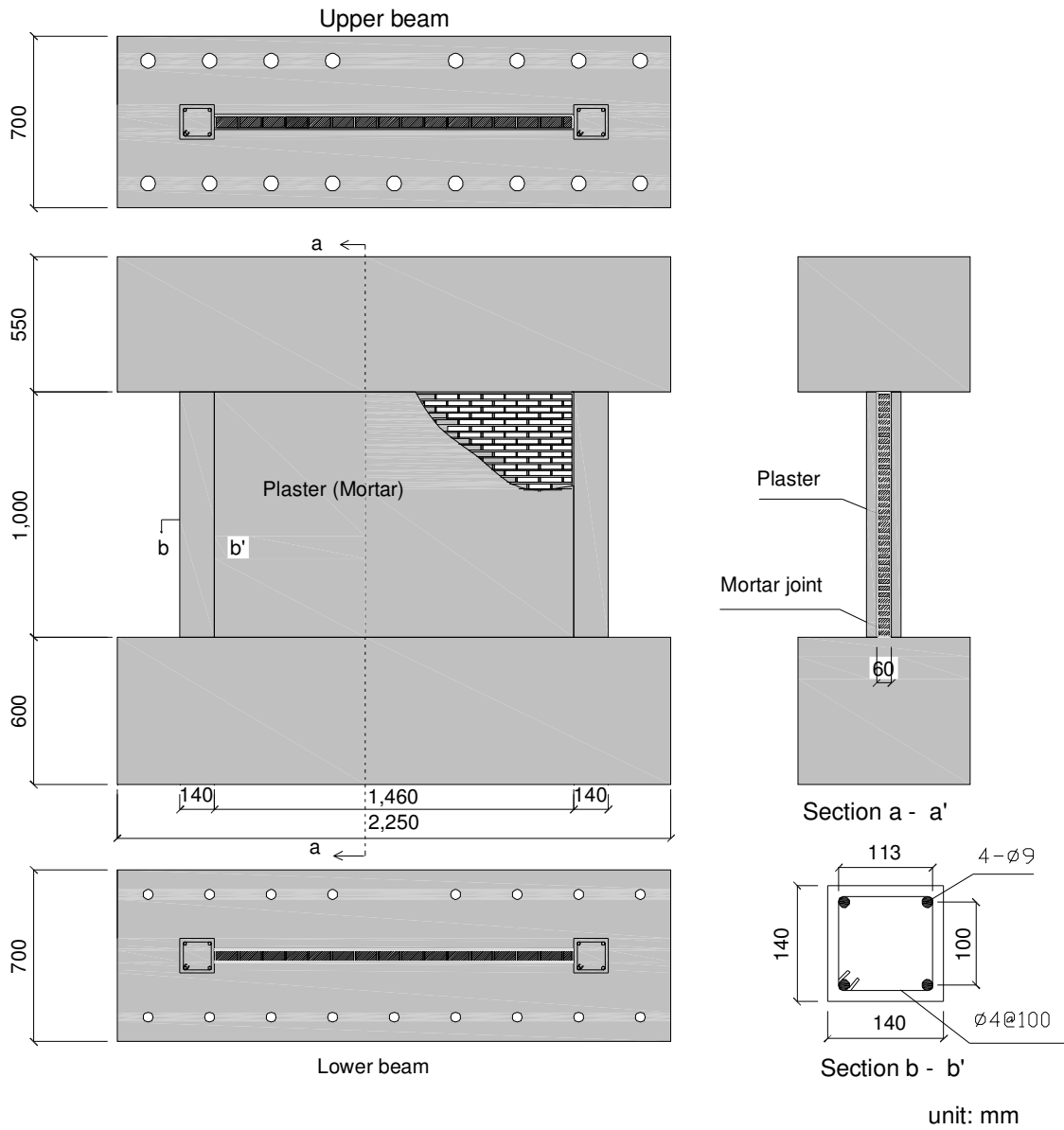


Figure 4.3. Detailed drawing of IF_SB specimen.

Table 4.2. Material properties of specimens

Concrete				
Specimen	Material age	Compressive strength	Tensile strength	Young modulus
	Day	N/mm ²	N/mm ²	N/mm ²
BF	44	19.6	1.89	17862.7
IF_FB	37	20.6	1.96	18968.3
IF_SBw/oFM	63	26.6	1.90	22447.2
IF_SB	67	27.3	1.98	23931.2
Masonry prism				
Specimen	Material age	Compressive strength	Tensile strength	Young modulus
	Day	N/mm ²	N/mm ²	N/mm ²
IF_FB	Unknown	2.91	0.55	789.0
IF_SBw/oFM	42	16.3	2.28	4374.0
IF_SB	46	18.5	2.28	8650.3
Mortar				
Specimen	Material age	Compressive strength	Tensile strength	
	Day	N/mm ²	N/mm ²	
IF_FB (only for boundaries)	42	40.8	3.33	
IF_SBw/oFM	42	44.7	2.33	
IF_SB	46 for infill 44 for finishing	48.6 for infill 42.9 for finishing	3.26 for infill 2.89 for finishing	
Reinforcing bar				
Bar number	Yield strength	Tensile strength	Young modulus	
	N/mm ²	N/mm ²	N/mm ²	
9 (BF, IF_FB)	355	440	2.02×10 ⁵	
4 (BF, IF_FB)	507	631	2.14×10 ⁵	
9 (IF_SBw/oFM, IF_SB)	338	382	2.0 x 10 ⁵	
4 (IF_SBw/oFM, IF_SB)	497	778	2.12×10 ⁵	

4.3 Material Properties

Material properties of test specimens were obtained from material tests on each group of material pieces of concrete cylinders, masonry prism, mortar cylinders and steel bars. The test cylinders of concrete were prepared at the same time of concrete casting of test structures. The masonry prism and mortar cinders were constructed at the same time of constructing the brick infill wall. All material pieces were kept in the same environmental condition as the test structures.

Three uniaxial compression tests were performed for each group of concrete and mortar cylinders and masonry prism and three split tension tests were conducted for concrete and mortar cylinders on the day after the static cyclic loading experiment. The tension tests on steel bars were performed for reinforcement's properties before the constructing of test structures. Table 4.2 shows the material test results, where the values represent the mean value of 3 samples in each test. The tensile strength of infill was represented by tensile strength of brick unit as the weakest component of infill.

4.4 Experimental Methods

4.4.1 Loading Method

The specimens were tested at the testing facility of the Toyohashi University of Technology. A schematic representation of the experimental set-up is shown in Figure 4.4. One horizontal hydraulic jack (2000 kN) and two vertical ones were equipped for the loading system.

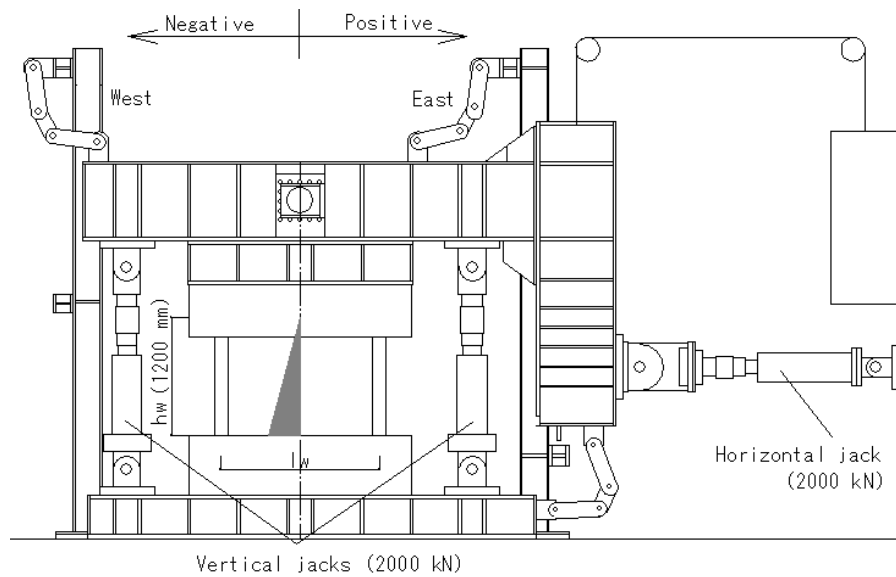


Figure 4.4 Schematic view of test set-up.

The specimens were subjected to a constant vertical load of 183.4 kN ($\approx 0.24 \times$ column sectional area \times compressive strength of concrete) based on the calculated weight of the surviving building. Then, reversed cyclic lateral loads were applied to the specimens by the use of hydraulic jacks. Drift angle R (rad.), ratio of lateral displacement to column height, was used to control incremental loading. Lateral loading program was initial cycle to $R = 1/800$ followed by two cycles to $R = 1/400, 1/200, 1/100, 1/50, 1/25,$ and $1/12.5$ for BF and IF_FB specimens and an initial cycle to $R=1/400$ followed by two cycles to $R=1/200, 1/100, 1/50, 1/25$ and $1/12.5$ for IF_SBw/oFM and IF_SB specimens, respectively. The cracks in column and wall were observed and marked at the maximum and zero position of loading. When the specimens failed, however, loading was stopped. Figure 4.5 shows the lateral loading history. The shear span to depth ratio ($= h_w/l_w$ in Figure 4.4) of the specimens was maintained at 0.75 throughout the tests so that lateral loads were applied at an assumed second floor height of 1200 mm.

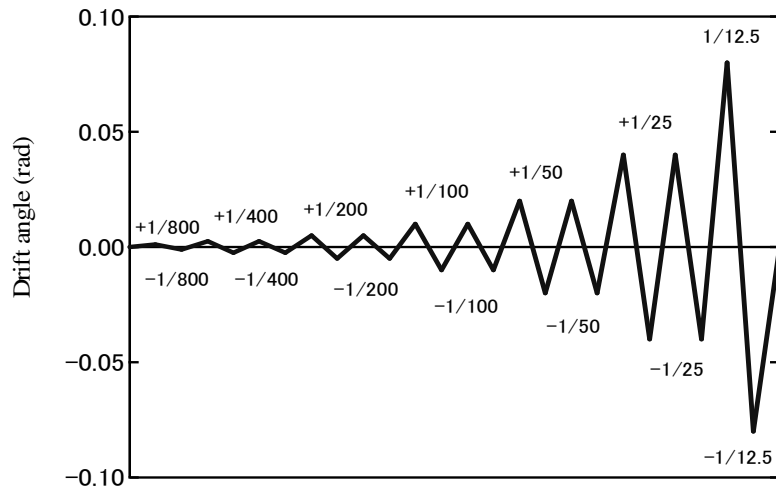


Figure 4.5. Lateral loading history.

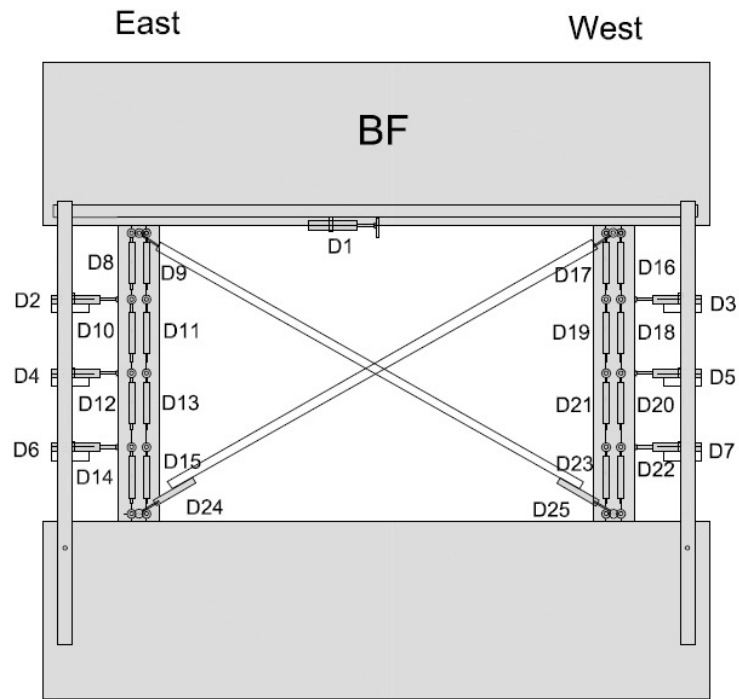
4.4.2 Measurement

The horizontal, vertical, and diagonal relative displacements of the specimens were measured with transducers (D1-D25), as shown in Figure 4.6(a). Strains of reinforcements were measured using strain gauges pasted on rebars as shown in Figure 4.6(b).

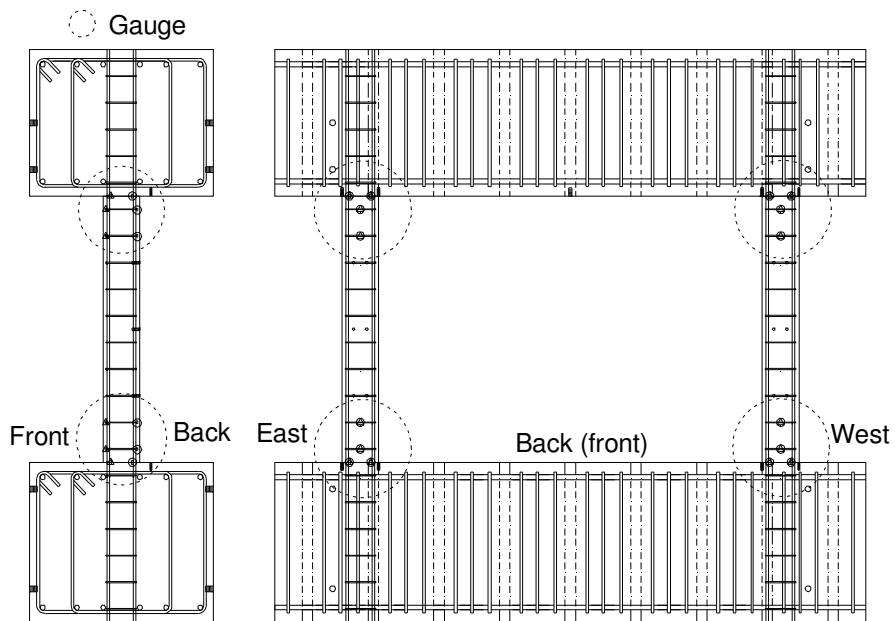
4.5 Experimental Results

4.5.1 Failure Process and Mechanism

During the testing, initiated cracks, crack propagation, and major crack widths were observed at every peak and residual drift to identify the failure mechanism of specimens which were generally similar for the infilled frame specimens. Table 4.3 and Figure 4.7 compare the failure process and the final crack patterns among the specimens, respectively.



(a) Transducers set-up



(b) Arrangement of strain gauges.

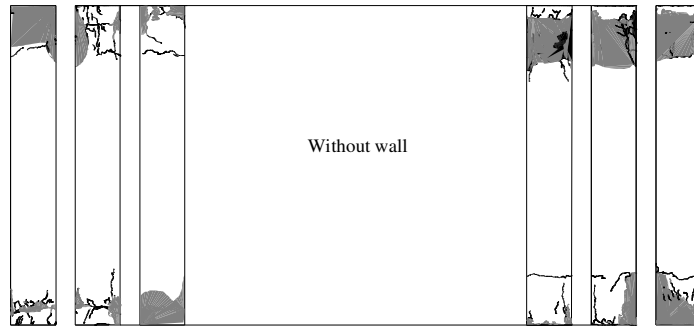
Figure. 4.6. Measurement.

Table 4.3(a). Failure Processes of BF and IF_FB

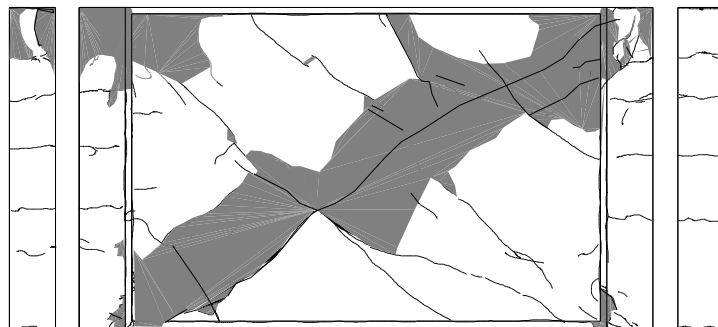
Cycle	BF specimen	IF_FB specimen	
(rad.)	Columns	Columns	Brick wall
Initial crack	None.	None.	As shown in Photo 4.3.
1/800	Initial flexural crack at the top of the compressive column.	Initial flexural crack at the top of the tensile column.	Separation cracks around the wall. Initial shear crack.
1/400	Flexural cracks at the top and bottom of both columns.	Flexural cracks at the top and middle of the tensile column.	Shear crack development.
1/200	Crack propagation in both columns.	Shear cracks at the top of the tensile column. Flexural cracks at the bottom of the compressive column.	Shear crack propagation.
1/100	Initial crushing of concrete at the bottom of the compressive column.	Shear cracks at the bottom of the compressive column. Initial yielding of longitudinal rebar.	Peeling off of plaster.
1/50	Concrete crush at the top and bottom of the compressive column. Initial yielding of longitudinal rebar.	Shear failure at the top of the tensile column. Buckling of longitudinal rebars. Spalling of cover concrete at the bottom of the compressive column. Initial yielding of hoop. Degradation of lateral strength.	Spalling of plaster.
1/25	Spalling of cover concrete. Degradation of lateral strength.	Loss of axial resistance.	Remarkable damage.
1/12.5	Buckling of longitudinal rebars in the tensile column. Loss of axial resistance.		

Table 4.3(b). Failure Processes of IF_SCw/oFM and IF_SB

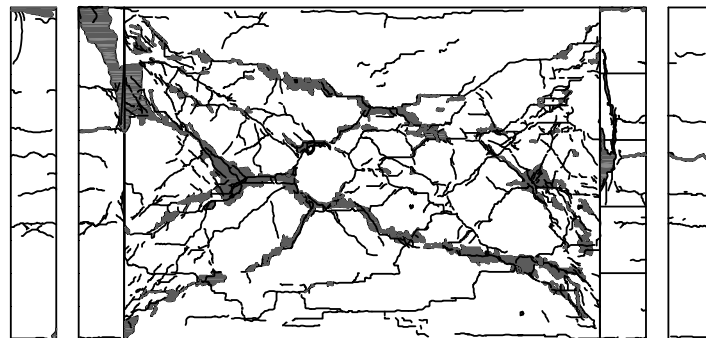
Cycle (rad.)	BF_SBw/oFM specimen		IF_SB specimen	
	Columns	Brick wall	Columns	Brick wall
Initial crack	None.	Separation cracks wall-stubs	None.	Separation cracks at the wall-stub boundaries.
1/400	Separation cracks between the wall and tensile column. Initial shear crack at the middle of tensile column. Initial flexural crack at the bottom of both columns.	Initial shear crack at the center of wall.	Initial flexural crack at the middle of tensile column. Initial shear crack at the top of tensile column.	
1/200	A flexural crack at the middle of tensile column. Yielding of longitudinal bar.	Development of shear cracks.	Initial yielding of main bar.	
1/100	Development of flexural cracks.	Initial compressive failure	Development of shear cracks. Spalling of concrete cover.	Peeling of plaster. Compressive failure of plaster.
1/50	Initial compressive failure of concrete in tensile column.	Crushing of mortar.	Compressive cracks at the bottom and top of compressive column.	Initial compressive failure.
1/25	Compressive failure at the middle and top of compressive column. Initial yielding of hoop. Buckling of main bar. Loss of axial resistance.	Large shear cracks in both diagonal directions.	Shear failure of column. Initial yielding of hoop.	A large vertical crack on panel. Loss of axial resistance



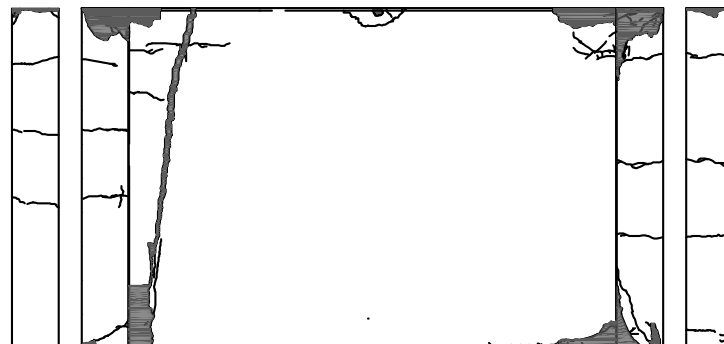
(a) BF Specimen ($R = 1/12.5$ rad.)



(b) IF_FB Specimen ($R = 1/25$ rad.)



(c) BF_SBw/oFM Specimen ($R = 1/25$ rad.)

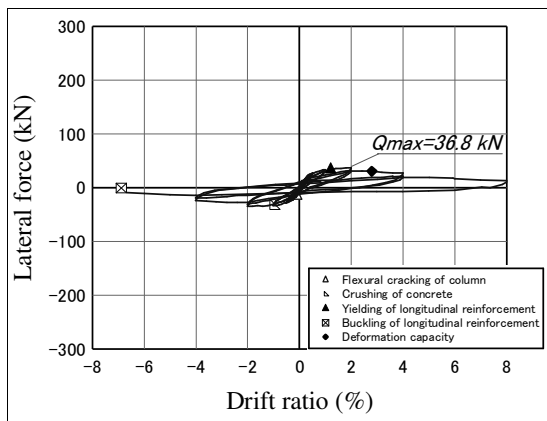


(d) IF_SB Specimen ($R = 1/25$ rad.)

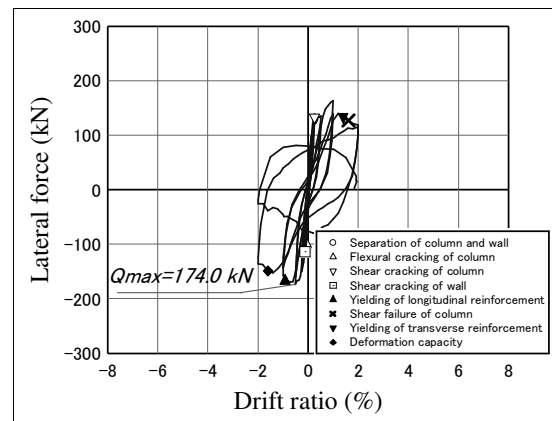
Figure 4.7. Final crack patterns.

4.5.2 Lateral Force-Drift Ratio Relationship

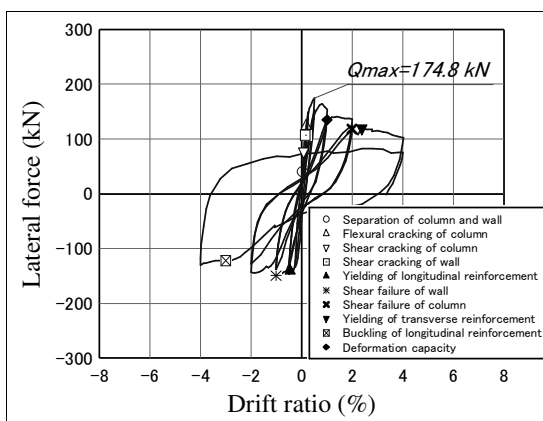
Figure 4.8 compares lateral force vs. drift ratio, R , relationships among the specimens. The maximum lateral strength of 36.8 kN was observed at 2.0% for the BF specimen. On the other hand, the maximum strengths reached 174.0 kN, 174.8 kN and 257.3 kN at 0.5%, 0.5% and 0.45% drift ratios for IF_FB, IF_SBw/oFM, and IF_SB, respectively. The deformation capacity, which was defined as a deformation where post-peak strength dropped to 80% of peak strength, was 2.8% for BF, whereas they decreased to 1.6%, 1.0% and 0.5% for IF_FB, IF_SBw/oFM, and IF_SB, respectively.



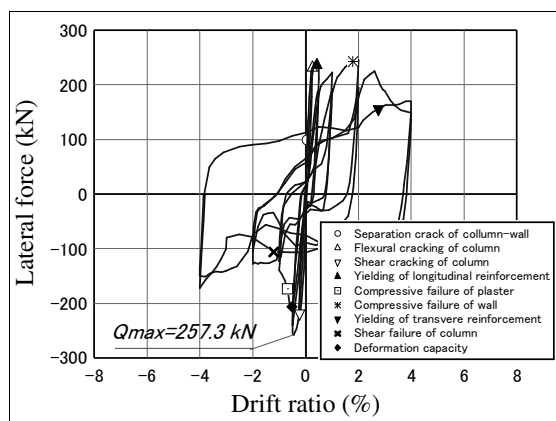
(a) BF specimen.



(b) IF_FB specimen.



(c) IF_SBw/oFM specimen



(d) IF_SB specimen

Figure 4.8. Lateral force-drift ratio relationships of infilled frames.

After installing the full scale nonstructural brick infill, strength increased to 4.7 times, but ductility decreased to about half. In the cases of the specimens with reduced infill, the lateral strengths of IF_SBw/oFM and IF_SB specimens are higher than those of IF_FB. It seemed because of the higher material properties of IF_SBw/oFM and IF_SB specimens, as shown in Table 4.2.

4.6 Summary

Four R/C one-bay frame specimens were constructed representing the first story of the moderately damaged building due to the 2007 Sumatra earthquakes. Moreover, three RC frames were installed by brick infill walls; one of brick wall was extracted from the referential damaged building, transported to Japan from Indonesia. However, two other specimens were infilled with scaled bricks made in Japan, which had arranged by similar compressive strength to that of Indonesian brick. These specimens were prepared to experimentally clarify the effects of brick infill on the seismic performance of the earthquake-damaged buildings. Major findings from experimental and analytical investigations are summarized as follows.

1. Seismic loading tests on the specimens were carried out to quantitatively obtain the structural contributions of the brick infill to the seismic performance of RC frame. As a result, the brick infill was found to significantly increase the strength of the overall frame by the compression strut mechanism but decreased the deformation capacity.
2. Flexural failure was experimentally observed on columns of the bare frame. On the contrary, shear failures were identified on brick wall and columns of infilled frames. It was exhibited that the presence of masonry infill altered the failure mode of RC frame structure.

Chapter 5

Analytical Modeling of RC Infilled Frames

5.1 Introduction

The experimental results showed that the brick masonry infill significantly contributed to the seismic performance of RC frame structures. Therefore, the brick infill should be considered as a parameter for seismic design of RC buildings.

The seismic performance of a masonry infill in a frame structure is commonly evaluated focusing on diagonal compression struts caused in the masonry infill. A number of researchers have studied analytical models for evaluating contribution of masonry infill to frame structures based on diagonal struts caused in masonry infill, as reported in section 2.5. However, according to the existing methods, varied analytical results of seismic performance were obtained for brick masonry infilled frames. Therefore, this study proposes a new equivalent strut model based on infill-frame interface for determining infill/frame contact length with simplified equations. In this study, a masonry infill is replaced by a diagonal compression strut, which represents a

distributed compression transferred diagonally between infill/frame interfaces. The infill/frame contact length can be determined by solving two equations, i.e., static equilibriums related to the compression balance at infill/frame interface and lateral displacement compatibility.

The proposed analytical method was verified through structural test results of brick infilled frames, which were described in the previous chapter, to verify the validity of the proposed method. Comparisons were performed on experimental results and numerical simulations using the proposed method.

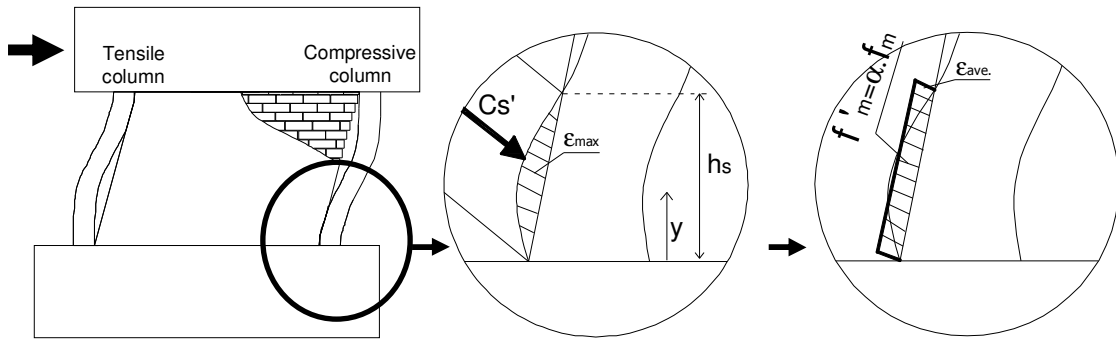
5.2 Proposal of Simple Model for Evaluating Infill-Frame Interaction

This study targets brick masonry infilled RC frames with relatively stiff beams which are typically used in Indonesian buildings, as shown in Figure 5.1(a). Such infilled frames may also represent the lower part of multi-story confined masonry structures where beam flexural deformation is constrained by the existence of infill. When they deform under lateral loads, contact/separation is caused between the bounding column and infill due to column flexural deformation and infill shear deformation, as shown in Figure 5.1(b). In this study, the contact length was derived from a simple procedure for the seismic performance evaluation of the targeted structures.

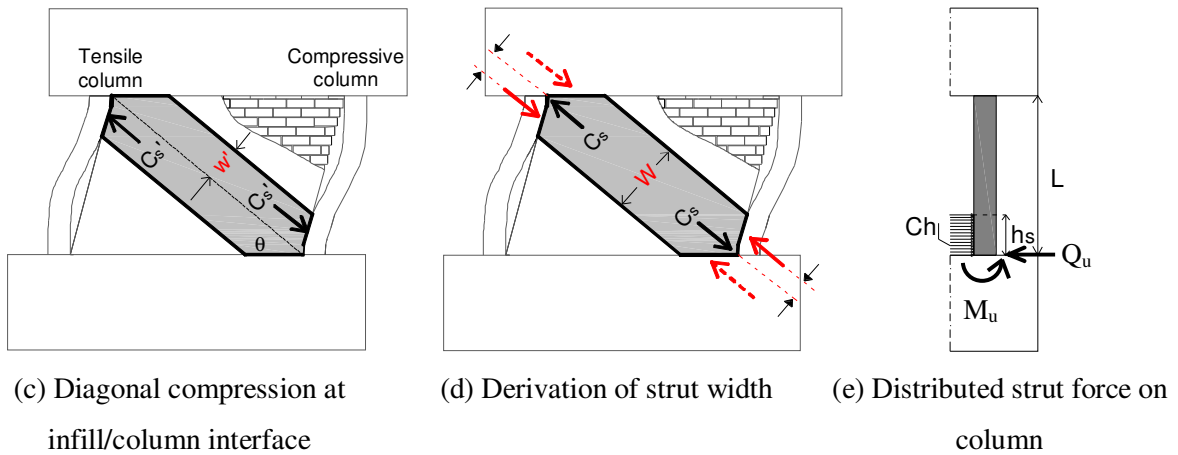
The masonry infill panel was replaced by a diagonal compression strut having the same thickness and material properties as those of the panel. In this model, a compression stress distribution at the infill/frame interface was replaced by an equivalent rectangular block, as shown in Figure 5.1(b), where the averaged compressive strength, f_m' , was evaluated by multiplying the uniaxial compressive strength of infill, f_m , by a reduction factor, α , which was evaluated by Equation 5.1a. The diagonal compression, C_s' , which acts on the bottom/top of the compressive/tensile column as shown in Figure 5.1(c), is given by Equation 5.2a. However, assuming reaction forces at the column ends, an unbalanced moment causes a rotation of a free



(a) RC building with brick infill



(b) Lateral deformation of infilled frame



(c) Diagonal compression at infill/column interface

(d) Derivation of strut width

(e) Distributed strut force on column

Figure 5.1. Modeling of masonry-infilled frame.

body of the infill, as shown by the solid red arrows in Figure 5.1(d). Therefore, reaction forces were considered at the beam ends, as shown by the dashed arrows in the figure. As a result, the total diagonal compression, C_s , was represented by twice as C_s' , as given by Equation 5.2b. Then, C_s was resolved into the horizontal and vertical components, which were represented by the distributed forces along column height, as shown in Equations 5.2c and 5.2d.

$$\alpha = \frac{\varepsilon_{average}}{\varepsilon_{max}} = \frac{\int_0^{h_s} \varepsilon(y) dy / h_s}{\varepsilon_{max}} \quad (5.1a)$$

$$\varepsilon(y) = \frac{\delta_s(y) - \delta_f(y)}{dl(y)} \quad (5.1b)$$

$$C_s' = 1/2 w' t f_m' \quad (5.2a)$$

$$C_s = W t f_m' \quad (5.2b)$$

$$c_h = t f_m' \cos^2 \theta \quad (5.2c)$$

$$c_v = t f_m' \sin \theta \cos \theta \quad (5.2d)$$

in which, α is reduction factor, $\varepsilon(y)$ is strain distribution at interface obtained by Equation 5.1b, $\delta_s(y)$ is shear deformation of infill, $\delta_f(y)$ is flexural deformation of column, $dl(y)$ is diagonal length of infill along column height, ε_{max} is maximum strain at the interface, w' is half strut

width from diagonal axis, t is thickness of infill, W is strut width, $W=2w'$, θ is inclination angle of strut, as shown in Figure 5.1(c).

Assuming that the compressive column yields in flexure at the bottom, the moment distribution along column height, ${}_cM(y)$, is obtained with Equations 5.3. Yield moment, however, is calculated with Equation 5.4 based on the Japanese standard (JBDPA, 2005).

In the case of $0 \leq y \leq h_s$

$${}_cM(y) = {}_{y=0}M_u - Q_u y + 1/2 C_h y^2 \quad (5.3a)$$

In the case of $h_s \leq y \leq L$

$${}_cM(y) = {}_{y=0}M_u - Q_u y + C_h h_s y - 1/2 C_h h_s^2 \quad (5.3b)$$

$$M_u = 0.8 a_t \sigma_y D + 0.5 N D \left(1 - \frac{N}{b D F_c} \right) \quad (5.4)$$

where, h_s is infill/column contact height, as shown in Figure 5.1(b), L is clear column height, as shown in Figure 5.1(e), M_u is flexural strength of column, Q_u is shear force at column bottom, which is determined with Equation 5.6, a_t is total cross-sectional area of tensile reinforcing bars, σ_y is yield stress of longitudinal reinforcement, D is column depth, N is axial force, b is column width, and F_c is compressive strength of concrete. However, the axial force at the bottom of the column was calculated as a summation of building weight (initial axial load), N_a , axial force due to shearing force in the beam, N_b , and vertical component of the strut force, $C_v h_s$, as shown in Figure 5.2.

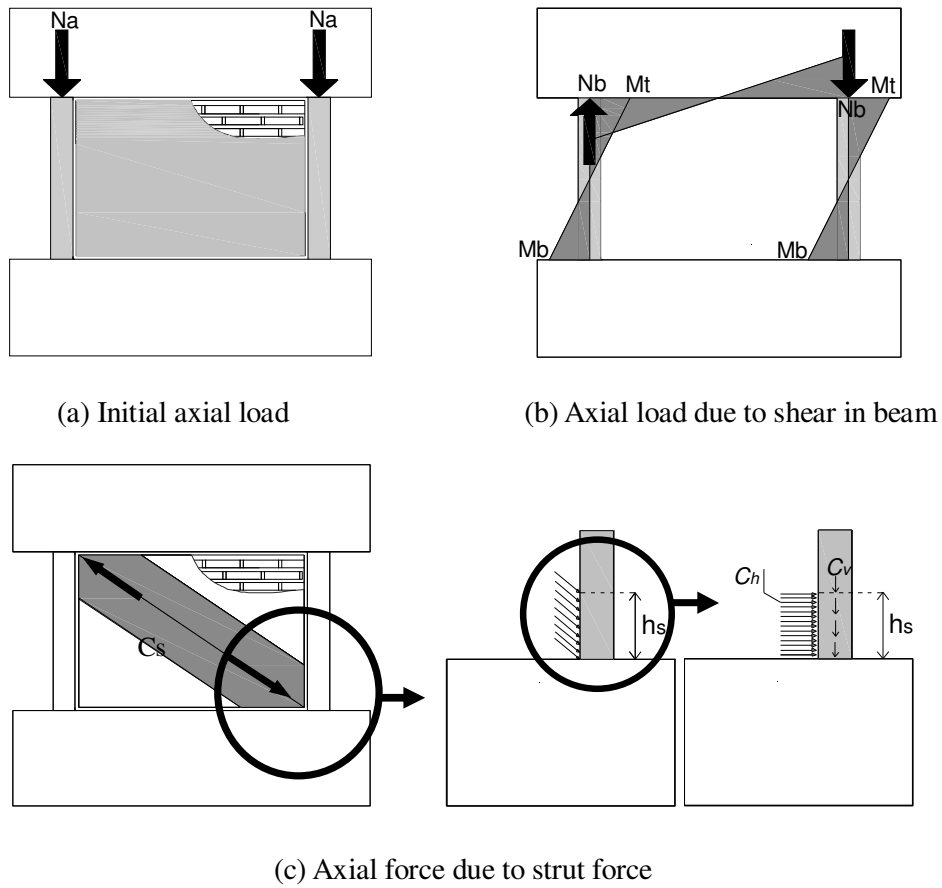


Figure 5.2. Considering of axial force at column bottom.

Lateral displacement along column height, ${}_c\delta(y)$, is produced by double integrals of Equation 5.3/ EI , which is shown by Equation 5.5.

In the case of $0 \leq y \leq h_s$

$${}_c\delta(y) = \frac{1}{EI} \left(\frac{1}{24} C_h y^4 - \frac{1}{6} Q_u y^3 + \frac{1}{2} M_u y^2 \right) \quad (5.5a)$$

In the case of $h_s \leq y \leq L$

$${}_c\delta(y) = \frac{1}{EI} \left(\left(\frac{1}{6} C_h h_s - \frac{1}{6} Q_u \right) y^3 + \left(\frac{1}{2} M_u - \frac{1}{4} C_h h_s^2 \right) y^2 + \frac{1}{6} C_h h_s^3 y - \frac{1}{24} C_h h_s^4 \right) \quad (5.5b)$$

where, E and I are Young's modulus and the second moment of inertia of columns.

Shear force at the bottom of compressive column, Q_u is given by Equation 5.6 when assuming a rotation of zero at the column top.

$$Q_u = \frac{2M_u}{L} + C_h h_s - \frac{C_h h_s^2}{L} + \frac{C_h h_s^3}{3L^2} \quad (5.6)$$

On the other hand, lateral deformation along infill height, ${}_i\delta(y)$, is defined by Equation 5.7, assuming uniform shear strain, ${}_i\theta$. Therefore, intersection height between column and infill can be evaluated by solving Equation 5.8, as shown in Figure 5.3. The figure shows that intersection height should equal h_s . The unknown h_s is obtained through an iteration after satisfying $y=h_s$. In this study, the Newton Raphson method was used to find h_s . The procedure above is presented in the flowchart in Figure 5.4.

$${}_i\delta(y) = {}_i\theta y = \frac{{}_c\delta(y=L)}{L} y \quad (5.7)$$

$${}_c\delta(y) = {}_i\delta(y) = \frac{{}_c\delta(y=L)}{L} y \quad (5.8)$$

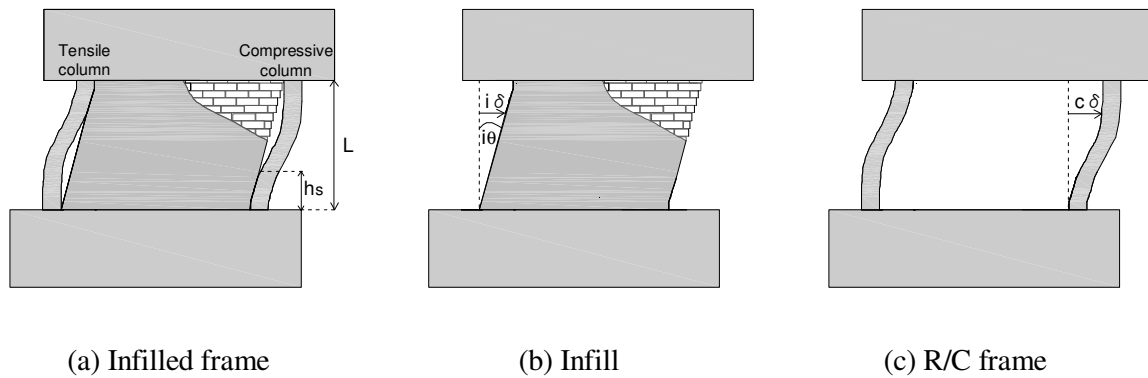


Figure 5.3. Lateral displacement compatibility between column and infill.

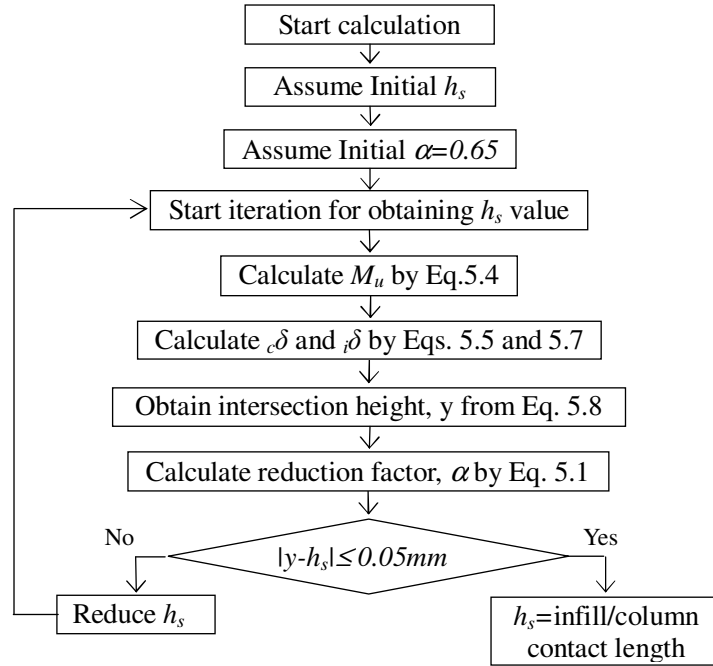


Figure 5.4. Flowchart for identifying infill/column contact length.

Consequently, the width of compression strut, W , is determined as a function of infill/column contact height, by Equation 5.9, however, which is defined as the smallest contact lengths between both ends of the strut.

$$W = 2h_s \cos \theta \quad (5.9)$$

5.3 Experiments for Verification

The proposed method was verified through experimental test results of RC bare frame (BF), full brick infilled frame (IF_FB) specimens, scaled brick infilled frame without finishing mortar on wall surfaces (IF_SBw/oFM), and scaled brick infilled frame (IF_SB) which have been described in chapter 4. Based on the test results, as shown in Figure 4.8, the infill contribution was extracted by evaluating the difference between lateral forces of infilled frames

(IF_FB, IF_SBw/oFM, and IF_SB), and bare frame (BF) specimens at each load step (at the same drift ratio), as shown in Figure 5.5.

5.4 Verification of Analytical Model

5.4.1 Seismic Contribution of Brick Masonry Infill

The envelope curve of infill was simulated by a trilinear model, in which the cracking force, V_c , and displacement, δ_c , of infill were defined by Equations 5.10 and 5.11, respectively, assuming that the infill/column independently behaved at a small drift considering the imperfect connection between both.

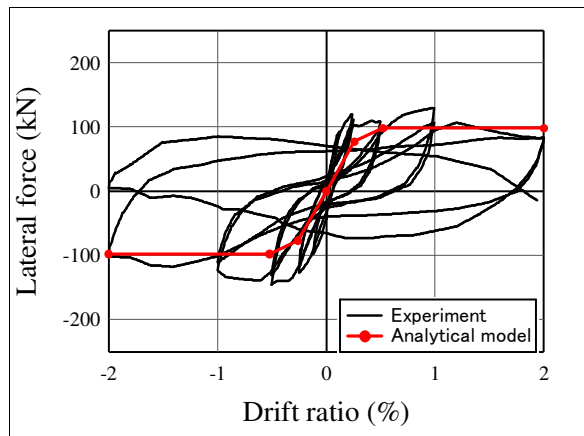
$$V_c = \tau A_w \quad (5.10)$$

$$\delta_c = \frac{\nu' V_c h}{G A_w} \quad (5.11)$$

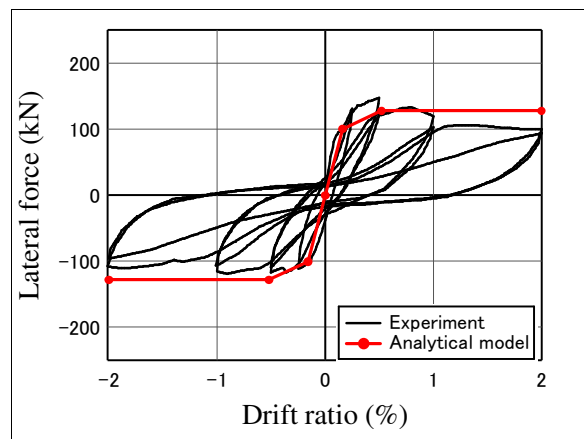
$$G = \frac{E_m}{2(1 + \nu)} \quad (5.12)$$

where, τ is shear strength of infill obtained by $\tau = f_t$, in which f_t is tensile strength of brick unit as the weakest component of infill, A_w is cross-section area of infill, ν' is shear deformation coefficient which is equal to 1.2 for a rectangular cross-section, h is height of infill, G is shear modulus of infill obtained by Equation 5.12, E_m is elastic modulus of masonry infill, ν : poisson ratio of masonry wall.

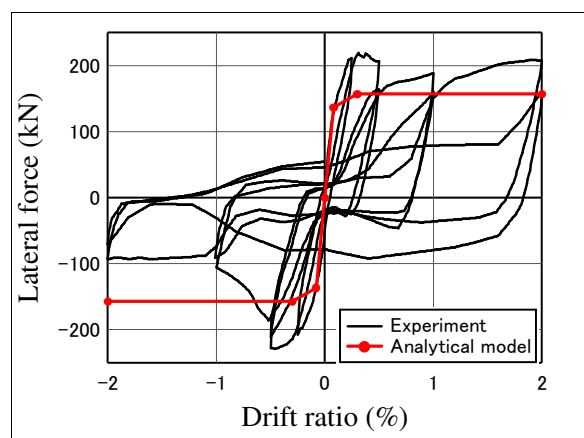
According to the proposed analytical method, infill/frame contact lengths, h_s , were evaluated to be 269.2 mm, 202.7 mm, and 159.8 mm for IF_FB, IF_SBw/oFM and IF_SB, respectively, hence the strut width was obtained by Equation 5.9. Equations 5.13 and 5.14 give



(a) IF_FB specimen



(b) IF_SBw/oFM specimen



(c) IF_SB specimen

Figure 5.5. Lateral force-drift ratio relationships of infill.

the lateral strength, V_m , and secant stiffness, K , at yielding of strut, respective.

$$V_m = C_s \cos \theta = W t f'_m \cos \theta \quad (5.13)$$

$$K = \frac{E_m W t}{d_m} \cos^2 \theta \quad (5.14)$$

where, E_m is elastic modulus of infill, and d_m is diagonal length of infill.

The performance curves evaluated as above are compared to envelopes of experimental results in Figure 5.5. Good agreements were obtained between both, which verified that the proposed method could be used reasonably for estimating the seismic performance of masonry infill.

Figure 5.6 shows the comparison of lateral strength of infill at yield between several analytical methods and experimental results for three specimens. The proposed method provides good correlation to experimental results as shown in the figure.

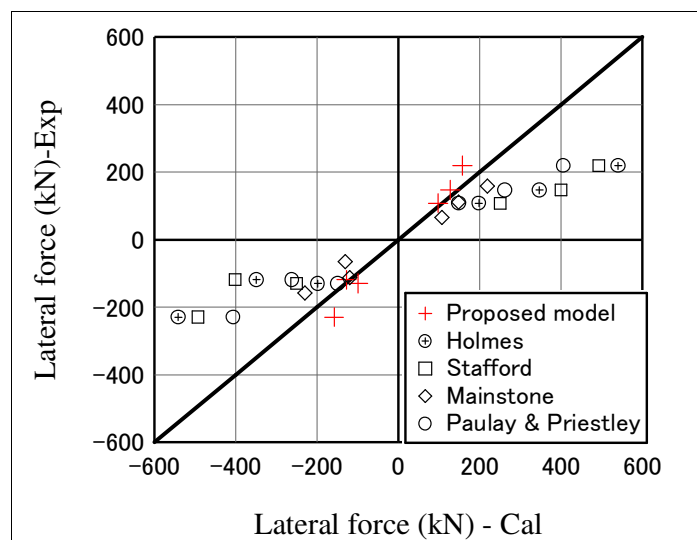
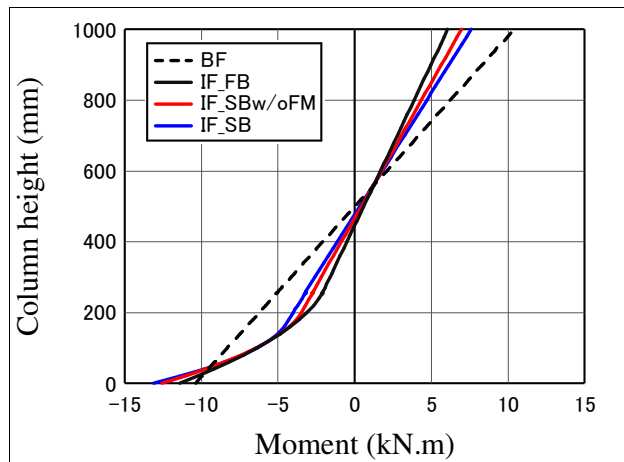
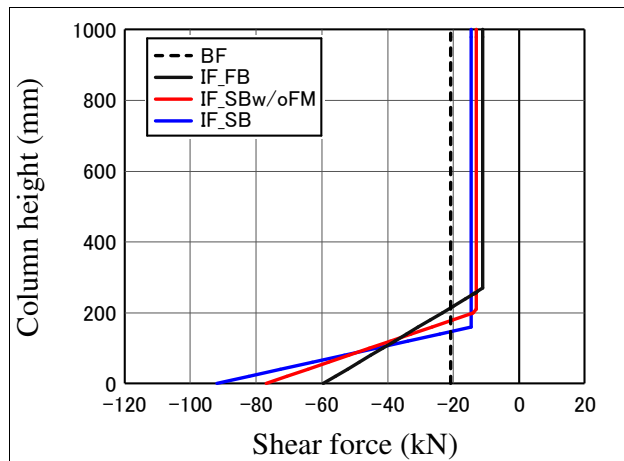


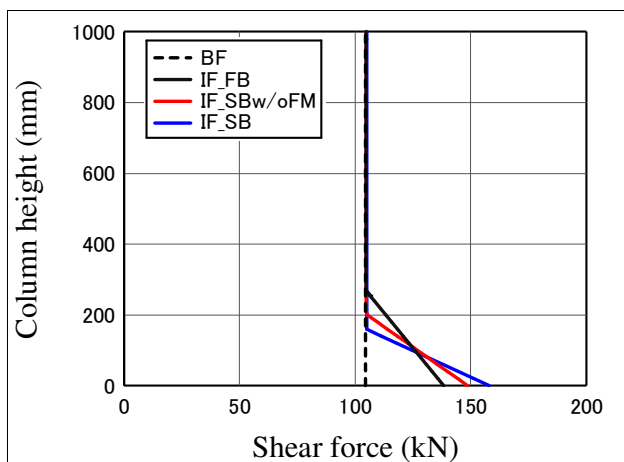
Figure 5.6. Comparison of lateral strength of infill between analytical and experimental results.



(a) Moment



(b) Shear force



(c) Axial force

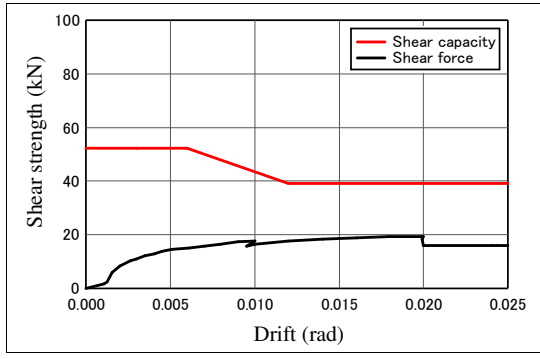
Figure 5.7. Stress diagrams of compressive column.

5.4.2 Effects on Columns

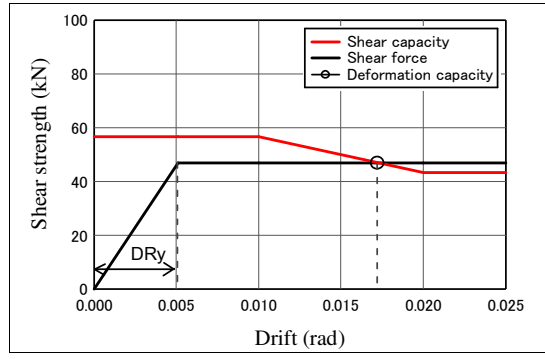
Distributions of bending moment, shear and axial forces along the compressive column height can be identified by the proposed method as shown in Figure 5.7. These figures identify that the infill affects to distributions of moment, shear and axial forces along the compressive column height. Bending moments at the base of the column were 11.4 kN.m, 12.6 kN.m and 13.1 kN.m for IF_FB, IF_SBw/oMF and IF_SB, respectively. Shear forces at the column bottom were 59.5 kN, 77.0 kN and 91.9 kN for IF_FB, IF_SBw/oMF and IF_SB, respectively. Axial forces at the bottom of compressive were 138.2 kN, 148.6 kN, and 157.8 kN for IF_FB, IF_SBw/oMF and IF_SB, respectively. Compared to the moment of 10.4 kN.m, shear forces of 20.7 kN, and axial forces of 104.6 for BF, it was found that the masonry infill increased not only the strength of the overall frame, but also local bending moment, shear and axial forces acting on the column. Therefore, the deformation capacities of infilled frame specimens were much lower than that of the bare frame specimen.

5.4.3 Evaluation of Column Ductility

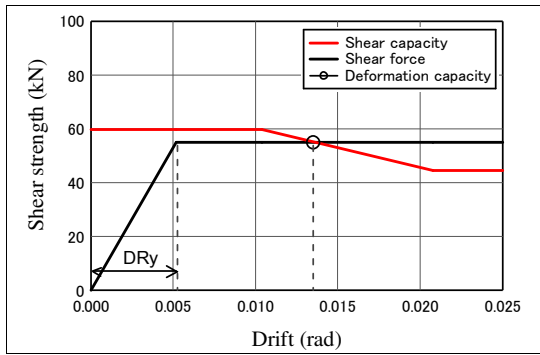
Moreover, the performance of compressive column was also replaced by a bilinear model, as shown in Figure 5.8. In the figure, however, the maximum shear was represented by the average of shear force distribution, ${}_cQ(y)$ which is the first differential of Equation 5.3, along the column height equal to column depth ($y=D$) from the end, because the severe damage occurred across this section. The drift at the maximum shear, D_{Ry} , should be given by Equation 5.15 considering the lateral displacement compatibility. On the other hand, the shear capacity of column was evaluated by Equation 5.16 (Priestley et al., 1994), where V_c is shear strength is contributed by concrete is given in Equation 5.16a, V_s and V_p are the transverse reinforcement contribution and axial load effect were calculated by Equations 5.16b and 5.16c, respectively. The parameters of P and a were evaluated considering the strut effects.



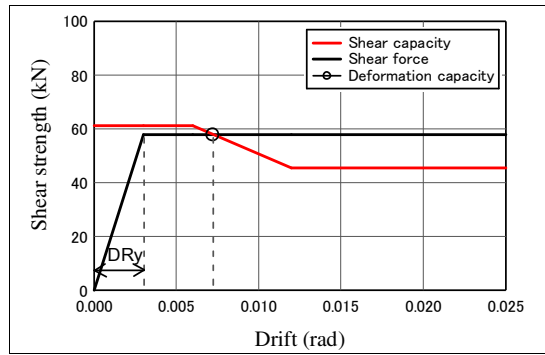
(a) BF specimen



(b) IF_FB specimen



(c) IF_SBw/oFM specimen



(d) IF_SB specimen

Figure 5.8. Performance curves of compressive column.

The deformation capacity of column was defined as a drift where shear force attained to the capacity, as shown in Figure 5.8. Consequently, they were 0.017 rad., 0.014 rad., and 0.007 rad., for IF_FB, IF_SBw/oFM and IF_SB, respectively which agreed with the experiment.

$$D_{Ry} = V_m / (K.L) \quad (5.15)$$

$$V_n = V_c + V_s + V_p \quad (5.16)$$

$$V_c = k \sqrt{F_c'} (0.8 A_g) \quad (MPa) \quad (5.16a)$$

$$V_s = \frac{A_v f_y D'}{s} \cot 30^\circ \quad (5.16b)$$

$$V_p = \frac{D - c}{2a} P \quad (5.16c)$$

where, k is degradation of concrete strength which is 0.29 MPa to 0.1 MPa for displacement ductility of 2 to 4, as shown in Figure 5.9, A_g is gross cross-sectional area, A_v is cross-sectional area of transverse reinforcement, f_y is yield stress of transverse reinforcement, D' is distance between the centers of perimeter hoop measured to parallel to the applied shear, s is spacing of hoop along the axis, c is neutral axis depth, P is axial load, a is shear span (distance from maximum moment section to point inflection).

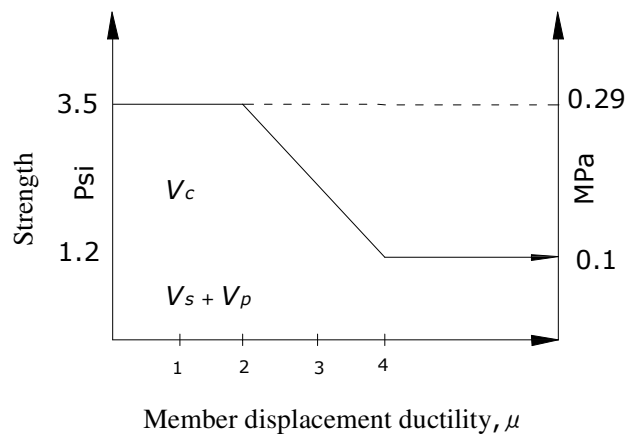
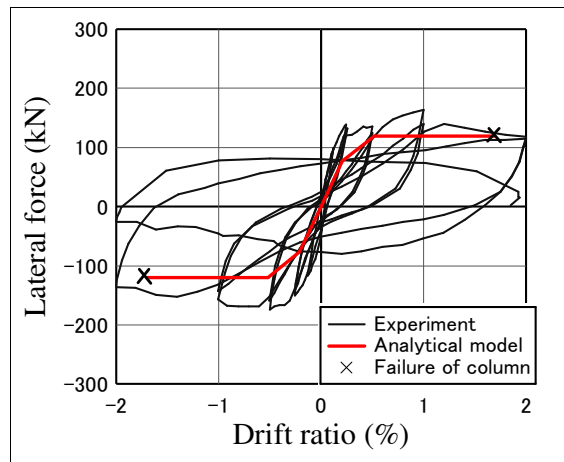


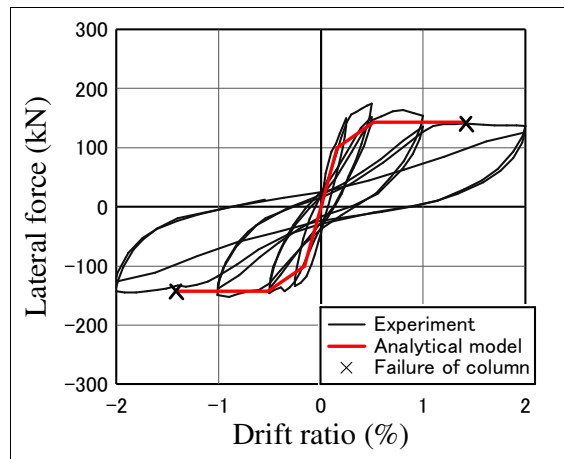
Figure 5.9. Concrete strength degradation with displacement ductility.

5.4.4 Performance Curves of Infilled Frames

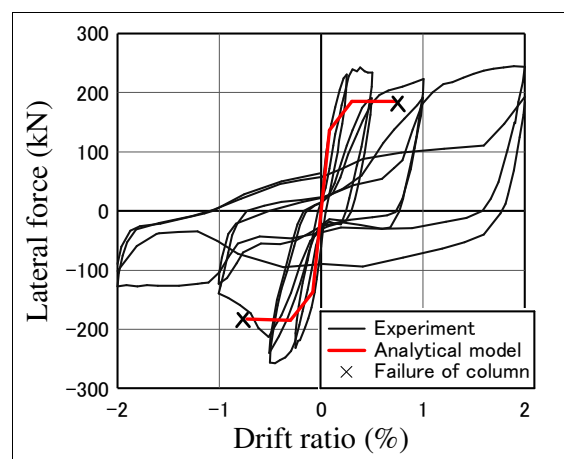
The performance curves of infilled frames can be predicted based on shear forces at the base of structures. As the results, Figure 5.10 compares the performance curves of infilled frames to experimental results. The strengths of infilled frames degraded regarding to deformation capacities of columns as shown in the figure.



(a) IF_FB specimen



(b) IF_SBw/oFM specimen



(c) IF_SB specimen

Figure 5.10. Comparison of experimental and analytical performance curves of infilled frames.

5.5 Summary

A simplified analytical method was proposed to evaluate infill contribution to the seismic performance of masonry infilled RC frames, and then it was verified through a series of structural tests. The following conclusions were obtained from analytical model proposed in this study.

1. The masonry infill panel is replaced by diagonal compression strut in the proposed simplified analytical method.
2. Contact length between column and infill was evaluated based on the compression balance at the infilled/frame interface and lateral displacement compatibility under column flexural and infill shear deformations.
3. Compression strut width is determined as the function of contact length which is based on the smallest evaluated contact length on tensile and compressive columns. It was found on three infilled frames that the contact length on infill-tensile column is smaller than those on infill-compressive column.
4. The performance curve of the infill in the experimental specimens was simulated by the proposed method. Consequently, good agreements were observed between experimental and analytical results. Based on comparison between the proposed model and other models, the proposed model provides nearer correlation to experiments than others.
5. An infill can increase local bending moment, shear and axial forces of bounding columns, which decrease the deformation capacities of bounding columns.
6. The performance of infilled frames can be predicted based on shear force at the base of structures.

Chapter 6

Application of Proposed Model to Seismic Performance

Evaluation of RC Buildings

6.1 Introduction

The proposed analytical model was implemented to nonstructural brick infill in two Indonesian earthquake-damaged buildings. However, the seismic performance of both buildings was evaluated on the basis Japanese standard (JBDPA, 2005), the proposed analytical method is implemented for nonstructural walls in two buildings considering the brick infill effects. Two calculations for seismic performance evaluation were conducted—one with infill and one without infill.

The seismic performance of both buildings was calculated in E-W direction for the first story presented by the basic seismic index of structure, E_0 , which was given as a product of the strength index, C , and the ductility index, F , based on Japanese standard (JBDPA, 2005) as described in section 3.6. The comparison of seismic performance of both buildings between

without and with infill effects is discussed.

6.2 Application of Proposed Model

The proposed analytical study was implemented to nonstructural brick walls in single and multi-span infilled frames in the collapsed and surviving buildings. The first floor plan and infilled frame arrangement of both buildings are shown in Figure 6.1.

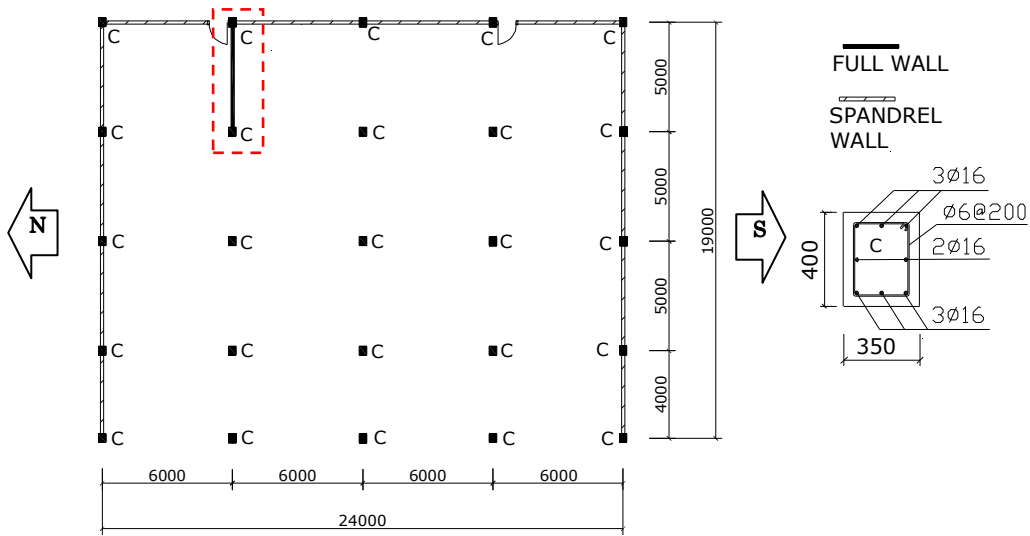
Although the brick infill walls were considered as analytical parameter, wing walls or walls with openings were neglected based on the past study (Ho Choi et al., 2005). While, the spandrel walls were considered to evaluate the clear height of columns.

The strength index, C , of column with infill effects in single infilled frame was evaluated according to the ultimate shear force of column given by Equation 5.6. On the other hand, for columns in multi-span infilled frames as shown in the Figure 6.1(b) and 6.2, each column was evaluated by considering the strut effect which was modeled for an exterior tensile column, interior column and exterior compressive column as shown in Figure 6.3(a), (b) and (c), respectively. In particular, distributed forces due to the strut were antisymmetrically applied to the bottom and top of interior column, as shown in Figure 6.3(b). Consequently, shear force at interior column end was determined by Equation 6.1.

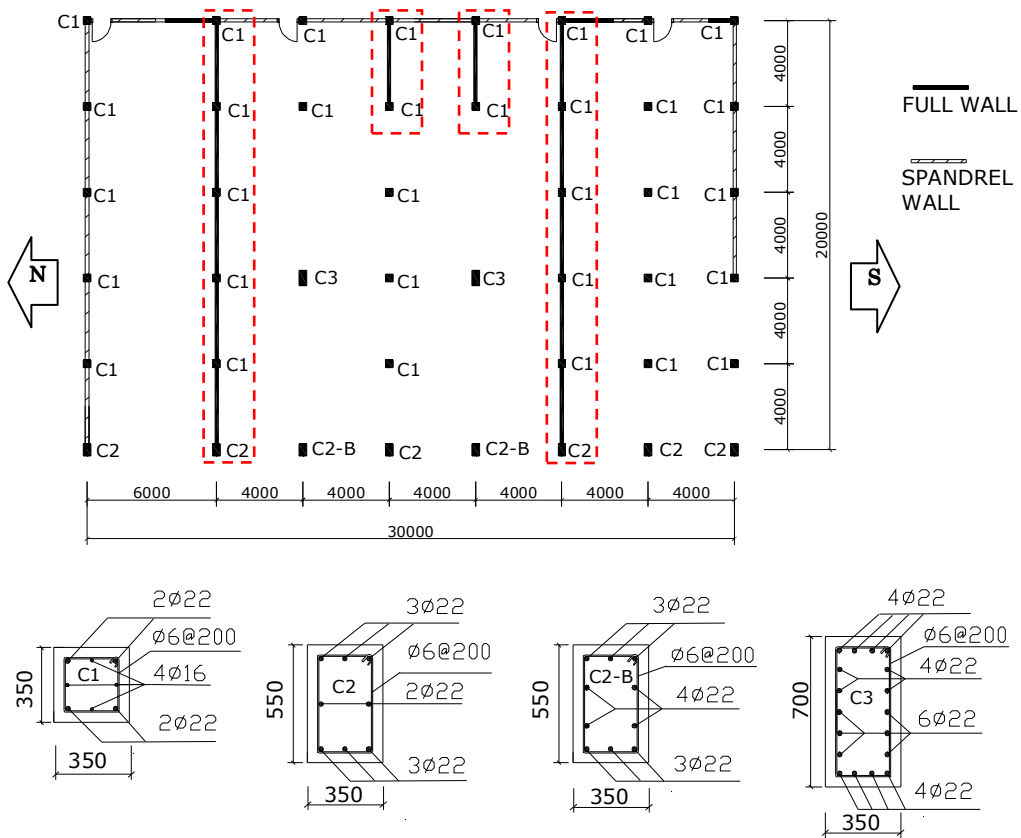
$$Q_u = \frac{2M_u}{L} + C_h h_s - \frac{C_h h_s^2}{L} \quad (6.1)$$

where, h_s is the smallest contact length between both ends of strut with columns.

The ductility index, F represents deformability of column was calculated according to structural specifications based on the reference. In the case of columns with infill effects, a deformation capacity of the columns was evaluated in the same manner as section 5.4.3.



(a) Collapse building



(b) Surviving building

Figure 6.1. Infilled frames and column detail on the first floor plan of RC frame buildings.

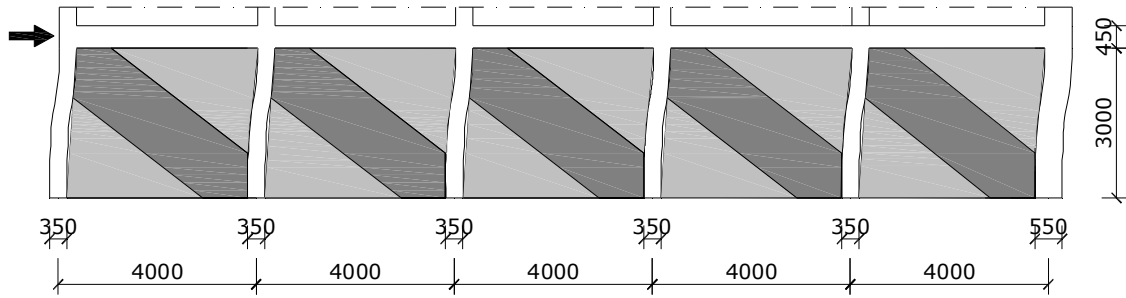
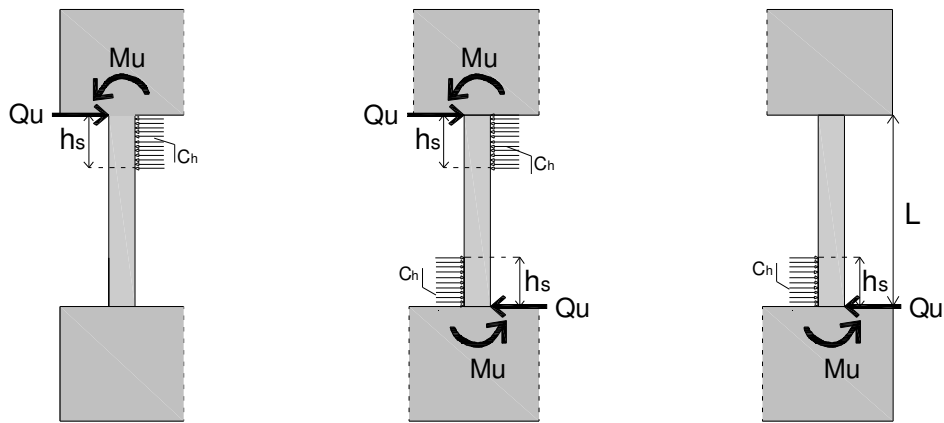


Figure 6.2. Strut model of infill in multi-span infilled frames.



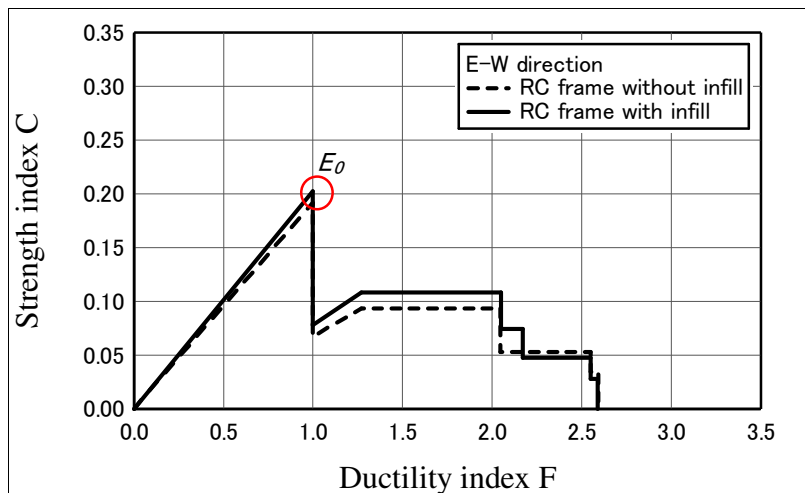
(a) Exterior tensile column (b) Interior column (c) Exterior compressive column

Figure 6.3. Assumed distributed forces due to strut at column ends.

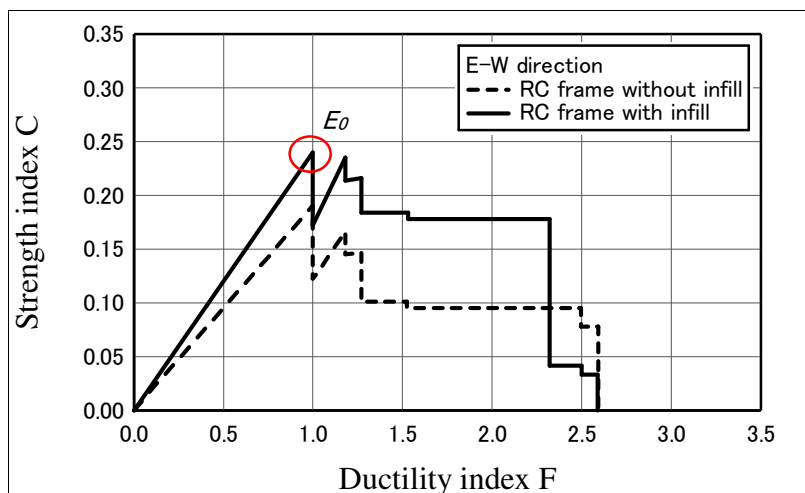
6.3 Seismic Performance Evaluation of Earthquake-Damaged RC Buildings

Figure 6.4 compares the calculated seismic performance of both buildings with and without brick infill effects in E-W direction. A distinct difference was observed between the maximum strengths of buildings in the case considering the infill. The strength of collapsed building drastically dropped at a 1.0% drift after shear failure of several short columns with spandrel walls, as shown in Figure 6.4(a). On the other hand, the strength of surviving building whose amount of nonstructural brick walls was larger than that of collapsed one was maintained until more than 2.0% drift, as

exhibited in Figure 6.4(b). This is a possible reason why one of the buildings could survive during severe earthquake ground motions which was assumed in E-W direction. This result indicates that the nonstructural infill significantly contributed to prevent the surviving building from collapsing during the earthquakes.



(b) Collapsed building



(b) Surviving building

Figure 6.4. Comparison of seismic performance of damaged buildings.

6.4 Summary

The seismic performance of two RC frame buildings with brick masonry infill damaged by the 2007 Sumatra earthquakes, one totally collapsed and others moderate damage, were evaluated according to the current Japanese standard. Two calculations were conducted on both buildings—one with infill and one without infill. The performance of brick infill in single and multi-span infilled RC frames was evaluated by applying the proposed analytical model. The major findings of analyses are summarized as follows.

1. The strength of collapsed building drastically dropped after shear failure of several columns with spandrel wall. On the other hand, the strength of surviving building whose amount of nonstructural brick walls was larger than that of collapsed one was still relatively high although several columns with spandrel wall have collapsed. It indicates that the nonstructural infill significantly contributed to the seismic resistance and prevented the surviving building from collapsing during the earthquakes.
2. The proposed analytical method can be applied reasonably for estimating the seismic performance of existing RC buildings with masonry infill.

Chapter 7

Summary, Conclusions and Recommendations

7.1 Summary

Masonry infill walls in RC frame structures have been long known to affect behavior of whole structures particularly increasing the lateral strength and stiffness of infilled frame structures. A lot of extensive analytical and experimental studies have been conducted by a number of researchers to investigate the effect and behavior of masonry infill in RC frame structures. However, there have been neither well-developed design recommendation nor well-accepted analytical procedures for masonry infilled frames. Therefore, in the seismic area such as Indonesia, the masonry infill is still considered as a non-structural element and ignored in seismic design calculations of buildings.

This study focused on evaluating the brick infill contribution to seismic performance of RC frames. The study was prefaced by a field investigation of earthquake-damaged RC buildings in Indonesia to observe the typical damage of RC frame structures with masonry walls.

Detailed investigation was carried out on two RC frame buildings, one totally collapsed and other moderately damaged, which were standing side by side and had structural similarities. The surviving building had an infill wall ratio much higher than that of collapsed one. It seemed the brick infill gave much contribution to seismic resistance of whole structure during the earthquakes. Therefore, to evaluate the brick infill effect to RC frame structure, an experimental study on bare frame and brick infilled frame structures representing the first story of the moderately damaged building was conducted. A brick wall was extracted from the surviving building, transported to Japan, and then installed into the bare frame. Both types of structures were tested under quasi-static cyclic loading to investigate the effect of brick masonry on RC frame. As the results, the brick infill increased the lateral strength of overall frame and decreased the deformation capacity.

Moreover, based on the test results, a new analytical model of infill was proposed for estimating the seismic performance of masonry infilled frames. In this model, the brick masonry infill was replaced by a diagonal compression strut. The infill/column contact length on the tensile and compressive columns was evaluated based on the compression balance at the infilled/frame interface and lateral displacement compatibility under column flexural and infill shear deformations. Compression strut width was determined according to the evaluated infill/column contact length which was defined as the smallest contact lengths between both ends of strut with compressive/tensile columns. The proposed method was verified through a series of structural tests of several brick masonry infilled RC frames. Good agreement were obtained between analytical and experimental results, which verified that the proposed method could be used reasonably for estimating the seismic performance of masonry infill/masonry infilled frames.

The proposed analytical model was applied for evaluating the contribution of brick infill to seismic performance of earthquake-damaged buildings. Consequently, the nonstructural infill

significantly contributed to the seismic resistances and prevented the surviving building from a total collapse during the earthquakes.

7.2 Conclusions

As the results of the current study, the following conclusions have been reached.

1. According to field investigation conducted after the 2007 Sumatra earthquakes in Padang city and nearby areas, it revealed that several RC structures with URM walls suffered severe damage such as shear failure of columns, buckling of column longitudinal reinforcements, and collapse of brick walls.
2. Detailed investigation on one of the collapsed RC frame buildings and its neighboring building which had a higher masonry wall ratio was conducted. The surviving building was classified into moderate damage level. Thus, it exhibited that the masonry infill possibly contributed to preventing the moderately damaged building from collapsing during the earthquakes.
3. Comparing the seismic performance of RC frame specimens with and without brick infill through quasi-static cyclic loading tests, wall contributions were quantitatively evaluated. The brick infill seemed to significantly increase the strength of the overall frame by the compression strut mechanism.
4. Flexural failure was experimentally observed on columns of the bare frame. On the contrary, shear failures were identified on brick wall and columns of infilled frames. It revealed that the presence of masonry infill altered the failure mode of RC frame structure.
5. A simple model of infilled frames was proposed in this study for determining the contact length between column and infill based on the compression balance at the infilled/frame interface and lateral displacement compatibility under column flexural and infill shear deformations.

6. A masonry infill in frame was replaced by a diagonal compression strut, which represented a distributed compression transferred diagonally between infill/frame interfaces. The Compression strut width is determined as a function of infill/column contact height, however, which is defined as the smallest contact lengths between both ends of the strut.
7. The performance curves of the infill in the experimental specimens were simulated by the proposed method. Consequently, good agreements were observed between experimental and analytical results.
8. An infill can increase local bending moment and shear force at bounding columns, which decreases the deformation capacities of bounding columns.
9. Applying the proposed analytical method to evaluate the seismic performance of Indonesian earthquake-damaged buildings, it was shown that the nonstructural infill significantly contributed to preventing the surviving building from collapsing during the earthquakes. It indicates that the proposed analytical method can be applied reasonably for estimating the seismic performance of existing RC frame buildings with masonry infill

7.3 Recommendations

According to analytical and experimental results, the presence of masonry walls has significant impacts on the seismic performance/response of RC frame structures. Hence, the masonry infill in RC frame structures should be considered as possible structural elements for more accurate seismic performance/response evaluation of this type of structure.

In current study, the analytical method was developed for RC frame structures with much stiff beams. In the future, the model is necessary to be verified by applying it to RC infilled frames with slender beams. Thus, additional tests on infilled frame structures are necessarily conducted.

The proposed model can be applied to evaluate the seismic performance of existing RC

buildings. It will be a realistic method for screening existing buildings for strengthening in high seismic areas.

References

Architectural Institute of Japan (AIJ). (1994). "AIJ Structural Design Guidelines for reinforced concrete buildings", Tokyo, pp 207

Architectural Institute of Japan (AIJ). (2007). "Report on the damage investigation of the 2006 central java earthquake."

Baran M., and Sevil T. (2010). "Analytical and experimental studies on infilled RC frames." *Int. J. of the Physical Sciences*, 5(13), 1981-1998.

Bertero VV, and Brokken ST. (1983). "Infills in seismic resistant building." *J. Struct. Eng.*, 109(6), 1337-1361.

Brokken,ST., and Bertero,VV. (1981). "Studies on effects of infills in seismic resistant RC construction." *Earthquake Engineering Research Center*, University of California, Berkely. UCB/EERC 81/12.

Decanini L., Mollaioli F., Mura A., and Saragoni R. (2004). "Seismic performance of masonry Infilled R/C Frames." *Proceeding of 13th World Conference on Earthquake Engineering*, Vancouver, B.C., Canada.

Earthquake Engineering Research Institute (EERI). (2009). "Learning from earthquakes, the Mw 7.6 Western Sumatra earthquake of September 30, 2009." *EERI Special Earthquake Report*.

EEFIT (2008). "The wenchuan, China earthquake of 12 May 2008." *A Preliminary Report by EEFIT*.

Fiorato AE, Sozen MA and Gamble WL. (1970). "An investigation of the interaction of reinforced concrete frame with masonry filler walls." *Report UILU=ENG-70-100*. Department of Civil Engineering, University of Illinois, Urbana Champaign IL, USA.

Hashemi A., and Mosalam KM. (2007). "Seismic evaluation of reinforced concrete buildings including effects of masonry infill walls." *Pacific Earthquake Engineering Research Center College of Engineering Uni. California, Berkeley*.

Ho Choi, Yoshiaki Nakano, and Yasushi Sanada. (2005). "Seismic performance and crack pattern of concrete block infilled frames." *Bulletin of ERS, No. 38*

Holmes M. (1961). "Steel frames with brickwork and concrete infilling." *Proceedings of the Institution of Civil Engineers, 19*, 473-478.

Humar JM., Lau D., and Piere JR. (2001) "Performance of buildings during the 2001 bhuj earthquake", *Can. J. Civ. Eng.* 28, 979–991.

International Association for Earthquake Engineering. (2004). "Regulations for seismic design." *A World List – 2004*.

Kahn,L.F., and Hanson,R.D. (1979). "Infilled walls for earthquake strengthening." *Journal of the Structural Division, ASCE, Vol. 105, No. ST2*.

Kaplan H., Bilgin H., Yilmaz S., Binici H., and Aztas A. (2010). "Structural damages of L'Aquila (Italy) earthquake", *Nat. Hazards Earth Syst. Sci.*, 10, 499–507.

Klingner RE, and Bertero VV. (1976). "Infilled frames in earthquake resistance construction." *Earthquake Engineering Research Center, University of California at Berkeley, Report EERC 76-32*.

Liau TC and Kwan KH. (1984). " Nonlinear behavior of non-integral infilled frames." *Comp. and Struct.*, 18, 551-560.

Mehrabi AB., Shing PB, Schuller MP., and Noland JL. (1994). "Performance of masonry-infilled R/C frames under in-plane lateral loads." *Rep. CU/SR-94-6*, Dept. of Civ., Envir., and Arch. Engrg., Univ.of Colorado, Boulder, Colo.

Mehrabi AB., Shing PB, Schuller MP., and Noland JL. (1996). "Experimental evaluation of masonry-infilled RC frames." *J. Struc. Engg.* 122(3), 228-237.

Maidiawati and Sanada Y. (2008). "Investigation and analysis of buildings damaged during the

September 2007 Sumatra, Indonesia earthquakes.” *Journal of Asian Architecture and Building Engineering*, 7 (2), 371-378.

Mainstone, R.J. (1971). “On the stiffness and strength of infilled framed.” *Proceedings, Institution of Civil Engineers*, Supplement IV, 57-90.

Mosalam K., Glascoe L., Bernier J. (2009) “Mechanical properties of unreinforced brick masonry.” *section 1, LLNL-TR-417646*.

Murty CVR., and Nagar A. (1996). “Effect of brittle masonry infills on displacement and ductility demand of moment resisting frames.” *Proceedings of 11th World Conference on Earthquake Engineering*, Auckland, New Zealand.

Murty CVR., and Jain K. (2000). “Beneficial influence of masonry infill walls on seismic performance of Rc frame buildings.” *Proceeding of 12th World Conference on Earthquake Engineering*, Auckland, New Zealand.

Nakano Y., Maeda M., and Kuramoto H. (2004). “Guideline for post earthquake damage evaluation and rehabilitation of RC buildings in Japan”. *Proceeding of 13th World Conference on Earthquake Engineering*, Vancouver, B.C., Canada.

Page A. W. (1996). “Unreinforced masonry structures an Australian overview.” *Bulletin of the New Zealand National Society for earthquake Engineering*, 29(4).

Paulay T, and Priestley MJN. (1992). “Seismic design of reinforced concrete and masonry buildings.” *John Wiley & Sons, Inc., New York, USA* 1992. ISBN 0-471-54915-0.

Paulay T. (1996). “Seismic design for torsional response of ductile buildings.” *Buletin of The New Zealand National Society for Earthquake Engineering*, 29(3).

Polyakov SV., (1956). “Masonry in framed buildings.” *Godsudarstvenoe isdatel'stvo Literatry Po Stroidal Stvui Architecture*, Moscow.

Priestley MJN, Verma R and Xiao Y. (1994). “Seismic shear strength of reinforced concrete columns.” *Journal of Structural Engineering*, 120(8), pp.2310-2329.

Shing PB, and Mehrabi AB. (2002). “Behaviour and analysis of masonry-infilled frames.” *Prog. Struct. Engng Mater.* 4, 320-331.

Stafford Smith BS, and Carter C. (1969). “A method of analysis for infilled frames.” *Proc. ICE.*, 44, 31-48.

The Japan Building Disaster Prevention Association (JBDPA). (2005). “English version, 1st, standard for seismic evaluation of existing reinforced concrete buildings, 2001.”

The National Disaster Management Coordinating Board of Indonesia (BAKORNAS): <http://bakornaspb.go.id/website> (in Indonesian).

USGS Website: <http://earthquake.usgs.gov/>.

Zovkic J, Sigmund V., and Gulkas I. (2012). “Cyclic testing of a single bay reinforced concrete frames with various types of masonry infill.” *Earthquake Engng Struct. Dyn.*, DOI:10.1002/eqe.2263.

Appendix A

An Example to Demonstrate the Calculation of Contact Length and Strut Width of Infill by the Proposed Model

A1. IF_FB Specimen

The RC frame infilled with full scale brick wall (IF_FB) specimen, shown in photo A.1, consist of 140 x 140 mm cross-sectional dimensions of the columns, 1000 mm clear height of column, 1460 mm clear length of infill, and 140 mm infill's thickness. The longitudinal rebars and transverse hoops of columns were 4- $\phi 9$ and 2- $\phi 4@100$, respectively. The procedures how to calculate the contact length and strut width of infill as the structure is subjected to lateral load are presented in this section.

The material properties of IF_FB specimen were $f_c = 20.6 \text{ N/mm}^2$, $E_c = 18968.34 \text{ N/mm}^2$, $I_c = 32013333.33 \text{ N/mm}^2$, $a_t = 127.17$, $\sigma_y = 355 \text{ N/mm}^2$, $a_g = 254.34 \text{ mm}^2$, and axial force on column based on upper floor weight $N_a = 92160 \text{ N}$.



Photo A.1. IF_FB specimen.

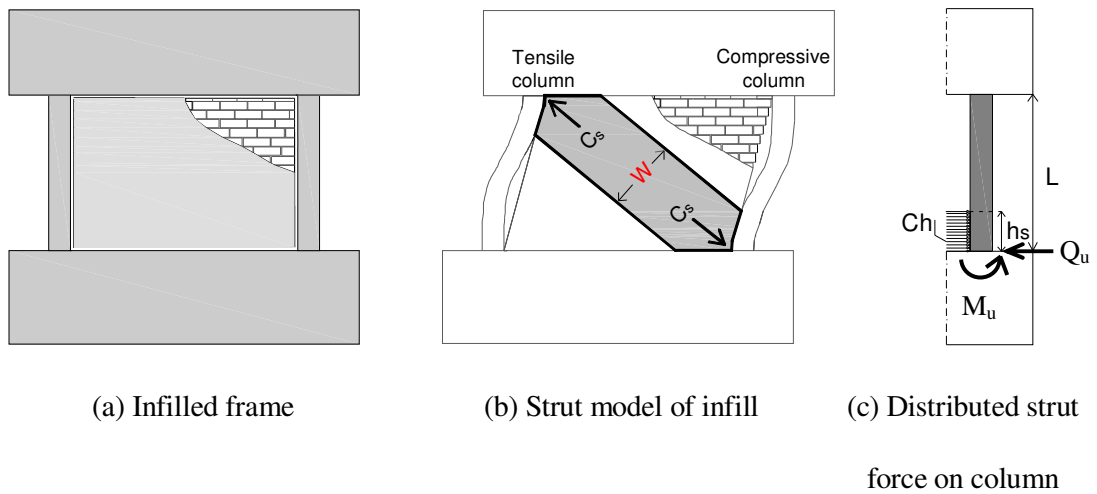


Figure A.1. Modeling of infilled frame.

A2. Infill-Column Contact length

The infilled frame structure suffered lateral deformation as lateral load was applied to the structure. Shearing force in the beam occurred with bending moment of columns simultaneously, and affected to axial force of surrounding columns. Table A.1 shows the calculating and

balancing process for shearing force in the beam. The M_u of both columns was evaluated by Equation 5.4,

$$M_u = 0.8 a_t \sigma_y D + 0.5 N D \left(1 - \frac{N}{b D F_c} \right)$$

where, $N = N_a$. Thus, axial force due to shearing force in the beam, $N_b = 12509.79$ N.

Table A.1. Balancing process of beam shear affect to columns' deformation.

step	axial on west column (N)	axial on east column (N)	M_u of west column (N.mm)	M_u on east column (N.mm)	Shear on beam (N)
1	92160	92160	10034964.36	10034964.36	12543.71
2	79616.29	104703.71	9530467.95	10484903.02	12509.61
3	79650.39	104669.61	9531913.32	10483753.86	12509.79
4	79650.21	104669.79	9531905.47	10483760.1	12509.79

Assuming the initial $h_s = 350$ mm from bottom end of compressive column and from top end of tensile column, as shown in Figure A1(b). The initial reduction factor was assumed as $\alpha = 0.65$. Thus, the following results were obtained.

The vertical component of the strut: $C_v h_s = h_s t \alpha f_m \cos \theta \sin \theta = 42302.1$ N.

The horizontal component of the strut: $c_h = t \alpha f_m \cos^2 \theta = 180.24$ N.

The axial force on bottom of compressive column: $N = N_a + N_b + C_v h_s = 147871.89$ N.

The axial force on top of tensile column: $N = N_a - N_b - C_v h_s = 36448.11$ N.

Yield moment, M_u , at bottom compressive column and at top of tensile column was

evaluated by equation 5.4 by considering the axial force, N , for each column.

$$M_u = 11616379.44 \text{ N.mm (bottom compressive column).}$$

$$M_u = 7377330.7 \text{ N.mm (top tensile column)}$$

The shear force at bottom of compressive column and at top of tensile column was evaluated by Equation 5.6.

$$Q_u = \frac{2M_u}{L} + C_h h_s - \frac{C_h h_s^2}{L} + \frac{C_h h_s^3}{3L^2}$$

The results for compressive and tensile columns:

$$Q_u = 66809.82 \text{ N (bottom compressive column).}$$

$$Q_u = 58331.72 \text{ N (top tensile column)}$$

The lateral displacement along the column height and infill was evaluated by Equations 5.5, as following equations.

In the case of $0 \leq y \leq h_s$.

$${}_c \delta(y) = \frac{1}{EI} \left(\frac{1}{24} C_h y^4 - \frac{1}{6} Q_u y^3 + \frac{1}{2} M_u y^2 \right)$$

In the case of $h_s \leq y \leq L$.

$${}_c \delta(y) = \frac{1}{EI} \left(\left(\frac{1}{6} C_h h_s - \frac{1}{6} Q_u \right) y^3 + \left(\frac{1}{2} M_u - \frac{1}{4} C_h h_s^2 \right) y^2 + \frac{1}{6} C_h h_s^3 y - \frac{1}{24} C_h h_s^4 \right)$$

Displacement of infill

$${}_i\delta(y) = {}_i\theta y = \frac{{}_c\delta(y=L)}{L} y$$

Intersection height, y , between infill displacement and column displacement was evaluated by Equation 5.8. Substituting the Equation 5.5a into 5.8, it can be presented as

$${}_c\delta(y) = {}_i\delta(y) = \frac{{}_c\delta(y=L)}{L} y$$

$$\frac{1}{EI} (1/24 C_h y^4 - 1/6 Q_u y^3 + 1/2 M_u y^2) = {}_i\theta \cdot y$$

$$1/24 C_h y^4 - 1/6 Q_u y^3 + 1/2 M_u y^2 - {}_i\theta \cdot y \cdot EI = 0$$

In this case, the Newton-Raphson method can be used to find the intersection point, y , which gives.

$$y_{i+1} = y_i - \frac{f(y_i)}{f'(y_i)}$$

where, the nonlinear equation, $f(y) = 0$, and $f'(y)$ can be written as

$$f(y) = 1/24 C_h y^4 - 1/6 Q_u y^3 + 1/2 M_u y^2 - {}_i\theta \cdot EI \cdot y$$

$$f'(y) = 1/6 C_h y^3 - 1/2 Q_u y^2 + M_u y - {}_i\theta \cdot EI$$

Considering the compressive column, the lateral displacement at the top column, $c\delta_{(y=L)}$, was evaluated to be 1.39 mm. thus, the uniform shear strain of infill, $i\theta=c\delta_{(y=L)}/L$, was 0.001387. The iteration processes to find y value of infill-compressive column by Newton-Raphson method are shown in Table A.2. The iteration started with an initial guess of $y_0 = 250$. The table shows that the intersection point between infill and column displacements was 232.3 mm. by the same manner as infill-compressive column, the intersection height between infill and tensile column displacements was evaluated to be 41.3 mm.

Table A.2. Newton-Raphson method for finding the intersection height

Iteration number	y_i	$f(y_i)$	$f'(y_i)$	$y_{i+1} = y_i - \frac{f(y_i)}{f'(y_i)}$
0	250	7735445706	443142000.8	232.544
1	232.544	103211742.2	430132081.9	232.304
2	232.304	27506.03412	429902581.5	232.304
3	232.304	0.001983643	429902520.2	232.304

As requirement of the proposed model that the h_s is indicated as contact length height if $|y-h_s| \leq 0.05$. Because of the y values of both columns were not eligible, the $h_s = 350$ was not indicated as the contact length between infill and column. The reduction factor, α , was evaluated by Equation 5.1 and it was obtained to be 0.653.

The calculation was continued by iteration process to find the contact length of infill-column by reducing the h_s value. The same way was applied as first step to the new values of h_s and α until satisfied the condition of $|y-h_s| \leq 0.05mm$.

Finally the contact lengths, h_s , were observed to be 311.34 mm and 269.2 mm for infill-compressive column and for infill-tensile column, respectively, and the reduction factor, α ,

of 0.656. The following demonstrates the calculation process of h_s of infill-tensile column.

The h_s was reduced to be $h_s = 269.17 \text{ mm}$, and α was evaluated to be $\alpha = 0.566$. Then,

$$C_h = 181.9 \text{ N}, \quad C_h h_s = 33531.57 \text{ N}, \quad \text{and} \quad N = 46118.64 \text{ N}.$$

$$M_u = 0.8 a_t \sigma_y D + 0.5 N D \left(1 - \frac{N}{b D F_c} \right) = 7915837.48 \text{ N.mm}.$$

$$Q_u = \frac{2M_u}{L} + C_h h_s - \frac{C_h h_s^2}{L} + \frac{C_h h_s^3}{3L^2} = 52795.89 \text{ N}.$$

$$\delta(y=L) = 0.95 \text{ mm}, \text{ then } \theta = \delta(y=L)/L = 0.00095.$$

Establishing a linier equation, $f(y)=0$ and $f'(y)$ as described above, the intersection height between infill and column displacement can be identified by Newton-Raphson method, as shown in Table A.3.

Table A.3. Iteration process for finding the contact length.

h_s	Iteration number	y_i	$f(y_i)$	$f'(y_i)$	$y_{i+1} = y_i - \frac{f(y_i)}{f'(y_i)}$
269.17	0	250	-4420654226	227164349.5	269.46
	1	269.46	68088582.26	233811758.7	269.169
	2	269.169	12453.104	233726178.6	269.169
	3	269.169	0.000397	233726162.9	269.169

A3. Strut Width of Infill

The strut width of infill is determined by Equation 5.9, which h_s is the smaller contact length between infill-compressive column and infill-tensile column. The smallest contact length was observed on infille-tensile column of 269.17 mm. Therefore, the strut width of infill on

IF_FB specimen is $W = 2h_s \cos \theta = 2 \times 269.17 \times 0.825 = 444.13 \text{ mm}$.

A4. Lateral Strength of Infill

The total diagonal compression force was evaluated based on obtained strut width by Equation 5.2b. $C_s = W t f_m' = 444.13 \times 140 \times 0.656 \times 2.91 = 118695.83 \text{ N} = 118.7 \text{ kN}$.

The lateral strength of infill at yielding of strut was obtained by Equation 5.13,

$$V_m = C_s \cos \theta = W t f_m' \cos \theta = 97.92 \text{ kN}$$

A5. Lateral Stiffness of Infill

The lateral stiffness of infill at yielding of strut was evaluated by Equation 5.14.

$$K = \frac{E_m W t}{d_m} \cos^2 \theta = 18868.63 \text{ N/mm}.$$

The drift of infill at yield was given by $D_{Ry} = V_m / (K.L) = 0.005$. The performance of infill of IF_FB specimen is shown in Figure 5.5(b).

Appendix B

Moment, Shear and Axial Force Distributions of Column

Table B1 shows the moment, shear and axial forces distribution of compressive column of IF_FB specimen with the contact length of infill-column, h_s , was 269.17 mm, yield moment, M_u , and shear force, Q_u , at based of column are 11.42 kN.m and 59.46 kN. The stress diagrams along the column height are shown in Figure 5.7.

Table B.1. Moment, shear and axial forces of compressive column of IF_FB specimen.

<i>Column height (mm)</i>	<i>M(y) (kN.m)</i>	<i>Q(y) (kN)</i>	<i>N(y) (kN)</i>
0	11.42	59.46	138.20
20	10.27	55.86	135.71
40	9.18	52.25	133.22
60	8.18	48.65	130.73

Table B.1. Moment, shear and axial forces of compressive column of IF_FB specimen

(continuation)

<i>Column height (mm)</i>	<i>M(y) (kN.m)</i>	<i>cQ(y) (kN)</i>	<i>N(y) (kN)</i>
80	7.24	45.05	128.24
100	6.37	41.44	125.74
120	5.58	37.84	123.25
140	4.86	34.23	120.76
160	4.21	30.63	118.27
180	3.64	27.02	115.78
200	3.13	23.42	113.29
220	2.70	19.81	110.80
240	2.34	16.21	108.30
250	2.19	14.41	107.06
252	2.16	14.04	106.81
253	2.14	13.86	106.68
254	2.13	13.68	106.56
255	2.12	13.50	106.44
256	2.10	13.32	106.31
258	2.08	12.96	106.06
260	2.05	12.60	105.81
269.17	1.94	10.95	104.67
280	1.82	10.95	104.67
300	1.60	10.95	104.67

Table B.1. Moment, shear and axial forces of compressive column of IF_FB specimen

(continuation)

<i>Column height (mm)</i>	<i>M(y) (kN.m)</i>	<i>cQ(y) (kN)</i>	<i>N(y) (kN)</i>
311.34	1.48	10.95	104.67
320	1.39	10.95	104.67
340	1.17	10.95	104.67
360	0.95	10.95	104.67
380	0.73	10.95	104.67
400	0.51	10.95	104.67
420	0.29	10.95	104.67
440	0.07	10.95	104.67
460	-0.15	10.95	104.67
480	-0.37	10.95	104.67
500	-0.59	10.95	104.67
520	-0.80	10.95	104.67
540	-1.02	10.95	104.67
560	-1.24	10.95	104.67
580	-1.46	10.95	104.67
600	-1.68	10.95	104.67
620	-1.90	10.95	104.67
640	-2.12	10.95	104.67
660	-2.34	10.95	104.67
680	-2.56	10.95	104.67

Table B.1. Moment, shear and axial forces of compressive column of IF_FB specimen

(continuation)

<i>Column height (mm)</i>	<i>M(y) (kN.m)</i>	<i>cQ(y) (kN)</i>	<i>N(y) (kN)</i>
700	-2.78	10.95	104.67
720	-2.99	10.95	104.67
740	-3.21	10.95	104.67
760	-3.43	10.95	104.67
780	-3.65	10.95	104.67
800	-3.87	10.95	104.67
820	-4.09	10.95	104.67
840	-4.31	10.95	104.67
860	-4.53	10.95	104.67
880	-4.75	10.95	104.67
900	-4.97	10.95	104.67
920	-5.18	10.95	104.67
940	-5.40	10.95	104.67
960	-5.62	10.95	104.67
980	-5.84	10.95	104.67
1000	-6.06	10.95	104.67

Appendix C

An Example to Demonstrate the Calculation of Column Performance

C1. Shear Capacity of Column

An example to demonstrate the calculation of shear capacity of compressive column IF_FB specimen is presented. Shear capacity of column was evaluated by Equation 5.16

$$V_n = V_c + V_s + V_p$$

$$V_c = k \sqrt{F'_c} (0.8 A_g) \quad (MPa)$$

$$V_s = \frac{A_v f_y D'}{s} \cot 30^\circ$$

$$V_p = \frac{D - c}{2a} P$$

where, $k= 0.29$ Mpa up to a drift of 0.01 and 0.1 Mpa at a drift 0.02 based on Figure 5.9, $f_c=20.6$ N/mm², $A_g=19600$ mm², $A_v=25.12$ mm², $f_y=507$ N/mm², $D'=113$ mm, $s=100$ mm, $D=140$ mm, $c=70$ mm, $P=143455$ N, and $a=446.6$ mm.

Consequently, the shear capacity of column, V_n , was observed to be 56.78 kN. The shear strength of column started to degrade at a drift of 0.01. The axial failure of column occurred at 0.002 drift as the shear strength was 43.26 kN, as shown in Figure 5.8(b).

C2. Performance of Column

The performance of compressive column was presented by shear force, as shown in Figure 5.8(b), which the maximum shear force of 47 kN was represented by the average of shear force distribution, ${}_cQ(y)$ in Table B1 along the column height of 140 mm where column height, y , equal to column depth, D , from the end. The deformation capacity of column of 0.017 rad was defined as a drift where shear force attained to the capacity, as shown in Figure 5.8(b).

Publications

A. Reviewed/Journal Papers with Referee's Review

1. Maidiawati and Yasushi Sanada, Investigation and Analysis of Buildings Damaged during the September 2007 Sumatra, Indonesia Earthquakes, *Journal of Asian Architecture and Building Engineering*, Vol. 7 No. 2, 371–378, 2008.
2. Maidiawati, Yasushi Sanada, Daisuke Konishi and Jafril Tanjung, Seismic Performance of Nonstructural Brick Walls Used in Indonesian R/C Buildings, *Journal of Asian Architecture and Building Engineering*, Vol. 10 No. 1, 203-210, 2011.

B. International Conference with Referee's Review

1. Maidiawati, Yasushi Sanada, and Thandar Oo, Modeling of Compression Strut in Masonry Infill Panel for Seismic Performance Evaluation of Masonry Infilled RC Frame Structure, Joint Conference Proceedings 9th International Conference on Urban Earthquake Engineering / 4th Asia Conference on Earthquake Engineering, Tokyo, 6-8 March, 2012.
2. Maidiawati, Thandar Oo, and Yasushi Sanada, A Simple Approach for Determining Contact Length between Frame and Infill of Brick Masonry Infilled R/C Frames, 15th World Conference on Earthquake Engineering, Lisboa Portugal, 24-28 October, 2012.
3. Maidiawati, Yasushi Sanada, and Thandar Oo, Analytical Model for Strength and Stiffness Prediction of Brick Masonry Infill, The Fourteenth Taiwan-Korea-Japan Joint Seminar on Earthquake Engineering for Building Structures SEEBUS 2012, Osaka-Japan, 1-2 November, 2012.

4. Maidiawati and Yasushi Sanada, Analytical Method for Seismic Performance Evaluation of Infilled R/C Frames, Proceeding Managing Assets and Infrastructure in the Chaotic Global Economic Competitiveness, International Conference on Construction Industry, Facilities and Asset Management (ICCIFAM), Padang-Indonesia, 22-23 November, 2012.
5. Maidiawati and Y. Sanada, Modeling of Brick Masonry Infill and Application to Analyses of Indonesian R/C Frame Buildings, The Thirteenth East Asia-Pacific Conference on Structural Engineering and Construction (EASEC-13), Sapporo, Japan, 11-13 September, 2013.